DELFT UNIVERSITY OF TECHNOLOGY

MASTER THESIS

The Development of Downhole Separators in Series, Using Design Models Based on Computational Fluid Dynamics Verified By Laboratory Experiments

Author:
K. SALEH

Supervisors:
Prof. Dr. P.L.J. ZITHA
Dr. ir. R.A. SWANBORN
Dr. ir. A. BOS

March 7, 2015

TUDelft
Delft
University of
Technology

Title:	The Development Of Downhole Separators In Series, Using Design Models Based On Computational Fluid Dynamics Verified By Laboratory Experiments
Author:	K. Saleh
Date:	January 2015
Professor:	Prof. Dr. P.L.J. Zitha
Supervisors:	Dr. ir. R.A. Swanborn and dr. ir. A. Bos
Postal address:	Section for Petroleum Engineering
	Department of Geoscience & Engineering
	Faculty of Civil Engineering & Geosciences
	Delft University of Technology
	P.O. Box 5028
	The Netherlands
Telephone:	+31 15 278 1328 (secretary)
Fax:	+31 15 278 1189

Abstract

One of the major problems associated with oil and gas production is the large volume of produced water. Operators around the world are facing significant costs with the treatment and disposal of produced water. Downhole separation, a relatively new technique, has been developed to reduce the costs of produced water and increase oil production. Downhole separation is the technique where oil and gas from the produced water is separated at the bottom of the well and re-inject some of the produced water into another formation, while the oil and gas are pumped to the surface. The reduction in cost is owed to the downhole treatment of the produced water since most of the topside produced water treatment facilities are reduced in number. Since most of the produced water does not reach the surface this creates an added value of minimizing the opportunity for contamination of underground sources of drinking water through leaks in casing and tubing during the injection process.

The goal of this project was to design a downhole liquid-liquid separator and to evaluate the performance at downhole conditions with the aid of computational fluid dynamics. The separation performance is evaluated experimentally.

A dedicated test rig has been designed and built at ProLabNL, a sister company of Ascom Separation, to test the separation efficiency of the downhole separator. The designed system consisted of three hydrocyclone stages in series to polish the water to the desired injectate quality of 100 ppm oil in water, and was operated under downhole conditions, i.e. high temperature (70 - 80 °C), high watercut (90 - 95%) and relatively large oil droplets (ranging from 500 - 1000 [μm]) dispersed in the continuous phase. The system design and the operational method are fully outlined.

At the tail-end of production, reservoir pressure is depleted causing increased sand production. In the existing commercial downhole separators, the solids that are produced are re-injected downhole leading to potential plugging of the disposal zone. The proposed downhole fluid separation system is equipped with a de-sander to flush the separated sand with the oil rich stream to the surface. Computational fluid dynamics was used to evaluate the pressure balance and volume flux balance of the internals. An erosion analysis was conducted to investigate the wear due to the sand influx.

Furthermore, laboratory tests were conducted to evaluate the influence of a progressive cavity pump (PCP) on the shearing effect of an oil water mixture. The pressure-drop over the pump seems to play a crucial role on the amount of droplet breakup which leads to a decrease in separation efficiency of the downhole separator.

Keywords: downhole separator, DOWS, hydrocyclone, oil-water separation, produced water, fluid mechanics, computational fluids dynamics, de-oiling, separation efficiency, design, water quality, Navier-Stokes equation.

Acknowledgments

The project is carried out with Ascom Separation, division Research and Development. I would like to thank my supervisors at Ascom Separation, dr. Swanborn and dr. Bos as well as prof. dr. Zitha from the TU Delft for their guidance and supervision during this period. A special thanks goes to dr. Lammers who mentored me for my day to day tasks. Besides a devoted supervisor, I gained a good friend in all three my supervisors. Hopefully our paths will keep crossing.

Their mentorship assisted me in further development of my engineering and critical thinking skills. A special thanks goes to my colleagues that I have been sharing working place with over the past 12 months and for keeping up a good mood throughout the whole period of this work.

List of Figures

List of Tables

Contents

Chapter 1

Introduction

Maturing oil and gas fields tend to produce large amounts of water. Produced water includes formation and injection water. In conventional production processes the produced oil and water are separated and re-injected into the subsurface.

Although oil companies have the choice of either disposing or re-using the produced water, the public concern about the environmental impact is becoming a major issue. This does not only concern the fresh water contamination, but also the damage caused by spillages on the surface. So water management has become an important aspect for oil producing companies because of the enormous increase of water production, which leads to an enormous amount of water treatment costs (OPEX). In addition, as withdrawal of water continues over time, it will contribute to the reduction of reservoir pressure and to compensate this water injection is needed.

For treatment, traditionally large gravity separators have been used to separate oil and water. However, they have some limitations such as dynamic sensitivity (on a FPSO) and are space occupying, which is an issue on offshore platforms. One of the techniques for liquid-liquid separation is the hydrocyclone with its compact size and high efficiency and reliability, which can replace large surface gravity separators. The cyclonic device divides the liquid mixture into two streams, an oil-rich stream and a water-rich stream.

Downhole oil-water separation (DOWS) was introduced to the oil & gas industry in the 1990's. Basically this idea includes a separator subsurface where the oil and gas is being separated from the water, whereby the water is injected in another formation (usually below the producing formation). This is usually performed with an electric submersible pump (ESP) where the oil and/or gas flow is brought up to the surface. The position of the ESP mainly depends on the reservoir pressure and the relative position of the production and injection zones . If there is not enough pressure from the reservoir an ESP is needed to provide the inlet pressure to the separator. In case of cyclones in series another pump is needed in between. There are two types of downhole separators: gravity and /cyclonic-based separation. The Gravity separators rely on the specific density of the different fluids. The method has an attraction of generally low OPEX and CAPEX and is environmental friendly due to the lack of chemicals and excessive heating requirements. The separation process occurs in the annular space between the casing and the tubing.

The cyclonic separator is subdivided into a push trough and pull through system. This has to do with the configuration/position of the pump and separator. If the produced fluid enters the pump first and then the separator, it is called a push trough system. If the produced fluid enters the separator first followed by a pump, it is called a pull through system. This report will only focus on cyclonic, push-and-pull through system for oil-water separation.

With the gradual pressure decline of a gas reservoir, the produced water from the reservoir builds up in the well and cannot be carried away anymore. This will lead to the gas well to stop producing. Since the

density difference between gas and water is large, the separation occurs naturally in the well. The purpose of a DGWS is not so much of the separation of fluids, but of injecting the water downhole while allowing gas production. If it is a condensate, then there is no need for an injection zone when the two main streams are the oil and gas. However, a side note has to be made for this because if the liquid is referred to as water, then an injection zone is needed. The great advantage of separating the gas-oil mixture downhole is the prevention of slugging and flow assurance. When having both an annulus for the gas and oil production, the gas and oil can be produced separately.

Field tests should be performed in order to test the performance of the downhole separator. However, before an expensive assembly is built and tested a cheaper and more efficient manner is available to analyze the performance of several components with a model in Computational Fluid Dynamics (CFD). This means that the downhole separator will be translated into a mathematical model such, that elements like the flow assurance, erosion and pressure balance can be investigated. CFD is the simulation of fluid flow and heat and mass transfer by solving sets of conservation equations. Its capabilities and application have been widely expanded, and it has become a great predictive tool in many applications ranging from drilling to production and processing.

Although the hydrocyclone technology is showing great potential, with efficiencies of over 99% for hydrocyclone liners, a limiting factor is the feed concentration of 1000-3000 ppm oil which is equivalent to 0,1 to 0,3%. However, downhole oil in water concentrations can be as high as 10% (or higher) and in low-pressure reservoirs the presence of a pump (in case of a push through system) reduces the droplet size. However, when using a bulk de-oiling hydrocyclone, which is basically the same as a hydrocyclone but with bigger outlet orifices diameters allowing higher feed capacities going up to 50% oil in water (OiW), this can be used as a first stage separator after which comes the hydrocyclone as a second stage. Test results at ProlabNL, a mature oil field simulation facility, have shown that the water outlet of the bulk de-oiling hydrocyclone gives concentrations of about 1%, which is still on the higher side. This indicates that maybe an intermediate separation step is required.

Chapter 2

Background

2.1 Problem Statement

When the concept of downhole separation was first introduced, there was a huge amount of interest, peaking during the 1990s, as everyone in the industry noticed the potential that reducing the volume of produced water could bring. However, the main concerns included high costs and the complexity of the system (with the inverted pump section, by-pass tubes and the hydrocyclone). Coupled with the low reliability of the initial DOWS, the ongoing concern regarding exactly what was being injected, and the fact that there was no way to verify separation efficiency, the end result was a low confidence that the systems could deliver as designed. Therefore, despite widespread initial interest and the obvious benefits, attention to the technology faded and the number of installations tailed off such that in the five years prior to 2010, no installations transpired [11].

2.2 Cyclonic Separation

Hydrocyclones are widely used for oil/water separation in surface applications where their small size and simplicity can offer savings in facilities costs and reduced operational costs. Figure 2.1 shows the basic operation of a liquid-liquid hydrocyclone.
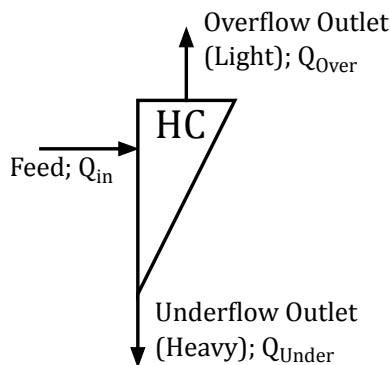
Figure 2.1: Colman-Thew hydrocyclone operation

The pressurized fluid mixture is fed to the hydrocyclone through one or more tangential inlets, forcing rotation of the fluids within the device. The conical shape of the hydrocyclone causes the fluid flow to accelerate into a

helical pattern, setting up a free vortex and creating large centrifugal forces. The centrifugal forces cause the lighter materials (e.g., oil, free gas) to migrate to the center of the hydrocyclone, while the denser materials (e.g., water, solids) are forced to the outer wall. By maintaining the underflow outlet at a higher pressure than that of the overflow outlet, the concentrated oil core of the vortex is forced to flow countercurrent to the main flow. The result is that a concentrated oil stream exits the overflow, while an oil depleted water stream exits the underflow. Most often hydrocyclones are used in oil production for de-oiling produced water, i.e., removal of trace hydrocarbons ($\ll 1\%$) prior to disposal of produced water by overboard discharge or downhole reinjection.

2.3 Downhole Oil-water Separation

One of the most important questions regarding downhole separation is the performance sensitivity. The operation principle of a hydrocyclone will remain the same, however the environment in which it operates will vary. The performance of a hydrocyclone mostly depends on its geometry, density difference between the continuous and dispersed phase and the oil droplet size distribution. The latter parameter is difficult to control. Janssen [17] has, in extensive laboratory experiments, investigated the droplet size distribution of oil-in-water mixtures leaving the reservoir. The author found that smaller droplets are produced for a reservoir with a low permeability and high linear velocity, the risk on breaking up droplets can diminished by either producing with a lower flow rate or altering the wettability of the near wellbore region to oil-wet. The first remedy may not be economically justified. Another natural important parameter for the performance of downhole separation is the injectivity. The presence of oil can have a negative effect on injectivity[1], leading to a reduction in permeability in the reservoir resulting in a situation where the pressure at the outlet of the hydrocyclone is so high that almost all of the flow is directed upwards to the overflow. This presence of oil is caused by the amount of smaller droplets at the inlet. In order to maintain a low oil-in-water concentration at the underflow, one should ensure a droplet size distribution with a low frequency for droplets smaller than 15 [μm].

DOWS systems have so far been installed where water cut is extremely high (90%). One of the reasons for this is the need to bring an oil stream to surface containing approximately 25-50% water in order to maintain injection water quality[2] [10]. The economic advantage of the DOWS system also decreases as the watercut of a well decreases. The result is that using the system in a well with less than 75% water cut has usually been unattractive. Typical oil-in-water levels at the outflow range between the 100-300 ppm [18]. Downhole monitoring of the oil-in-water concentrations should also be conducted in order to determine the efficiencies of the hydrocyclones. This can be done either real-time (Advance Sensors EX1000M) and/or installing capillary lines from the injection zone to the surface, where it is connected to the tubing at the bottom outlet of the hydrocyclone. From these surface placed tap points the oil-in-water concentrations can be determined. Another important issue is to know the droplet size distribution in order to estimate the efficiency of the hydrocyclones. If there is a large dispersion of droplets due to for example chokes and high-pressure differences, the efficiency of the cyclones will decrease significantly. However, in order to get a picture of what is happening to the droplets in the annulus an imaging device should be installed, but this is very complex and costly. The advantages of a DOWS are, as already stated, significant. One could argue that the surface processing is generally more efficient than downhole separation on a \$/barrel basis. However they require platform space and potentially other infrastructure to be implemented. Another important aspect that is not easily observed is the fact that surface facilities become under-occupied as candidate wells for the DOWS produce lower surface watercut. This provides opportunities for other high watercut wells to be ramped on [3]. This thesis will focus on the liquid-liquid centrifugal separation.

---

[1]Emulsion droplets can be forced (squeezed or snapped off) to enter the formation where they may be captured either by straining in pore constrictions and/or by deposition on pore surface causing in-depth permeability damage. Also oil droplets are likely to be in-site generated from residual oil with an even more drastic impact on injectivity [25]

[2]Detailed explanation in chapter 4

2.4 DOWS Completion Design

Throughout the years several design have been proposed and patented from initially one hydrocyclone mounted below the tubing to multistage bulk de-oiling hydrocyclones and hydrocyclones in series in combination with ESPs. The DOWS concept comes down to some basic principles. First of all, there is a need for a separation device, which is in most of the cases a hydrocyclone for its small size, high efficiency and having no moving parts. Secondly, pumps need to be installed in order for the fluids to enter the separator, injected into the reservoir and brought up to the surface. The configuration and the amount of the pumps depends mainly on the reservoir pressure and the relative position of the producing and injecting zones. However, as the DOWS is being implemented in brown fields, the pressures decreased enormously[3], there is a necessity for a pump. A second pump is needed for bringing the oil-rich stream to the surface. The driving force for the pumps may come from the surface or installed downhole. If it is installed downhole, naturally the system becomes more complex as a second motor is installed. It should be denoted that when one motor is installed both the pumps will work on the same frequency, because the drive shaft operates the two pumps. In addition, it is important to note that the motor should be bypassed with fluid for it to cool down. Figure 2.2 shows a typical design of a DOWS completion design.
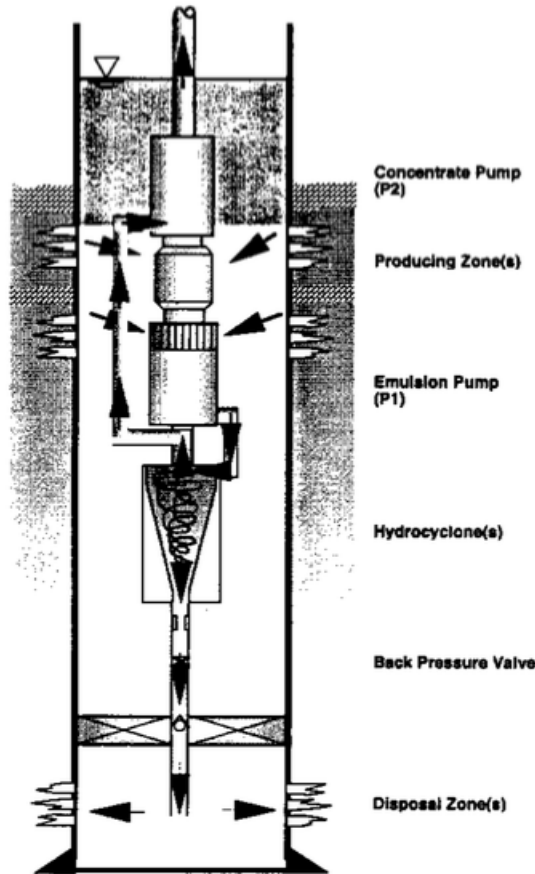
Figure 2.2: Typical design of a DOWS completion design [12]

---

[3]Initial pressure gradients are in the range of 9.8 to 11.0 kPa/m. Many reservoirs are located between 1500m to 4000m so that typical reservoir pressures on discovery are between 15 MPa and 40 MPa [26].

2.5 Multistage Separation

One approach for enhancing the DOWS efficiency is to use multistage separation. In this scenario, the first stage hydrocyclone is optimized to remove as much water as possible from the production. The first stage does not produce an injection-quality water stream. A second stage of hydrocyclones is used to clean the water discharged from the first stage to injection quality. In this way, water to the surface can be significantly reduced as compared to the use of a single stage system [10]. However, the need for a possible third stage depends on the oil inlet concentration. The efficiency of the separator decreases at every stage due to removal of the "easier" droplets in the first (and second stage). As the target injection concentration is to inject below 100 ppm, and assuming an oil well with a watercut of 90%, a three-stage separation is required.

2.6 Downhole Water Sink

Downhole water sink (DWS) technology is an alternative for controlling water production in wells producing hydrocarbons from reservoirs with bottom water drives[4] and strong tendencies for water coning[5]. With DWS, a well is dually completed[6] for oil production (upper completion) and water drainage (lower completion or water sink) with the two completions separated by a packer. Basically, by adjusting rates of both the upper (oil) and lower (water) completions, one controls the position of the interface at the wellbore and the resulting fluid cuts in each completion. Quality of the drained formation water depends upon DWS completion design and rate adjustment [19].

2.7 Fluid Shear

Shear implies that there is a gradient in the velocity of a fluid stream measured across the axis of flow. A high shear rate is normally encountered where there is an abrupt change in flow velocity or where a high velocity stream flows through a static channel, and is normally indicated by a significant change in pressure exerted on (or by) the flowing fluid. High shear conditions upstream of an oil/water separator are avoided because of the negative effect on the droplet size distribution of the dispersed phase. Since de-oiling hydrocyclone separator performance is directly related to oil droplet size, excessive shear upstream of a hydrocyclone separator should be avoided. High shear rates occur within process devices such as piping, control valves, and pumps. In general the higher the pressure drop across a control valve, or the lower the hydraulic efficiency of a pump, the greater the shear rate and the more negative the effect on separation performance. High shear rates can also occur within the hydrocyclone itself. In particular, the tangential inlets of a typical de-oiling hydrocyclone expose the oil/water mixture to extremely high flow velocities and resulting high shear rates. It has been observed that oil in water dispersions where the mean oil droplet size is already very small ($\ll 50$ μm) are less susceptible to further reduction in droplet size as a result of high shear rate. Additionally, it is known that dispersions of low gravity crude oils are less susceptible than dispersions of lighter crude oils to droplet size reduction as a result of shear. Based on these observations, a number of "shear tolerant" hydrocyclone geometries and process design practices have become common for produced water treatment applications. Modern de-oiling hydrocyclone designs are able to remove very small oil droplets from water, and "reasonable" levels of shear do not prevent these hydrocyclones from achieving their design goal: removal of trace amounts of oil from water [10].

---

[4]Water drives are drive mechanism and a source of natural energy to move the oil and gas towards the wellbore.

[5]The change in oil-water contact or gas-oil contact profiles as a result of drawdown pressures during production.

[6]Some wells have a dual completion, which means two tubings, each producing from a different reservoir at a different depth [17].

2.8   Sand Production

Important in this work is the use of a de-sanding cyclonic unit. From several reports [1] [2] it has been concluded that sand production has played a crucial role in the performance of the DOWS. The injectivity of the reservoir decreased enormously due to excessive sand production and the hydrocyclones were worn out due to erosion. The sand production of a well increases with increasing watercut. At watercut levels of 35% sand production commences. Sand production dramatically increases as watercut increases, with sand levels in excess of 0,3% by volume in the worst cases (this equates to approximately 450 kg/1000 barrels of fluid). Over time the sand levels then tend to stabilize back to 0,05% to 0,1% [20].

The problem of a de-sander upstream of the liquid-liquid separator, as above stated, is the breaking up of droplets. The particle size and the viscosity of the inlet fluid influence this. The smaller the particles and more viscous the fluid, the more pressure differential is required to gain a sufficient efficiency in the de-sander. In turn, this results in higher shear forces creating smaller oil and water droplets. So the de-sander benefits from bigger particles and lower viscosity.

2.9   Injectivity of Disposal Zone

As already mentioned, the presence of oil can have a negative effect on injectivity. Production from reservoirs with a relatively low permeability may lead to the presence of small oil droplets resulting in lower separation efficiency in the DOWS. This means that the underflow outlet of the hydrocyclone separator produces a higher concentration of oil. Little data have been published on the aspect of formation damage resulting from produced oily water injection. Tang (1982) investigated filtered and unfiltered produced water containing crude oil and solids. He indicated that the injection of produced water containing 600 ppm of oil and 14,2 ppm of solids could cause permeability reductions; the worst damage is caused by the invasion of oil rather than by the deposition of solids on the core face. He also commented that the oil content of the produced water needs to be decreased to 20 ppm in order to prevent severe formation damage [21].

Zang et al. conducted core flooding experiments to simulate formation damage associated with produced oily water injection. The results indicate that produced oily water containing oil droplets and solid particles can contribute to the permeability decline observed in the cores. The most severe decline occurred in the first 10 - 15 mm of the core. Oil droplets with a dimension significantly less than the pore throat diameter also led to permeability decline [21].

2.10   Failures

Failures can be classified into two basic categories, mechanical and process related failures. When all mechanical systems are working properly, failure of a DOWS system generally means there is incomplete separation. There are a number of process variables that directly affect separation performance. In most cases, these process variables result in the creation of an emulsion that cannot be adequately separated by the hydrocyclone separator. The biggest issues arise with plumbing, since tubular and conduits must be fitted into a very small cross-sectional area, which are also exposed to very high flow velocities. A small number of failures have resulted from problems with the isolation packer. In these cases, the packer has failed to isolate the production and disposal zones. The complexity of DOWS system installation can lead to problems in properly designing the ESPs. Because of the uncertainty about the injectivity index of the disposal zone, and the need to operate the separator at a proper flow split, it can be difficult to plan for the thrust load generated by the pump. Inadequate thrust bearings will result in premature failure. Excessive solids production has led to premature mechanical failure of the separator, pumps, or bypass tubing. In at least two cases, solids production was so excessive that the entire pump/separator assembly was packed with solids when inspected at the surface.

Solids also affect separation performance since oil-wet solids particles can cause oil to be drawn to the water outlet of the separator. Solids also tend to enhance the creation and stability of oil/water emulsions. The separation of heavy crude and water is more difficult due to small density difference between the oil and water and dewatering heavy crude oil is normally made difficult by the high viscosity of the crude. It has been observed in DOWS applications that heavy crude/water mixtures are much more likely to form stable water- in-oil emulsions when exposed to the shear induced by a push- through design using ESP's [10]. Control of the flow split, the ratio of the overflow rate to the inlet flow rate, is a crucial aspect for the separation performance. All DOWS systems to date have been installed with extremely limited capability to adjust pressure balance across the separator, thus limited ability to adjust flow split in response to changing production or injection conditions. This has resulted in inadequate separation and premature system failure in some cases [10]. If the rate of pressure difference is not set correctly, either oil will be carried to the underflow or excessive water will be lifted to the surface. However, the latter is more acceptable [2].

2.11   DOWS design constraints

The limitations of the DOWS can be identified by the failures. Based on these failures, the constraints are defined [7]. Wellbore space is very limited, the hydrocyclones designed for this particular operation must be narrow and tall, therefore, minimum casing size requirement is 5-1/2". In order to allow the cooling of the ESP-DOWS system, the engine must be installed below the productive area. Otherwise, shrouds are used to direct the fluids past the motor.

Reservoirs that have a history of sand production may not be suitable for this system due to the risk of plugging. Also, based on previous experience, the system worked better in carbonate formations compared to sandstone formations. For sufficient the minimum difference in specific gravity between oil and water should be 0.05. Oil content (typically between 10 and 200 ppm of oil) in the injection water can damage the formation, especially those that do not have residual oil saturation.

2.12   Reservoir Screening Criteria

Wells which have a depleted horizon, low static pressure or most likely to receive water injection, are potential candidates for the DOWS technology. The reservoir has to contain sufficient incremental reserves and provide a suitable disposal zone. Injection zone must have sufficient permeability and porosity to accept segregated produced water. From production perspective, only wells having water cut of 94% or more will be considered for this technology. In order to prevent the injected water to migrate to the production zone, a minimum distance of about 25 m must exist between the production and disposal zone. The characteristics of produced water must be compatible with the injection zone. It is usually inadvisable to mix water from carbonate and sandstone formations [10].

Chapter 3

Cyclonic Separation

Tangential de-oiling hydrocyclones have long been present on the upstream produced water treatment market. With governments around the globe restricting the maximum allowable oil-in-water discharge quantities to a maximum of 20 ppm, conventional hydrocyclones are no longer adequate to meet the new regulation requirements.

Contrary to conventional tangential or axial hydrocyclones, the ASCOM HiPer[1] (MixedFlow) hydrocyclone, shown in Figure 3.1, is based on a mixed-flow principle, which results in coalescing and consequently stabilizing effect on the oil-water flow. All available pressure energy is converted into a rotating motion within the hydrocyclone as the liquid passes flows through it. This generates much higher g forces that result in stable oil and water separation. Recent ASCOM tests with diesel and crude confirmed earlier findings that the ASCOM HiPer hydrocyclone showed both very high separation efficiency and a lower pressure drop. The MixedFlow hydrocyclone is a patented technology (USA and Europe) with full and sole ownership by ASCOM.
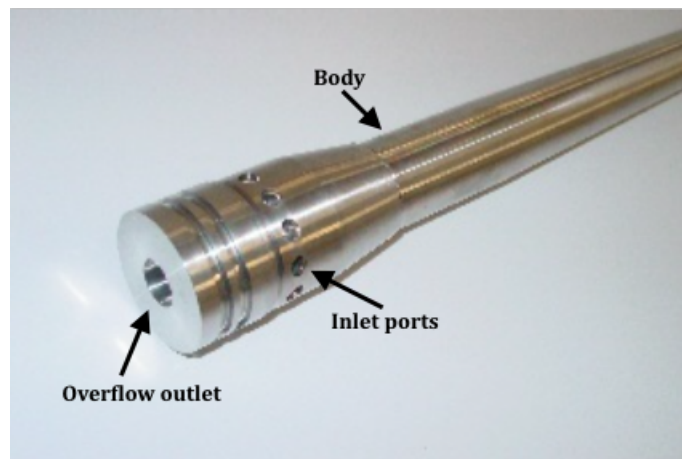
Figure 3.1: HiPer hydrocyclone liner inlet section with multiple inlet ports

---

[1]High Performance

3.1 Stoke's Law

Stokes' law applies to the sedimentation or flotation of non-flocculating, discrete and spherical particles, and is here modified to the application of oil droplets in produced water. Stokes' gives the terminal settling velocity of an oil droplet as shown in equation (3.1), assumes laminar flow, spherical particles and unhindered settling:

$$V_t = \frac{gD^2(\rho_w - \rho_o)}{18\mu} \tag{3.1}$$

Where D is the droplet diameter [m], ρ_w and ρ_o the continues (water) and dispersed (oil) phase density [kg/m^3] respectively and μ the viscosity of the continues phase [kg/(ms)].

Stokes' law shows that the settling velocities increases by either increasing the droplet diameter D, increasing the density difference between the phases $\rho_w - \rho_o$, decreasing the viscosity μ of the continuous phase, or increasing the acceleration g. It is still the droplet diameter that will affect the settling velocity the most (Husveg 2007).

If a hydrocyclone or other separation equipment based on centrifugal forces is used to separate the oil from the produced water, a slightly modified Stokes' law must be applied. For a particle that is forced to move in a circular path the acceleration acting on that particle is proportional to the square of the angular velocity, as shown in equation (3.2).

$$a = \omega^2 r \tag{3.2}$$

where, r the radius of the circular path [m] and ω the angular velocity [m/s].

Estimating g and a, and inserting equation (3.2) into Stokes' law as given by equation (3.1), gives the terminal settling velocity for an oil droplet affected by a centrifugal force:

$$V_t = \frac{\omega^2 r D^2(\rho_w - \rho_o)}{18\mu} \tag{3.3}$$

The droplet diameter is a major factor also in centrifugal separation, but the angular velocity is of equal influence to the terminal velocity. Equation (3.3) shows that there is a large potential for increasing the terminal settling velocity of the oil droplet, and this is used in all types of centrifugal separation [1].

3.2 The Colman and Thew Hydrocyclone

The geometry of the ASCOM HiPer hydrocyclones are based on the Colman and Thew model [18], the pioneers in the modern renaissance in de-oiling hydrocyclones. The Colman and Thew patents on de-oiling hydrocyclones cover a wide range of design ratios. The authors first conducted tests on commercial implementations of this hydrocyclone having the dimensions shown in figure 3.2. The effects of operational parameters on this design were investigated to establish a baseline. Then tests were conducted on an experimental hydrocyclone in which the various dimensions of the hydrocyclone could be varied incrementally in order to determine optimum design parameters. The goal of this research was to develop an optimized oil/water separation hydrocyclone to remove oil from water at maximum removal efficiency. Using these optimum design parameters, a prototype hydrocyclone was designed incorporating materials and manufacturing methods used in the production of existing solid/liquid hydrocyclones. The result was an economical, high throughput hydrocyclone for use in production operations where space, weight or other considerations exclude tankage-based separation facilities [18].

The reasons for multiple-coned Colman and Thew hydrocyclone:

1. As the outer vortex moves downwards, some fluid is lost inwards and the angular momentum loss in the outer vortex is compensated for by the multiple-stacked decreasing angle (i.e., narrowing radius). The decrease in cone angle reduces the cut size (i.e., improves separation efficiency).

2. The discharge of solids is in an area of low pressure and the solids are conveyed in the boundary layer towards the apex opening and are intercepted and smuggled by the transverse orifice.

Therefore, by varying the dimensions, number of cones and cone geometry of an industrial hydrocyclone, the angular momentum of flow can be conserved and hence efficiency can be enhanced.
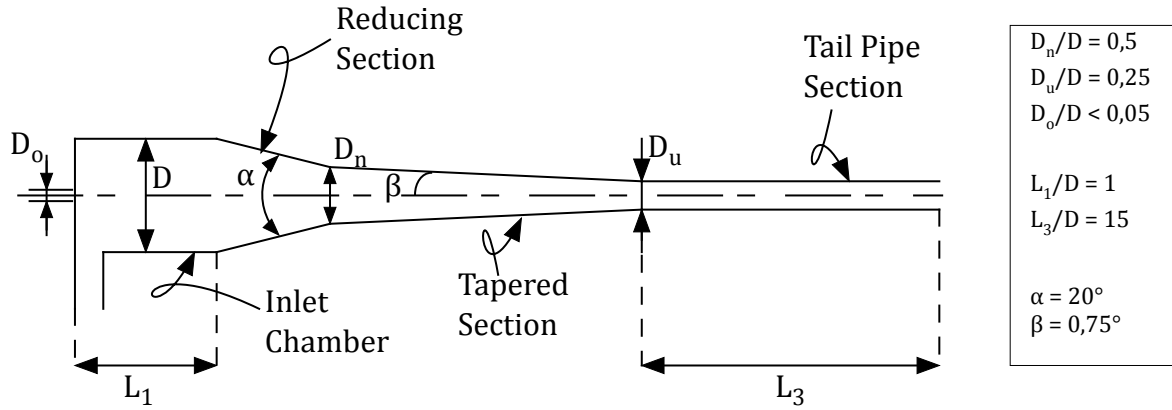
Figure 3.2: Colman-Thew hydrocyclone

3.3 Operation

Flow enters the hydrocyclone tangentially (figure 3.3), creating a spinning motion in the chamber. This spinning fluid causes the lighter oil to separate to the center where it forms a small core one to two millimeters in diameter. The bulk of the liquid reports to the underflow and the oil concentrate reports to the overflow. Typically, less than 5% of the inlet flow reports to the overflow.
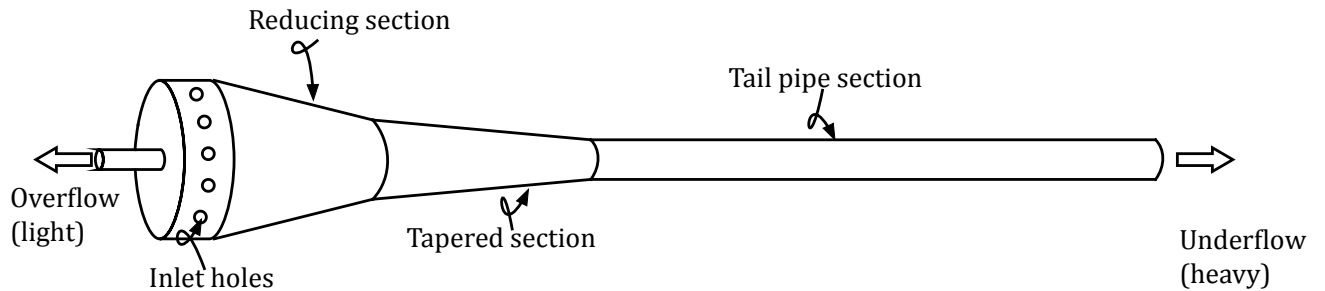
Figure 3.3: Colman-Thew hydrocyclone operation

3.4 Definition of performance parameters

The most important parameters used in this study are defined in this paragraph.The theoretical separation performance of the multi-stage separator is based on:

$$\eta = 1 - \frac{Q_{out}^{oil}}{Q_{in}^{oil}} \tag{3.4}$$

where Q_{out}^{oil} and Q_{in}^{oil} are referred to the underflow outlet and inlet oil in water concentration respectively. Based on extensive testing at ProLabNL, a mature oil field simulation facility, the efficiencies have been determined for several types of hydrocyclones and bulk de-oiling hydrocyclones for several parameters (i.e. flow rate, OiW, temperature, viscosity, density and droplet size). The resulting figure is usually the "grade efficiency" where the separation efficiency is set as function of the droplet size.

The split ratio R, also referred to as the reject ratio, is the overflow rate to the inlet flowrate, as given below:

$$R = \frac{Q_{over}}{Q_{in}} 100\% \tag{3.5}$$

where Q_{over} is the total flow rate at the upper outlet of the hydrocyclone and Q_{in} the total inlet flowrate.

Under normal operation there are two measured pressure-drops across a hydrocyclone. One is the pressure difference between inlet and the overflow, and the other is the difference between inlet and underflow. The former is always greater than the latter. The relationship between these two different pressure drops is called the pressure difference ratio (PDR) and is defined as:

$$PDR = \frac{P_{in} - P_{over}}{P_{in} - P_{under}} \tag{3.6}$$

The two outlets of the hydrocyclone are referred to as the underflow and overflow. However, it is not uncommon in the industry to refer to the overflow as the "reject". being the fluid that needs to be extracted from the system. The underflow is also referred to as the outlet.

Chapter 4

Multistage Separator Performance

The aim of this chapter is to examine the theoretical separation performance of the hydrocyclone liners and to present the framework of the downhole separator. In order to meet the required injectate quality of 100 ppm [18] oil in water concentration, it is important to know how many stages of hydrocyclone and bulk de-oiling hydrocyclones are needed. The hydrocyclone configuration in a downhole separator assembly depends on the downhole conditions, i.e. the watercut, sand production, reservoir pressure, injectivity and several other parameters.

4.1 Separator configuration

The aim of the design is to develop an integrated separation unit, with adequate dimensions to fit any kind of specified well bore. Due to the high flow rates numerous liners are needed to handle the amount of flow. This makes the use of space in the well bore more complicated. Based on the output of each cyclone (being the underflow outlet), it is possible to couple the separator stages such, that either the oil or water stream gets polished. In figure 4.1 these two basic configurations are depicted.

(a) Water polishing system

(b) Oil polishing system
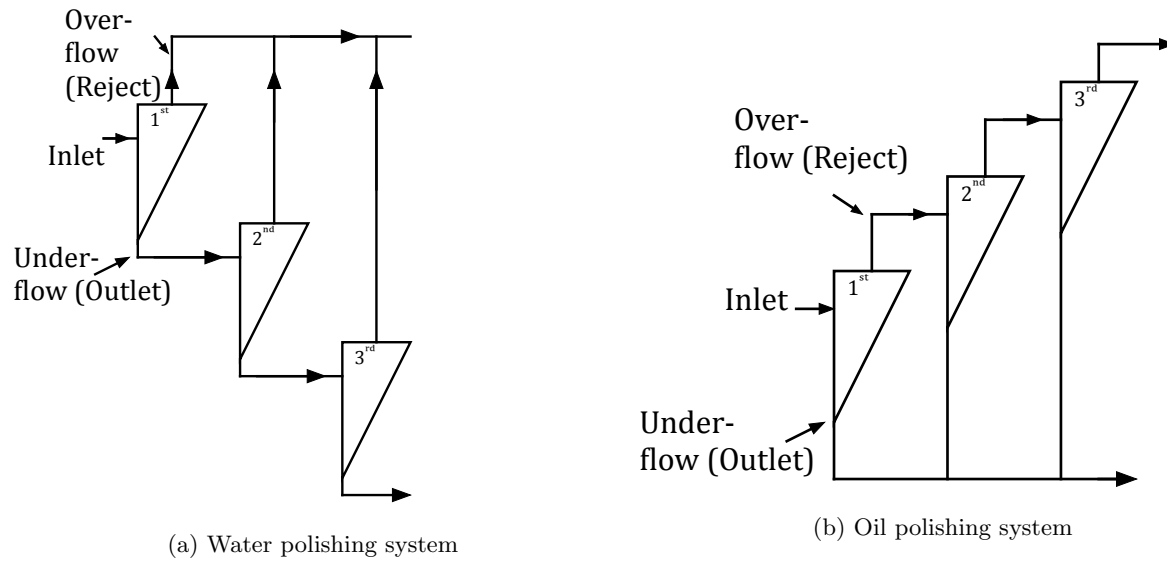
Figure 4.1: Hydrocyclone polishing systems

In figure 4.1a the underflow stream of each stage is the feed for the next stage. As a rule of thumb, at every stage the oil in water concentration is reduced by a factor of 10 (so from 1000 ppm to 100 ppm). The underflow of the last stage is injected in the reservoir. The overflow of each stage does not get polished and is brought together in a separate chamber from where it is drawn into the ESP. Since the aim of the downhole separator is not to get an as clean as possible oil stream to the surface, but to maintain the injectate below a concentration of 100 ppm oil. This makes the first configuration, as depicted in figure 4.1a, the most suitable. Since the separator assembly will be installed with a de-sander, the configuration will differ slightly. Therefore, the system becomes more complex due to the slurry outlet of the de-sander.

4.1.1 System description

The proposed produced water treatment system consists of 4 separation stages, as depicted in figure 4.2. The 1st stage is a de-sanding cyclone and should knock out most of the sand. The 2nd stage performs the bulk oil/water separation whilst the 3rd and 4th stages are polishing stages that reduce further oil concentration to injectate quality.

It can be seen that the heavy phase outlet of the first stage, being the slurry outlet of the de-sanding cyclone, is combined with the overflow of the second stage. Moreover, it should be noticed that the reject of the de-sanding cyclone is positioned at the underflow outlet. Since the slurry outlet of the de-sander will be directed to the surface, its velocity should be maintained at a minimum of 1 [m/s]. There are multiple ways to accomplish this like using smaller diameter tubing or increasing the flow. But a smaller diameter may result in higher pressure-drop and potential clogging. A viable option is to combine it with the rejects of the liquid hydrocyclone. In this way the minimum velocity can be maintained.
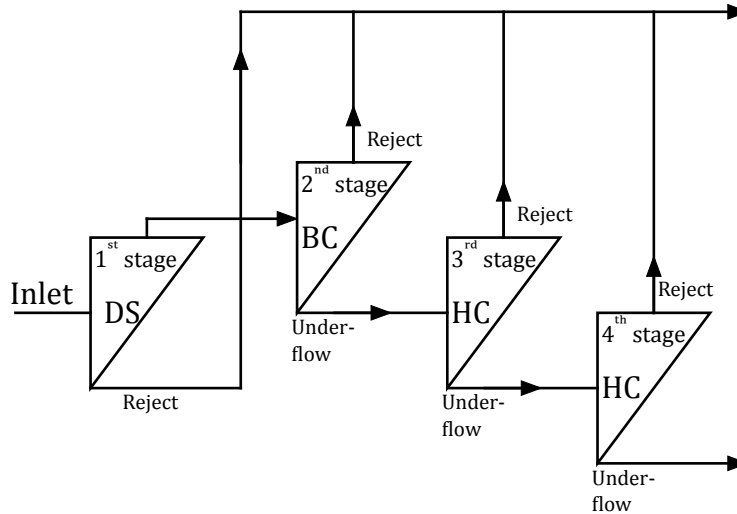
Figure 4.2: Schematic separation efficiency 4 stage system

4.1.2 Input Data

Data from a field test[1] plus the ASCOM hydrocyclone performance data [33] have been used as input parameters for the separator model. These parameters are shown below in tables 4.1 and 4.2. The output of the system gives the number of liners needed, injectate quality, volume of water and oil injected into the reservoir and volume of water and oil recovered to the surface. The reservoir pressure is not taken into

---

[1]These data were very generously provided by TAQA

account since it will be assumed that $P_{res} >> \Delta P_{DOWS}$ and is only playing a role when the bubble point[2] is known (for cavitation) whereby free gas can enter the separator system.

Table 4.1: Input parameters hydrocyclone liners

Stage		1	2	3	4
Liner type		De-sanding cyclone	Bulk de-oiling hydrocyclone FAB 041	Hydrocyclone FAB 081	Hydrocyclone FAB 103
Flow capacity	[m^3/h]	25	5	4	0,8
Reject rate	%	12	20	4	4
Efficiency	%	90	90	90	90

Table 4.2: Input parameters reservoir

		Water	Oil	Sand	Total
Flow rate	[m^3/h]	13,4995	1,5	0,0045	15,0
Concentration	%	89,97	10	0,03	100

One of the important parameter for the system is the reject rate. Since the choke valve is installed at the reject restricting the flow, this will subsequently determine how much oil is left in the oil-core-tail as shown in figure 4.3. When setting the reject rate at 2% (relative to the inlet flow), a larger volume of oil will stay in the core and consequently having a longer oil core tail. The longer this "tail" the more oil will leave through the underflow outlet, meaning a lower efficiency. However, setting the reject rate much higher does not necessarily mean a higher performance can be reached since more water will be produced leading to a turndown in performance.
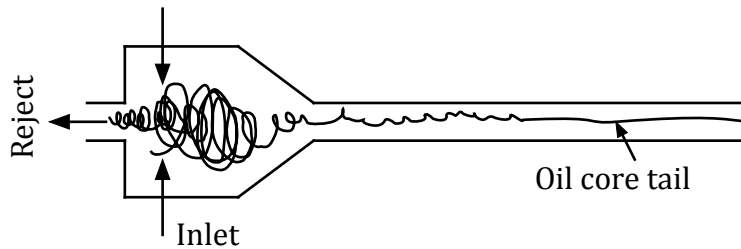
Figure 4.3: Oil core tail inside an hydrocyclone

---

[2]This is the pressure at which first gas is formed when oil is subjected to a decreasing pressure at a given temperature. If the pressure at the top of a reservoir is above the bubble point pressure, all gas is dissolved in the oil. However, if the top part of the reservoir is below bubble point pressure a gas cap exists, and the oil is gas-saturated. The bubble point pressure is therefore also known as the saturation pressure [17].

As a rule of thumb [1] the reject rate is set at 2 - 4 times the oil in water concentration of the inlet for hydrocyclones. In practice this means that the reject rate is set between 2% and 4%. However, for the 1" hydrocyclones the inlet feed is as low as 0,1% and by setting the reject rate at 0,2 - 0,4% this will lead to a very low oil production. Consequently this will be set at 2 - 4% as well. The following values are adopted for the bulk de-oiling hydrocyclones within ASCOM:

Table 4.3: Bulk de-oiling hydrocyclones reject rates setting

Inlet OiW concentration	Reject rate
OiW <4%	8%
4% < OiW < 10%	2×OiW%
OiW >10%	OiW% + 10%

4.2 Results

4.2.1 Separation efficiency

In order to calculate the oil concentration at the outlet (and subsequently in the overflow), the efficiency will be fixed at 90%. Even though this number is based on several parameters and could vary for changing conditions (i.e. flow rate, OiW, temperature and droplet size), it can be used as a conservative value for the separation efficiency downhole. Table 4.4 shows the the theoretical separation efficiency of the downhole separator. Each stage gives the fraction of oil, water and solid going through the overflow and underflow. Figure 4.4 illustrates the schematic separation efficiency, based on table 4.4.

Table 4.4: Separation efficiency

Separation stage	Oil	Water	Sand	
1^{st}_{under}	100000	899970	30	[ppm]
2^{nd}_{under}	10000	989963	38	[ppm]
3^{rd}_{under}	1000	998961	39	[ppm]
4^{th}_{under}	100	999859	41	[ppm]
1^{st}_{over}	100000	897720	2280	[ppm]
2^{nd}_{over}	460000	540000	0	[ppm]
3^{rd}_{over}	226000	774000	0	[ppm]
4^{th}_{over}	22600	977400	0	[ppm]

4.2.2 Mass balance

Table 4.5 shows the volume flux balance of the 4 separation stages in series together[3]. From the outlet of the last stage it can be seen that the injectate quality of 100 ppm (=0,01%) is reached. This results in three stages of liquid-liquid separation with one de-sanding stage upstream the bulk de-oiling hydrocyclone to separate out most of the sand. 91% of the sand is eliminated from the system, resulting in 9% of the total incoming sand flux from the reservoir to migrate through the three liquid stages and leaving the outlet of the 1" hydrocyclone.

Table 4.5: Volume flux balance

	Total	Water	Oil	Sand	
From reservoir	360000	323892	36000	108	[Liter/day]
To surface	126430	90355	35977	98,5	[Liter/day]
To reservoir	233570	233537	23	9,5	[Liter/day]
From reservoir	100,00%	89,97%	10,00%	0,03%	
To surface	100,00%	71,47%	28,46%	0,08%	
To reservoir	100,00%	99,99%	0,01%	0,00%	

---

[3]Table 4.5 illustrates the 4 hydrocyclone stages in figure 4.2 as one single element.

Figure 4.4 shows the oil, water and sand fractions in each stage. The second stage removes 90% of the oil to the overflow, which is due to a higher tolerance in the overflow (reject rate to 20%). Since the second stage' inlet receives only 1,2% oil, the overflow is set to 4% restricting the flow but in turn profiting from higher tangential velocities inside the swirl element for better separation.
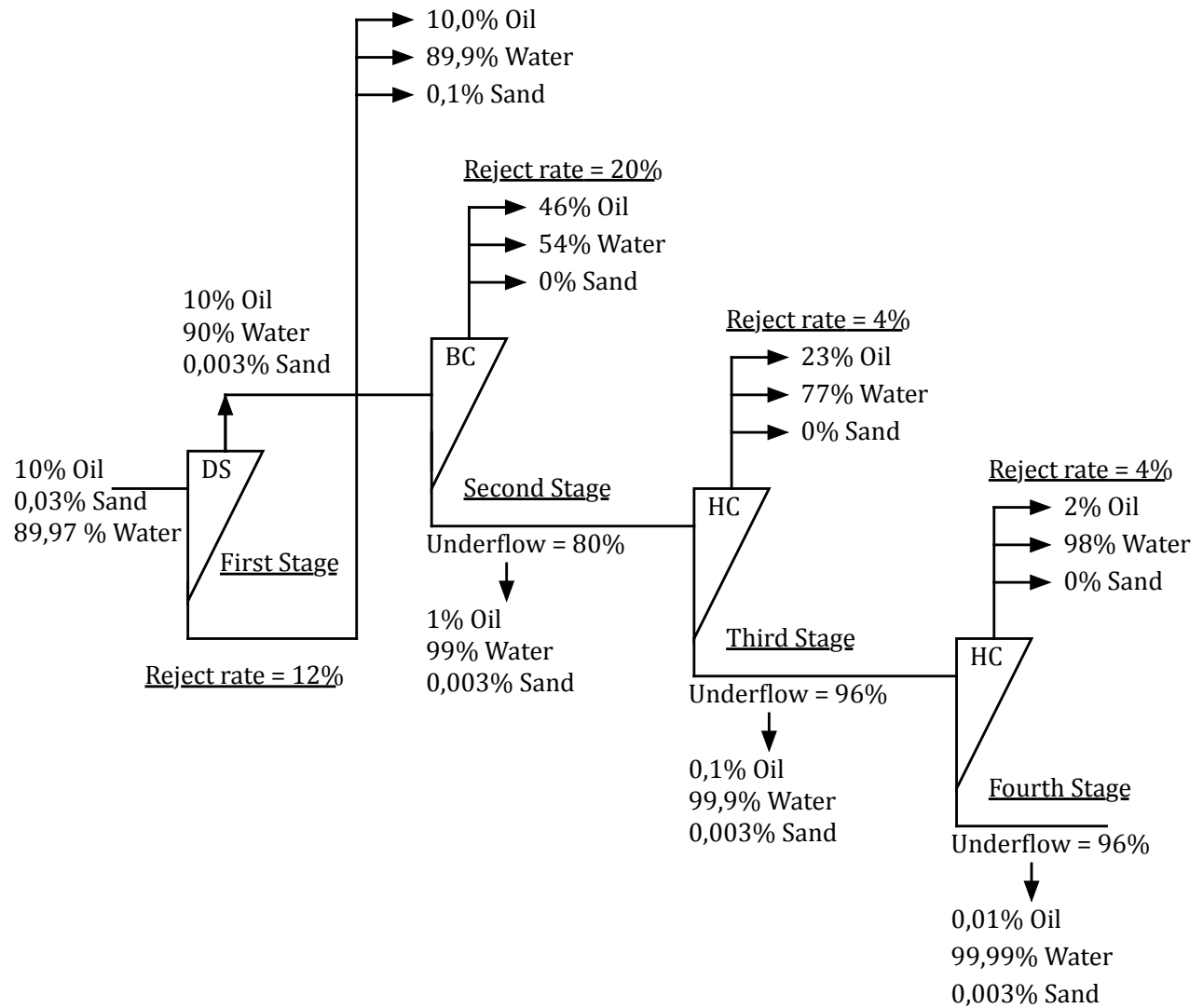
Figure 4.4: Schematic separation efficiency 4 stage system

Chapter 5

Physical design of separator assembly

The aim of the design is to solve the arrangement between the devices and flow channels in the relatively narrow well bore. Based on possible DOWS completion designs and the arrangement of the devices within the DOWS, sections 5.1 & 5.2 respectively, a completion model will be proposed. This is then followed by detailed analysis of the pressure and volume flux balance of the DOWS, sections 5.4 & 5.5 respectively, leading to two separator designs.

The intended field is situated in Block P15, 40 kilometers northwest of the Port of Rotterdam in 25 meters (82 feet) of water. The Rijn wells are connected to the Taqa-operated P15-ACD offshore production and processing facilities. Crude oil production is exported to the Port of Rotterdam via pipeline. The current production rate from the Rijn field is approximately 3,500 barrels of oil per day [23].

5.1 Possible DOWS completion designs

TAQA has provided a well with a water-bearing layer below the oil-producing layer with a minimum distance of 25 meters, which is one of the conditions for the downhole separator[1].

A packer is to be installed to provide isolation from the injection zone to the production zone. A second packer needs to be installed to ensure the fluid is only going through the separating assembly (and not up through the annulus).

Two types of reservoir configuration exist. The oil producing layer above the water injection zone and vice versa. Also the distance between these two zones influences the completion design of the separator assembly. Four reservoir configurations are depicted in table 5.1. The difference between reservoir configuration type 1 and 2, the latter is more complex. An advantage of the second reservoir configuration is the benefit of the "free" extra pressure due to the producing zone being below the injecting zone.

---

[1]The injected produced water can migrate back into the producing zone and then short circuit into the producing perforations, thereby recycling the produced water and causing oil production rates to drop sharply [8]
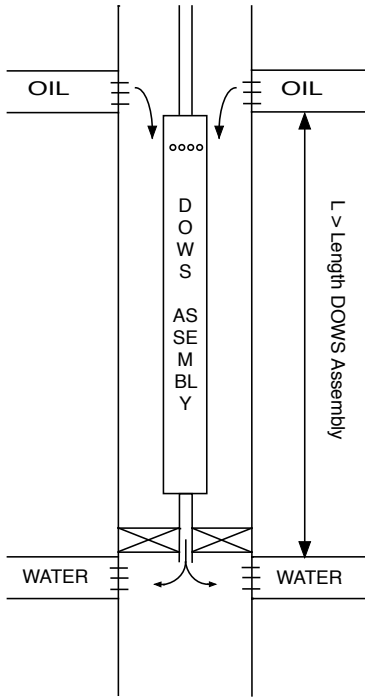
Reservoir configuration 1. Oil reservoir is above water injection zone. The distance between the two zones is larger than the separator assembly.
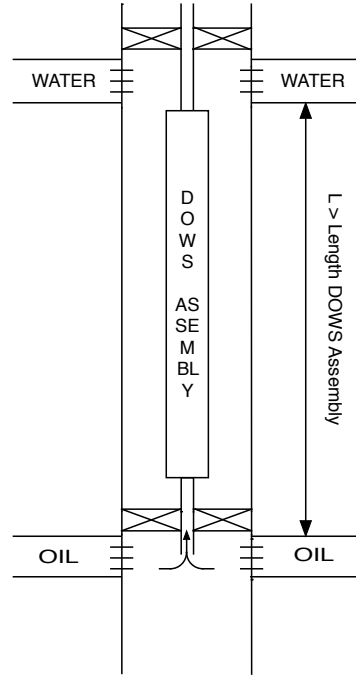
Reservoir configuration 2. Water injection zone above oil reservoir. Distance between both reservoirs is larger than separator assembly.
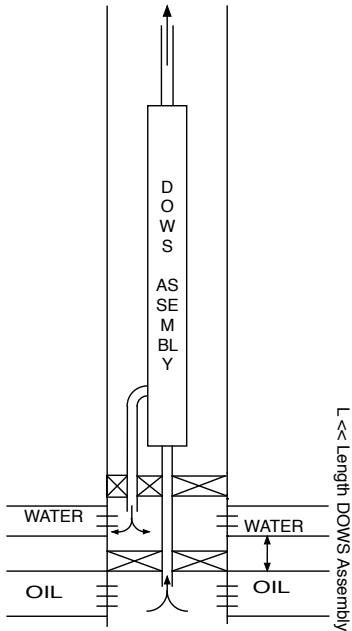
Reservoir configuration 3. Water injection zone is above oil reservoir. Distance between two zones is smaller than separator assembly.
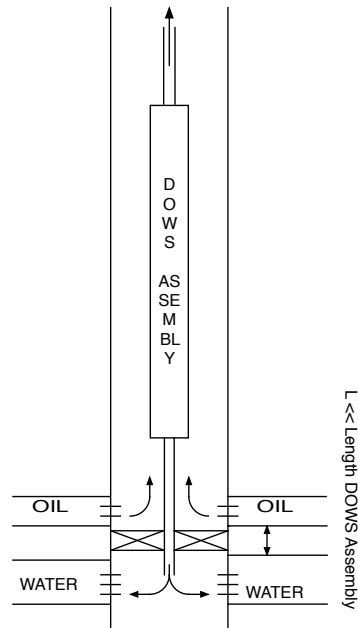
Reservoir configuration 4. Oil reservoir above the water injection zone. Distance between two zones is smaller than separator assembly.

5.2   Downhole separator configuration

The DOWS assembly basically consists of a separator, motor, seal (protects the motor), and a pump. Below four configurations are depicted based on the position of the pump. In this, it is assumed that one motor is providing the drive for the pumps.
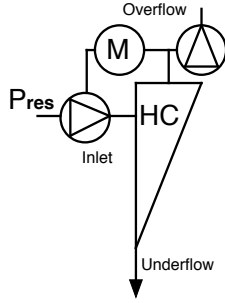
Pump configuration A. The reservoir pressure is not sufficient to provide the underflow with enough pressure to be injected in the reservoir. A second pump must be used boost the overflow, the oil rich stream, to the surface since the oil head in the well is more than the pressure at the overflow. Since the pump upstream of the separator creates severe droplet breakup, a minimum distance of 10 meters [2] is required for the droplets to coalesce. The motor installed will have two drive shafts meaning both pumps will operate on the same frequency and therefore less operating flexibility.
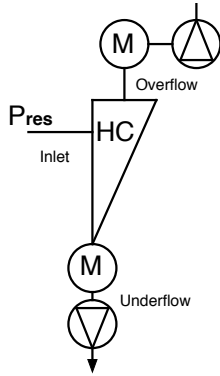
Pump configuration B. The reservoir pressure is sufficient enough to provide the required pressure drop through the multistage separator, however, the pressure at the underflow has decreased such that a pump is required to provide sufficient injection pressure into the reservoir. The advantage is the prevention of droplet breakup at the inlet, but there is a risk of cavitation at the underflow. A second motor needs to be installed to provide the drive for the reversed ESP downstream.
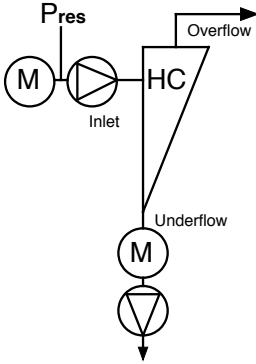
Pump configuration C. In this case the pump at the inlet compensates the pressure-drop over the overflow. This will decrease the complexity and cost of the system but the risk of lowering the efficiency of the separator is increased due to the severe droplet breakup of the pump. If the reservoir pressure is sufficient enough to lift the oil rich stream to the surface, the pressure-drop of the separator may make it practically impossible, than this configuration is suitable to overcome the pressure-drop caused due to the downhole separator. A second motor needs to be installed to provide the drive for the reversed ESP downstream.
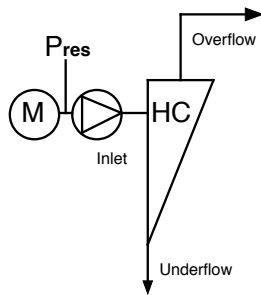
Pump configuration D. This configuration is suitable when sufficient reservoir pressure is available and with some extra pressure, a pump upstream of the separator, it is sufficient to both inject into the reservoir and lift the oil rich stream to the surface (This could be the case with an over pressured zone).

31

5.3   Proposed completion model

Basically the hydrostatic column and the injectivity of the reservoir determine the pump configuration. If the injection zone has a low injectivity, a pump needs to be installed either upstream or downstream the separator. But since the hydrocyclones are very sensitive to small oil droplets, the risk of forming them should be avoided at any cost. The author has therefore decided to position both a pump at the underflow and the overflow outlet of the multistage separator. A two-motor system is applied as there is sufficient space in the wellbore. If one motor would be applied its driveshaft should reach through the separator assembly making the diameter bigger and the design of the separator assembly more complex. Assuming two motors enables greater flexibility in the control of the system.
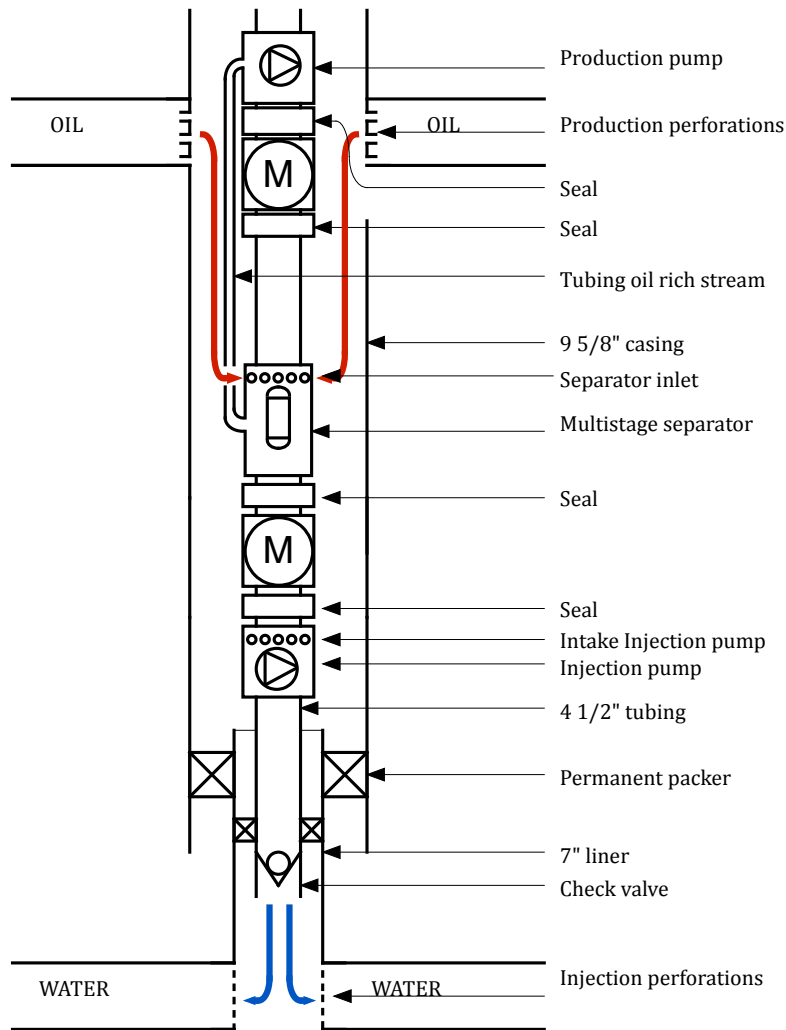
Figure 5.1: Bottom part of completion with oil reservoir on top in combination with push through system

Figure 5.1 shows how the fluid received from the reservoir through the perforations is led directly to the inlet of the separator assembly. The seals, above and below the motor, are there to protect from surrounding fluids. The injection pump pumps the polished water received from the outlet of the multistage separator into the aquifer. The oil rich stream is pumped through production tubing to the surface. A check valve is installed to prevent that fluid returns to the separator. At a certain point in time the well will be filled with

a water column and sand at the bottom of the well. In order to prevent the height of this water column to exceed the inlet of the multistage separator, which would potentially lead to influx of only water, the amount of hydrocyclone liners in the multistage separator should be capable of handling the total fluid influx from the reservoir.

5.4   Pressure balance

The elements that create a pressure- drop in the system are those where the flow is conducted through. More specifically, as can be seen from the design of the separator assembly in figure 5.5, these elements are the hydrocyclones and tubular. Moreover, there is an empirical relationship to be found between the pressure-drop at the underflow and the overflow of the hydrocyclone. This ratio is a characteristic of the type of hydrocyclone and holds that if the overflow is choked at a certain pressure, the pressure at the underflow will automatically become:

$$\Delta P_{under} = \frac{\Delta P_{over}}{PDR} \tag{5.1}$$

where PDR stands for pressure drop ratio, which is a function of the flow. In figure 5.2 this ratio is plotted for two reject rates, 2% and 4%. When the overflow outlet is choked to 2% reject rate, this will evidently create more pressure drop resulting in a lower PDR.
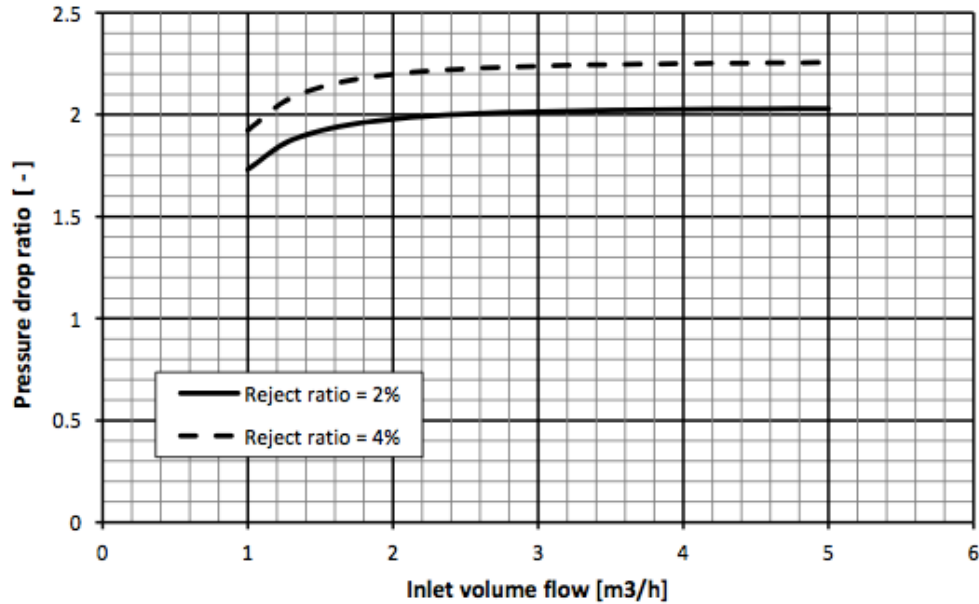
Figure 5.2: Pressure drop ratio as function of flow

The theoretical pressure drop for the whole system can be calculated using the characteristic PDR curves of the used bulk de-oiling hydrocyclone. The problem to be solved lies mainly in the compartments where outlets with different pressures come together. The pressure balance of the whole system is shown in figure 5.3. Based on this configuration the design of the downhole separator assembly can be made.

Figure 5.3: Pressure balance

Taking an inlet pressure (flowing bottomhole pressure) of 140 [bar], the pressure-drop for each cyclone is sequentially calculated resulting in an outlet pressure of 127 [bar]. This flow is injected into an aquifer positioned in a lower reservoir at a higher reservoir pressure by means of an ESP. The stepwise description of figure 5.3:

1. Hydrocarbons are received from the reservoir at the inlet (1) of the de-sander (DS). The lighter components, mainly the oil and water with a small fraction of sand, will be directed from the overflow (3) to the inlet of the second stage (4). A check valve is installed in every flow line to prevent back flow.

2. The heavier components leaving the underflow (2), mainly the sand with a small fraction of oil and water, will be combined with the reject of the second stage (5).

3. In order to prevent back flow from (14) into (5) a nozzle is installed downstream the DS to create the desired pressure drop from 138 [bar] to 132 [bar].

4. The underflow of the second (6) and the third stage (8) is the feed for the third (7) and fourth stage (10) respectively.

5. In order to combine the overflows of the third and fourth stage a jet pump is needed. This is a type of pump that uses the Venturi effect to convert the pressure energy of the motive fluid (9) to velocity energy, which creates a low-pressure zone that draws in and entrains a suction fluid (12) [19]. The working principle of a jet pump and its application for the aforementioned situation will be described in 5.7.

6. The outlet of jet pump (17) will similarly be combined with flow line (15) to a second jet pump (16).

7. From the collection chamber (18) the hydrocarbons will be drawn into an ESP from where it is directed to the surface.

5.5 Volume flux balance

The pressure-drop trough the system is a function of the flow. In order to see how the pressure drop is related for each element, the volume flux balance for the proposed four stage separation system is depicted in figure 5.4.
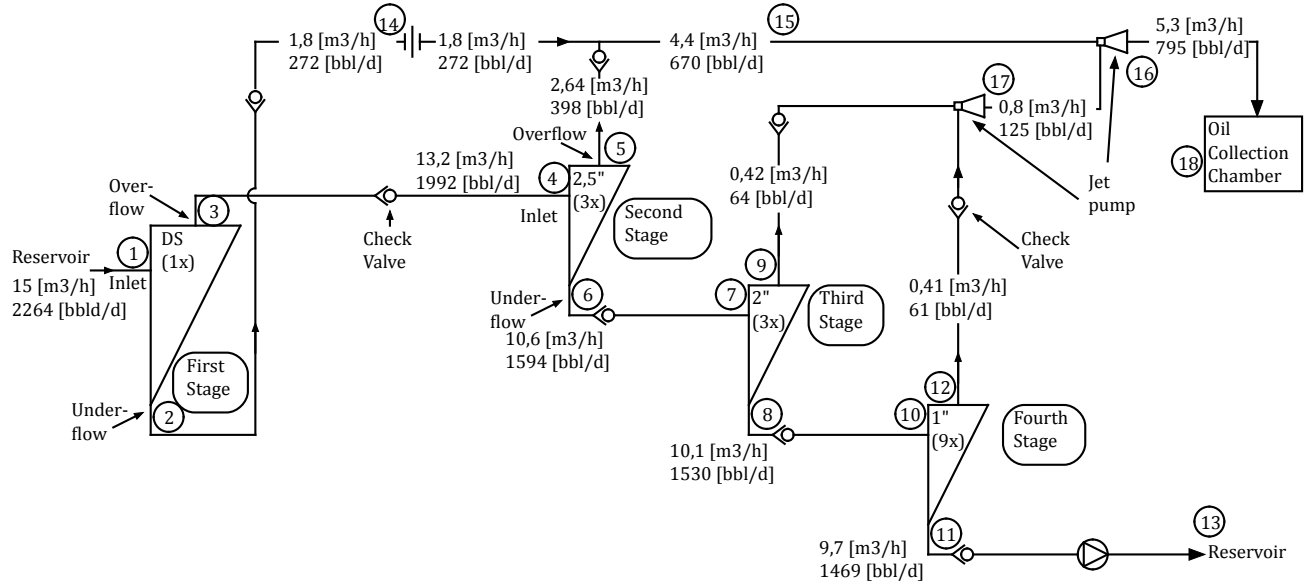
Figure 5.4: Volume flux balance

It can be seen that the flow being injected in the reservoir is about 1470 barrels a day and the flow brought to the surface is about $\pm$ 800 [bbld]. However, it is important to know what portion of this fluid is oil, which can be derived from the formula for efficiency:

$$\eta = 1 - \frac{out}{in} \tag{5.2}$$

This can be seen in table 4.4 and 4.5. As a minimum requirement for the oil industry the oil in water concentration for the discharged water should be no more than 100 ppm OiW, which is the case: 0,01%. Table 5.1 gives the volume flux balance for each stage. It should be noted that no separation is shown, only the volume flux of the oil and water together.

Table 5.1: Pressure and volume flux balance

Pressure Balance			Volume Flux Balance		
First Stage (DS 2")					
Inlet	140	[bar]	Inlet	15	[m^3/h]
Underflow	138,8	[bar]	Underflow	0,6	[m^3/h]
Overflow	138,8	[bar]	Overflow	14,4	[m^3/h]
ΔP_{under}	1,2	[bar]	Reject Rate	4%	
ΔP_{over}	1,2	[bar]	Number of liners	1	
Capacity Liner	25	[m^3/h]			
Second Stage (2,5" bulk de-oiling hydrocyclone)					
Inlet	138,8	[bar]	Inlet	14,4	[m^3/h]
Underflow	136	[bar]	Underflow	11,52	[m^3/h]
Overflow	132	[bar]	Overflow	2,88	[m^3/h]
ΔP_{under}	2,4	[bar]	Reject Rate	20%	
ΔP_{over}	7,1	[bar]	Number of liners	3	
PDR	3	[-]			
Intensity liner	3,84	[m^3/h]			
Third Stage (2" hydrocyclone)					
Inlet	136,44	[bar]	Inlet	11,52	[m^3/h]
Underflow	132,80	[bar]	Underflow	11,06	[m^3/h]
Overflow	128,23	[bar]	Overflow	0,46	[m^3/h]
ΔP_{under}	3,7	[bar]	Reject Rate	4%	
ΔP_{over}	8,2	[bar]	Number of liners	3	
PDR	2	[-]			
Intensity liner	3,84	[m^3/h]			
Fourth Stage (1" hydrocyclone)					
Inlet	132,79	[bar]	Inlet	11,06	[m^3/h]
Underflow	125,85	[bar]	Underflow	10,62	[m^3/h]
Overflow	117,45	[bar]	Overflow	0,44	[m^3/h]
dP_{under}	6,9	[bar]	Reject Rate	4%	
dP_{over}	15,3	[bar]	Number of liners	9	
PDR	2	[-]			
Intensity liner	1,23	[m^3/h]			

5.6 Separator design

Figure 5.5 (left assembly) refers to the embodiment of a fluid separation system installed within a wellbore. In the configuration shown the production formation is above the discharge formation. A wellbore casing is installed including a set of perforations to permit fluid transfer from/to the formations. This is not shown in the figure. Figure 5.5 (left assembly) illustrates a tubular housing **25** with its central opening at **1** through which the wellbore fluids enter and a lower opening **26** through which the discharged water exits to the injection pump. Disposed within the housing **25** are multiple hydrocyclones **27**, **28**, **29** in a generally longitudinal aligned relationship. The orientation of the hydrocyclones **27**, **28**, **29** is not considered important for functionality reasons, but is important for fitting the appropriate sized hydrocyclones and associated plumbing within the confines of the housing **25**. The wellbore fluids enter **1** from where it is directed to a tangential inlet opening **2** of the de-sanding cyclone **3**. Due to their tangential velocity the first separation step occurs and the first stream, being higher density fluids (primarily sand with small fraction of oil and sand), exits the de-sanding cyclone **3** through outlet **5** and conveys the collected stream to conduit **18**. An important feature of this embodiment is that the separated first stream, being primarily sand, does not need to be transported through a separate conduit to a remote location in the wellbore, but introduced with the rejects **7** of the bulk de-oiling hydrocyclones **27** to be transported to the surface. The second stream, being primarily oil and water, exits the de-sanding cyclone **3** through conduit **4** and conveys the collected second stream to the inlet holes **8**. Subsequently this fluid enters the first liquid-liquid separation stage through inlet ports **8** where they receive their tangential velocity. The fluid is separated into a first light stream, being primarily oil, and second dense stream, which is primarily water. This first stream exits the bulk de-oiling hydrocyclone **27** through **7** and is mixed with the sand from the de-sanding cyclone **3** into conduit **18** from where it flows to the second jet pump **20**. The second stream leaves **27** trough outlets **9** into the second inlet chamber **10**. Again this fluid receives a tangential velocity at the inlet ports **11**, after which being separated into a first light stream **26** and a second dense stream **13**, being primarily oil and water respectively. The first stream leaves the rejects of the three hydrocyclones **28** from where it is conveyed to reject chamber **12** after which it is directed to the first liquid jet pump **17**. This is another important feature of this embodiment where two fluid streams with a high and low pressure, **12** (motive liquid) and **23** (suction liquid) respectively, are mixed together into **24** whereby back-flow into the lower pressure conduit is prevented. The second dense stream **13** is directed to the inlet ports **14** of hydrocyclones **29** where it receives its tangential velocity. Again the separation process takes place inside the hydrocyclone **29** where the last bit of oil is separated out of the water and is led trough the reject **15** to the liquid jet pump **17**. The mixed liquid at the outlet of jet pumps **17** is conveyed through conduits **24** to jet pump **20**. The motive fluid in conduit **18** creates suction in jet pump **20** entraining the liquid in both conduits **17**. This leads to one single conduit from where the fluids are drawn into the ESP (not shown in this figure) through conduit **21**. Chamber **30** function is to allow repositioning of outlet **21** to a desired place for connecting to the PCP.

Figure 5.5 illustrates an alternate embodiment (right assembly) of the fluid separation system **25** wherein multiple hydrocyclones **27**, **28**, **29** are placed in a generally longitudinal aligned relationship. This alternate embodiment differs slightly from the prior design such that hydrocyclones **27** and **28** are directly connected in series. This means that the total outlet flow **9** (being primarily water) of bulk de-oiling hydrocyclones **27** will be directly forwarded to the inlet of hydrocyclone **11**. The advantage of such a system is the assembly and de-assembly of the parts since only a single tubular piece **30** needs to be replaced.

In addition, for the sake of clarity, 3D figures are shown to give a better view of the important features of the 2D downhole fluid separation system. Even though a 2D drawing could be as precise, it cannot reveal the actual configuration of the hydrocyclones.
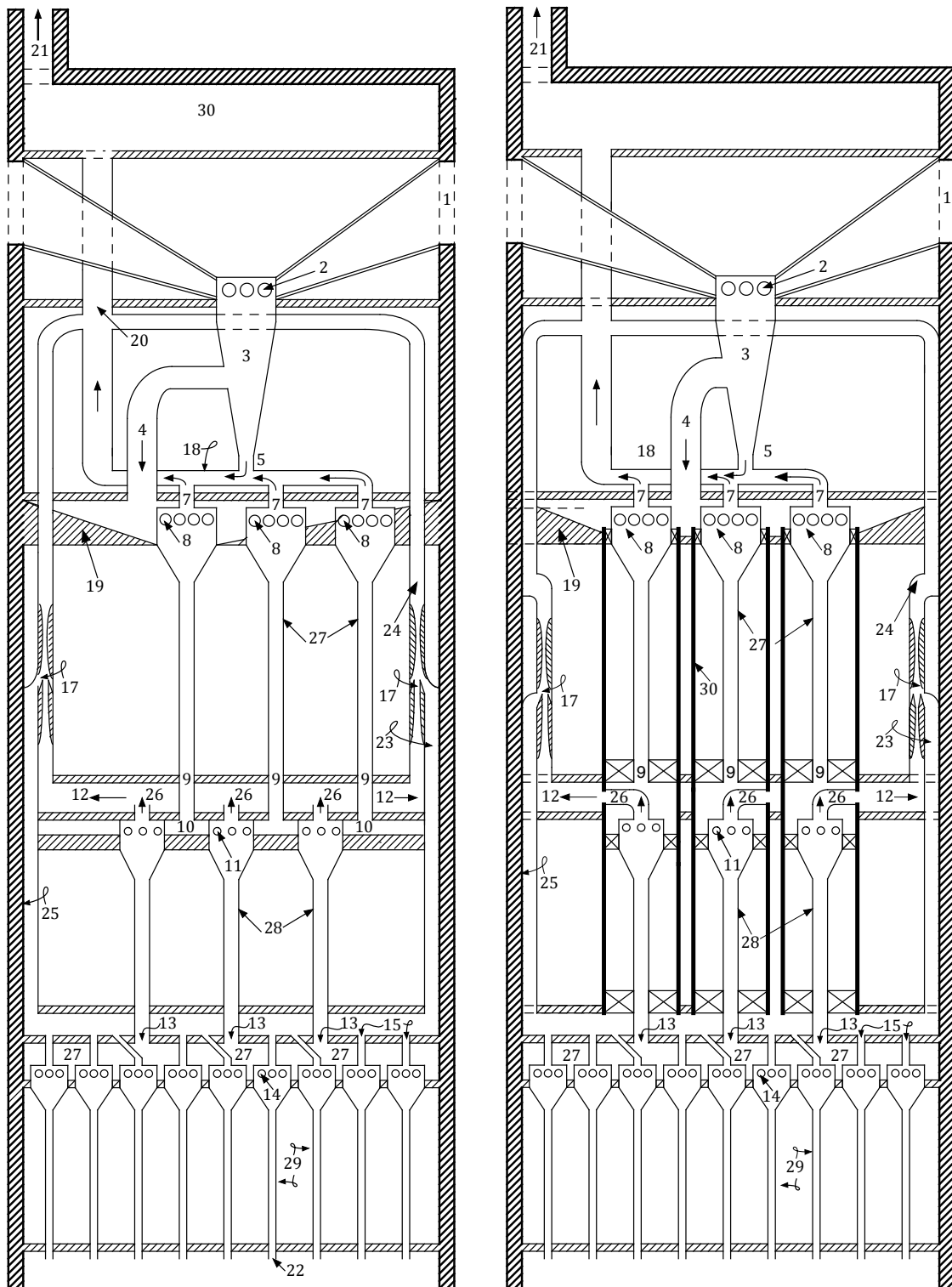
Figure 5.5: Vertical elevational view of the fluid separation system
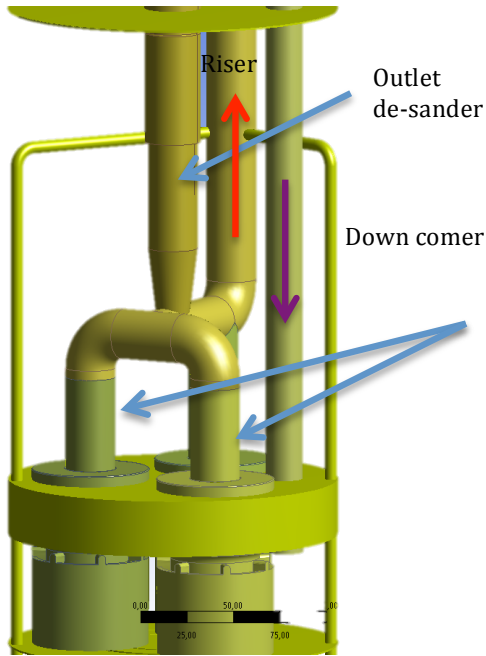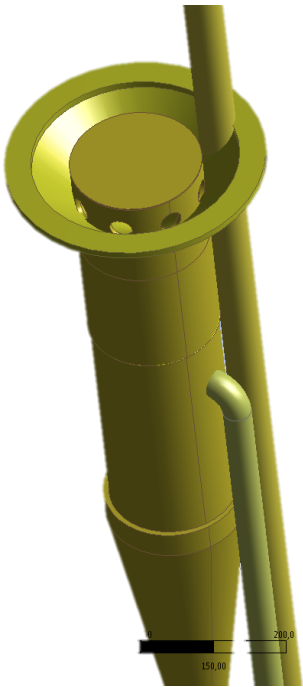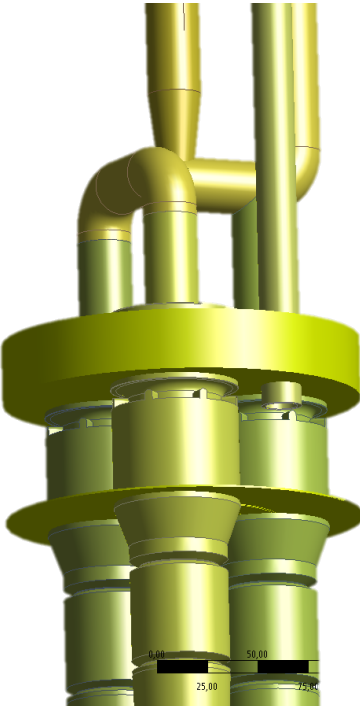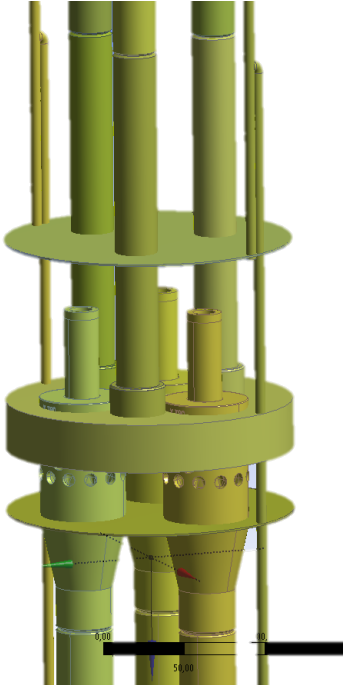
Rejects bulk de-oiling hydrocyclones with outlet de-sander	Inlet chamber de-sanding cyclone with downcomer and riser
Inlet chamber 2,5" bulk de-oiling hydrocyclones	Configuration 2nd and 3rd stage hydrocyclones

Table 5.2: 3D DOWS configuration
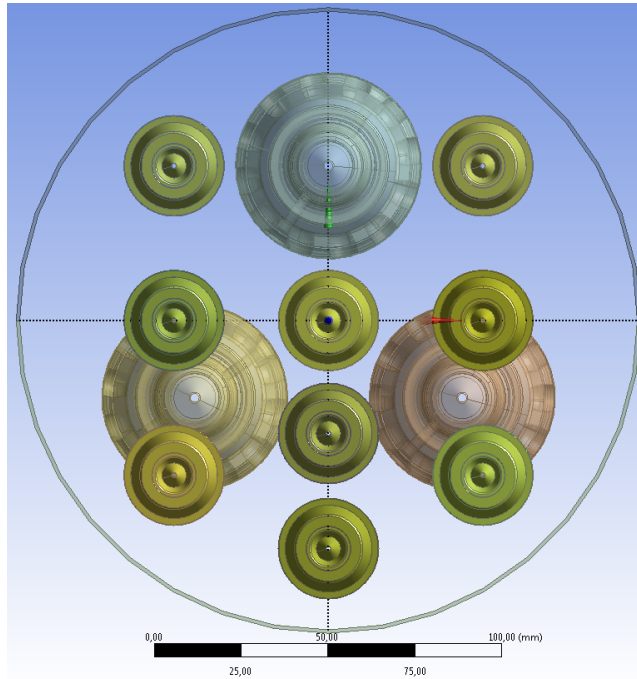
Figure 5.6: Configuration 1" and 2" liners - Bottomview
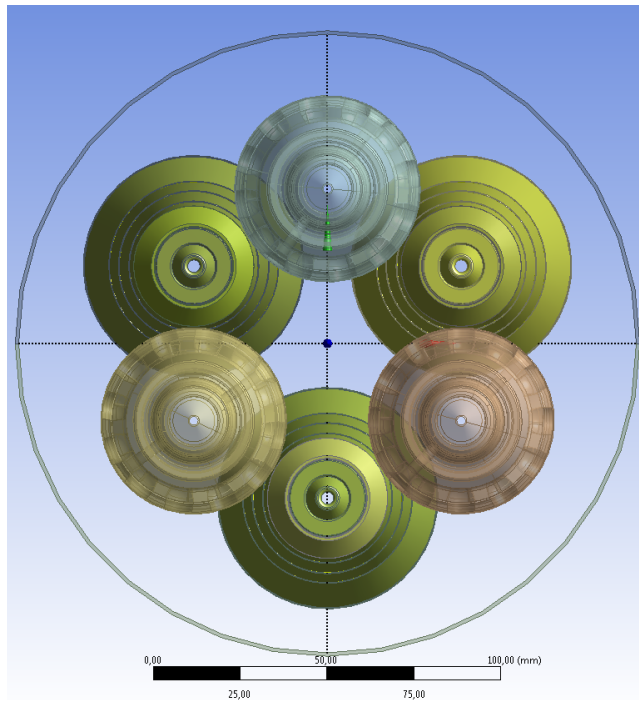
Figure 5.7: Configuration 2" and 2,5" liners - Bottomview

5.7 Jet pump

A jet pump converts highly pressurized power fluid to kinetic energy through the nozzle. This creates a suction effect, which drives the production fluid through the pump. At the diffuser the velocity head is converted into pressure, allowing the production fluid to flow to the surface through the return conduit [24]. A liquid M_0 is sucked in the jet pump by means of a motive liquid M_1 and mixed to liquid $\dot{M}$.

1 - Jet pump
2 - Pressure gauge
3 - Motive inlet
4 - Suction inlet
5 - Outlet
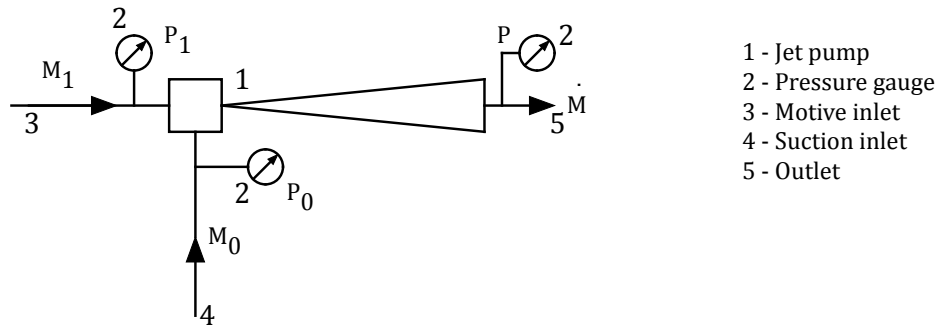
Figure 5.8: PFD jet pump

All jet pumps have three common features: inlet, suction and discharge. The figure below gives a more detailed view of how such a jet pump functions.
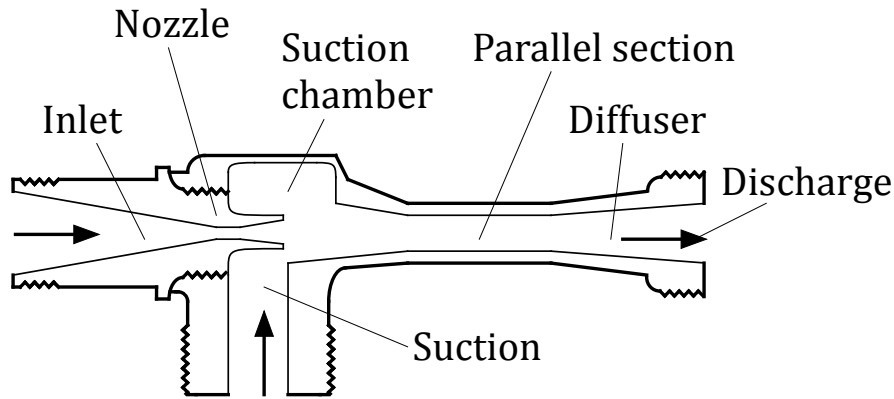
Figure 5.9: Typical layout jet pump

Inlet - the operating medium, in this case being the water and oil mixture, enters the inlet under pressure and travels through the nozzle to the suction chamber. The nozzle converts the pressure of the operating medium into a high velocity stream.

Suction - due to the high velocity stream emerging from the nozzle, the pressure in the suction chamber is lowered. This evidently results in a pumping action where after the fluid is caused to flow to the discharge.

Discharge - from the suction chamber, the fluid acquires a part of its energy back in the parallel section. In the diffuser part of the velocity of the mixture is converted to a pressure greater than the suction pressure but lower than the inlet pressure.

An important aspect of the pump is that there are no moving parts, it only consists of two major components: the nozzle and the body.

In this scenario the two inlet conditions are readily set, meaning the flow and pressure are known. Therefore it is important to investigate whether a jet pump is a solution to be implemented in the downhole separator system. Based on a performance chart provided by the company named "GEA Wiegand" [24] this can be easily investigated.

Below is a stepwise description of the performance calculation to investigate whether a jet pump can be used for this application.

1. Calculate density ratio between motive and suction fluid.

$$\varepsilon = \frac{\rho_1}{\rho_0} = \frac{950}{950} = 1 \tag{5.3}$$

Looking at figure 5.5, flow in the conduits **23** and **12** have approximately the same density. With a small fraction of oil in water, it will be assumed that the mixture density will be just a bit lower than that of water.

2. Calculate mass flow ratio between motive and suction fluid.

$$\mu = \frac{M_1}{M_0} = \frac{Q_1}{Q_0} \times \frac{\rho_1}{\rho_0} = \frac{0,46 \times 950}{0,44 \times 950} = 1,05 \tag{5.4}$$

with Q being the volumetric flow rate [m³/h] and ρ being the density [kg/m³].

3. Read the permissible pressure ratio difference from the graph [24].
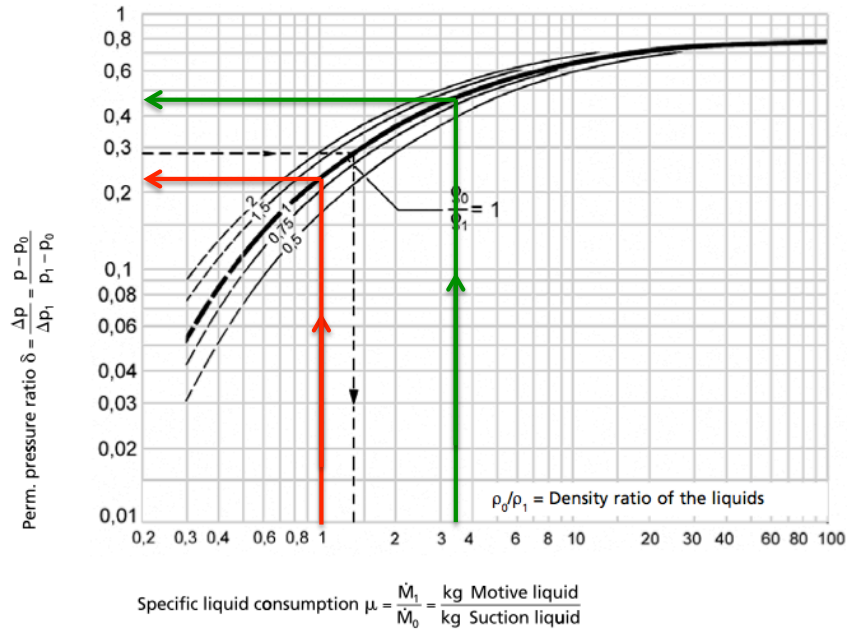
Figure 5.10: Pressure ratio vs. mass flow ratio

For a density ratio of 1 and mass flow ratio of 1,05, it can be read that a pressure ratio of 0,22 can be obtained (red line). Based on this the pressure of the mixed liquid $\dot{M}$ can be determined.

4. Calculate pressure mixed liquid P.

   Equation (5.5) gives the ratio between total delivery pressure in [barg] and the effective motive liquid. Having the pressure at the motive and suction inlet, P_1 and P_0 respectively, the mixed liquid pressure P can be obtained. The pressure can be either obtained from figure 5.3 or table 5.1.

$$\delta = \frac{\Delta P}{\Delta P_1} = \frac{P - P_0}{P_1 - P_0} = \frac{P - 120}{129 - 120} = 0,22 \tag{5.5}$$

$$P = \delta * (P_1 - P_0) + P_0 = 122[bar] \tag{5.6}$$

5. Sizing liquid jet pump.

   The size of the liquid jet pump is basically determined by the mixed mass flow.

$$\dot{M} = \dot{M_1} + \dot{M_0} = 401 + 385 = 786[\frac{kg}{h}] \tag{5.7}$$

This results in a jet pump with the following dimensions:

Table 5.3: Max. mixed flow, connections, dimensions and weights

Size		3"	5"	7"
Maximum mixed flow [kg/h]		1200	3500	6000
Dimensions [mm]	a	153	270	350
	b	42	60	65
	c	111	210	285
	d	80	85	100
Weight [kg]		5	10	13
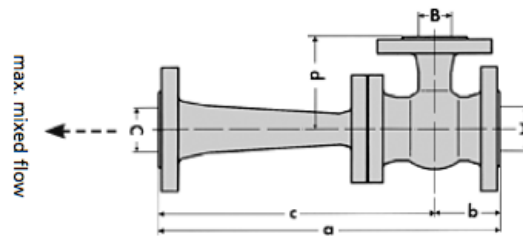
Figure 5.11: Dimensions jet pump

6. Pump size 3" is most suitable

Based on the above, the performance of the jet pump **20** can be calculated:

1. Calculate density ratio between motive and suction fluid.

$$\varepsilon = \frac{\rho_1}{\rho_0} = \frac{950}{950} = 1 \tag{5.8}$$

2. Calculate mass flow ratio between motive and suction fluid.

$$\mu = \frac{M_1}{M_0} = \frac{Q_1}{Q_0} \times \frac{\rho_1}{\rho_0} = \frac{4,4 \times 950}{0,8 \times 950} = 5,5 \tag{5.9}$$

3. Read the permissible pressure ratio difference from figure 5.10; a permissible pressure ratio of 0,55 can be found.

4. Calculate pressure mixed liquid P

$$P = \delta * (P_1 - P_0) + P_0 = 0,55 * (132 - 122) + 122 = 127,5[bar] \tag{5.10}$$

5. Sizing liquid jet pump

$$\dot{M} = M_1 + M_0 = 4218 + 787 = 5005[\frac{kg}{h}] \tag{5.11}$$

6. Pump size 7" is most suitable

Chapter 6

CFD modeling of the multistage separator

The total system will be divided in several subsystems to handle the complexity. The separation performance of the hydrocyclones will not be considered since CFD has a weak predicting-power[1]. However since hydrocyclones are placed in the system and therefore act as a resistance, their behavior with respect to pressure-drop will be mimicked as porous zones with a Venturi model. The following subsystems are analyzed:

Subsystem 1 - Pressure-drop mimicking of an hydrocyclone with Venturi model
Subsystem 2 - Coupling of the bulk de-oiling hydrocyclone Venturi model- and de-sander to riser
Subsystem 3 - Erosion analysis

6.1 Theory

Below is given the brief concepts in CFD simulations. Every fluid flow involves mass, energy and momentum conservation. Consequently, the continuity, the energy and the momentum equations are crucial in a CFD simulation.

6.1.1 Modelling Structure

CFD involves a number of aspects of modeling fluid flow, like creating the geometry, generating a mesh, defining boundaries, and then solving the model and finally post-processing. ANSYS is the name of a software in which numerical element methods can be solved. Within ANSYS several sub-packages are available, like DesignModeler where the geometry is made and Fluent where fluid flow can be modelled. Figure 6.1 shows the schematic CFD modeling structure. The first three steps shown in Figure 6.1 are called pre-processing.

---

[1]Theoretically this is due to the limits of computing power and hardware capacity.
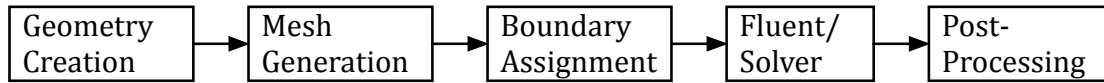
Figure 6.1: The steps that we need to undertake for the modeling of the DOWS in ANSYS CFD

Once the numerical model is set up, the solution is monitored and finally the results are examined to consider revision of the model if needed. Creation of a hydrocyclone model consists of a set of integrated cylindrical and conical sections for Fluent analysis [27].

6.1.2 Mesh Generation

After the geometry is created, the next step is to assign it with a mesh. Mesh generation is one of the most critical aspects of finite volume analysis[2]. This process subdivides the volume containing the fluid by a finite numbers of discrete cells. Too many cells may result in very long solver runs, and too few may lead to inaccurate results.

6.1.3 Fluent Model Solver

The following paragraphs will deal with assigning the physical model, flow regimes, materials and boundary conditions such as the inlet and outlet velocity and pressure conditions. Their setup corresponds with the steps that are needed to accomplish a running model, however the description will be limited to the numerical analysis aspects only. The mathematical instruments used in ANSYS Fluent to solve numerical equations are (explained in 6.1.4) segregated solver and coupled solver.

Both numerical methods use the Finite Volume Method (FVM), but their approach is different. This holds that the domain is divided into cells using a computational grid. Then the governing equations of the individual control volumes are integrated to construct algebraic equations for unknown parameters such as velocity and pressure. Linearization of the discretized equations and solutions of the resultant linear equation system to yield updated values of the dependent variables.

6.1.4 Solution Methods

Segregated Solution Method
Using this approach, the governing equations are solved sequentially (i.e., segregated from one each other). Because the governing equations are non-linear (and coupled), several iterations of the solution loop must be performed before a converged solution is obtained.

Coupled Solution Method
In contrast with the segregated solver, the coupled method solves the governing equations of continuity, momentum and energy transport simultaneously. However, in this study, the first method will be used leading to lower usage in CPU and faster (2x) convergence due to less complicated physical conditions. However, the results with a coupled solution are more accurate [27].

---

[2]The finite volume method is a discretization method which is well suited for the numerical simulation of various types (elliptic, parabolic or hyperbolic, for instance) of conservation laws; it has been extensively used in several engineering fields, such as fluid mechanics, heat and mass transfer or petroleum engineering. The equations are solved over a number of discrete volumes. FVM reforms the partial differential equations (mostly Navier-Stokes equations) in a conservative form after which the new equations are made. This way the conservation of fluxes happens through a control volume [16]

6.1.5 Models

Since no separation efficiency of the hydrocyclone itself will be investigated, it suffices to use single-phase flow. Fluent provides several models for multiphase flow and turbulent flow. For the latter, single-phase models such as $k - \varepsilon$ or Reynolds Stress Model (RSM) are used to model turbulence. When modeling multiphase flow additional terms will account for the secondary phase. If the phases are separated and the density ratio is of order 1 or if the particle volume fraction is low ($<10\%$), then a single-phase model can be used to represent the mixture.

6.1.6 Materials

Fluid properties of water are defined and the model is setup with physical properties in trials relevant to the scope of the problem.

Material	Density [kg/m^3]	Viscosity [kg/ms]
H$_2$O	998,2	0,001003

Table 6.1: Single phase fluid properties

6.1.7 Boundary Conditions

The parameters regarding the boundary conditions in this thesis are defined in terms of mass flow rate, volume fraction, velocity or pressure depending on the geometry and purpose. Since this part of the simulation can have significant impact on the result, it is of importance that the boundaries are correct and not poorly defined.

To avoid runoff error, Fluent will subtract atmospheric pressure from the absolute pressure resulting in the gauge pressure. All pressures computed in Fluent are gauge pressures. This relationship can be seen below:

$$P_{abs} = P_{gauge} + P_{atm} \tag{6.1}$$

Figure 6.2 depicts equation (6.1) better (absolute pressure is taken arbitrary):
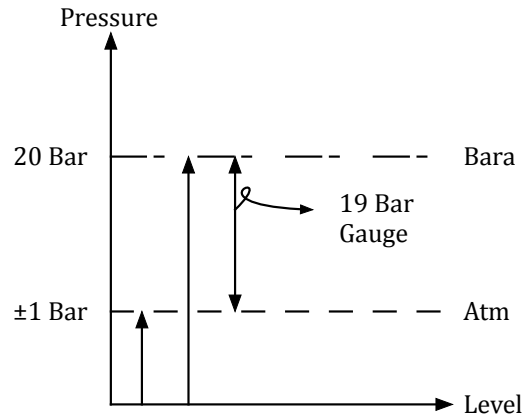
Figure 6.2: Gauge and atmospheric pressure

47

6.2 Experimental CFD setup

Two components of the downhole separator will be analyzed being the pressure balance between the rejects of the 1st and 2nd stage and the erosion rate. To build the first component in CFD, a preceding model will be build to mimic the pressure drop of the bulk de-oiling cyclones. This will then be coupled with the de-sander and the conduit leading to the riser. For the second component the erosion rate at the outlet of the de-sander is analyzed. The outlet is choked with a flow reducer leading to a narrowing of the tube diameter.

6.2.1 Subsystem 1 - Venturi model

1. Objective

A model is proposed with a Venturi geometry to describe the pressure drop/low pressure region for the Ascom hydrocyclone. This will then be implemented as a resistor in the total system. Due to an increase of the velocity in the narrow throat the pressure will significantly drop creating the same effect as in a hydrocyclone. In this manner the Venturi can be implemented as a resistance to pressure.

2. Simulation setup

The Venturi model consists of two thin membranes with known velocity characteristics, which are calculated with Excel. The aim is to derive a formula that describes the pressure drop in the throat of the Venturi with the addition of two porous jump coefficients C_1 and C_4 (thin membranes) to correct the PDR of the hydrocyclones. This idea is illustrated in figure 6.3. The reason for the Venturi geometry is because of the reduction in fluid pressure that results when fluid flows through a constricted pipe. A fluid's velocity must increase as it passes through a constriction in accordance with the principle of continuity, while its static pressure must decrease. This physical phenomenon is used to describe the pressure in a hydrocyclone since a pressure-drop occurs from the inlet $\rightarrow$ underflow and inlet $\rightarrow$ overflow. The derivation of the set of equations can be found in Appendix E.
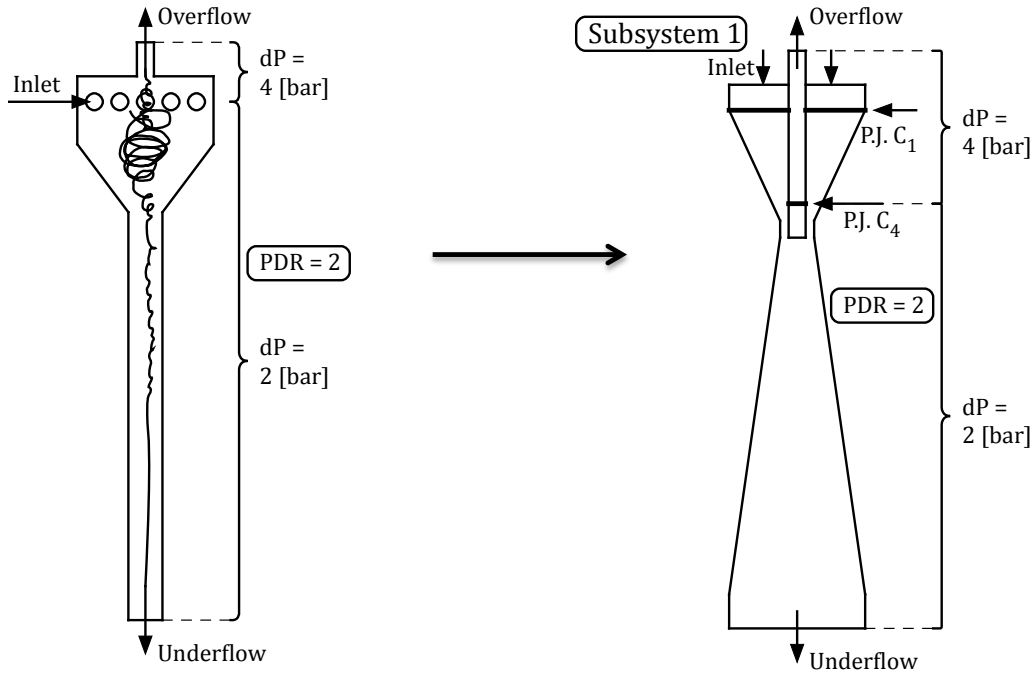
Figure 6.3: Hydrocyclone and Venturi pressure-drop model

The aim is to find the values of coefficient C_1 and C_4 such that the pressure-drop curve of the Venturi model fits the pressure-drop curve of the hydrocyclone. Since the downhole separator includes three types of hydrocyclones, each of them will be described with a Venturi model. Their diameter is scaled based on the hydrocyclone model. In the Excel fit, the diameters D_1, D_3 and D_4 are set as parameters meaning they can be adjusted to obtain the best fit. The final geometry can be seen in figure 6.4. The conduit in the centre is to convey the fluid from the constriction to the overflow outlet. It is placed such that it can benefit from the low-pressure region and with an extra porous jump C_4 the PDR can be reached. The length of the Venturi model is set at 1000 [mm], which is of the same order as the hydrocyclone. Fluent gives the following equation for a thin porous medium (porous jump) over which the pressure is defined, which is a combination of Darcy's law and an additional inertial loss term:

$$\Delta P = \left(\frac{\mu}{\alpha} v + C_2 \frac{1}{2} \rho v^2 \right) \Delta m \tag{6.2}$$

where μ is the laminar fluid viscosity, α is the permeability of the medium, C_2 is the pressure-jump coefficient, v is the velocity normal to the porous face, and Δm is the thickness of the medium [27]. By setting the permeability very high, e.g. 1e+20, the effect of turbulence will be neglected. The thickness of the medium will be set to 1.

The equation for the pressure drop from inlet to the underflow:

$$\Delta P_{P.J.1} = C_1 v_1^2 \tag{6.3}$$

And the equation for the porous jump at the overflow:

$$\Delta P_{P.J.4} = C_4 v_4^2 \tag{6.4}$$

Equating (6.2) with (6.3) & (6.4) yields for the Fluent C_2 coefficient:

$$C_2 \frac{1}{2} \rho v^2 = C_1 v_1^2 \iff C_{2;1} = \frac{2 C_1}{\rho} \tag{6.5}$$

$$C_2 \frac{1}{2} \rho v^2 = C_1 v_1^2 \iff C_{2;4} = \frac{2 C_4}{\rho} \tag{6.6}$$
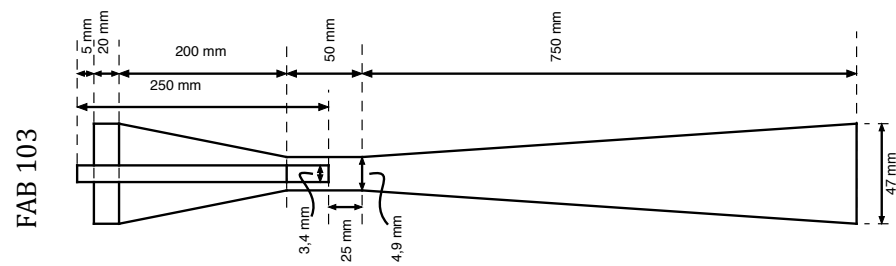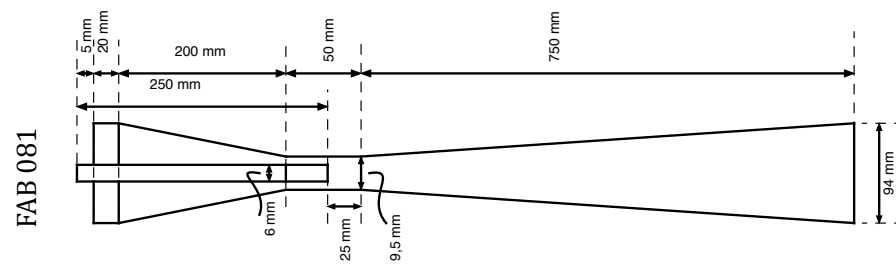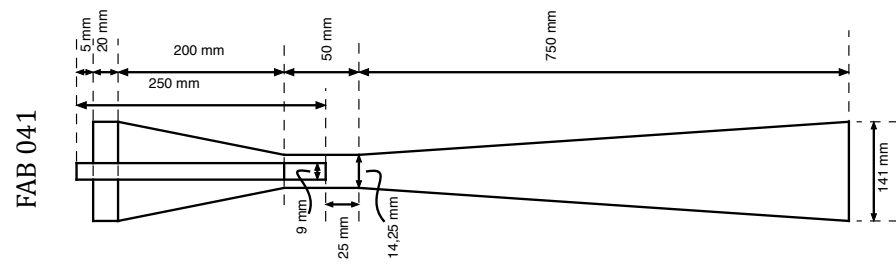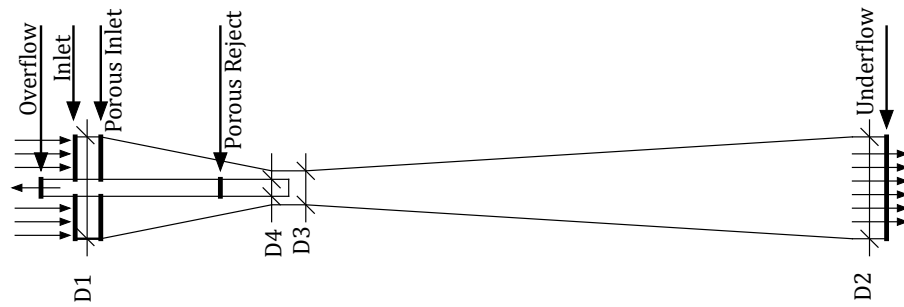
Figure 6.4: Dimensions of the three hydrocyclone Venturi models

3. Boundary Conditions

Once the porous jump coefficients C_1 and C_4 are found with the Excel fit, the Venturi model is designed in CFD and is built step by step to meet the correct pressure-drop curve.

In order to get the Venturi model running correctly, as described above, a first simulation will be performed to verify its performance. For the verification of the CFD Venturi model, its results are compared with an online JAVA applet [29]. Next a reject tube will be added, still without any porous jump values. Finally the second model will be added with the porous jump values.

1. Boundary conditions Venturi without reject tube and porous jump:

    (a) Inlet: Velocity Inlet

    (b) Underflow: Outflow

    (c) Overflow: -

2. Boundary conditions Venturi with reject tube, without porous jump:

    (a) Inlet: Velocity Inlet

    (b) Underflow: Outflow

    (c) Overflow: Outflow

3. Venturi with reject tube, with porous jump

    (a) Inlet: Velocity Inlet

    (b) Underflow: Outflow

    (c) Overflow: Outflow
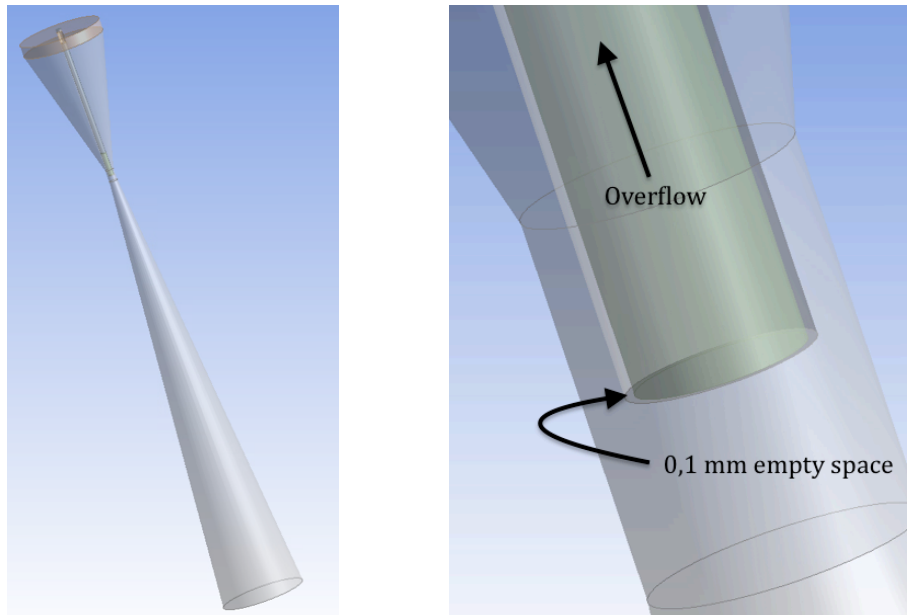
Figure 6.5: 3-D CFD Venturi Model

The 0,1 [mm] empty space is needed to function as a wall otherwise the two fluid components will interact with each other.
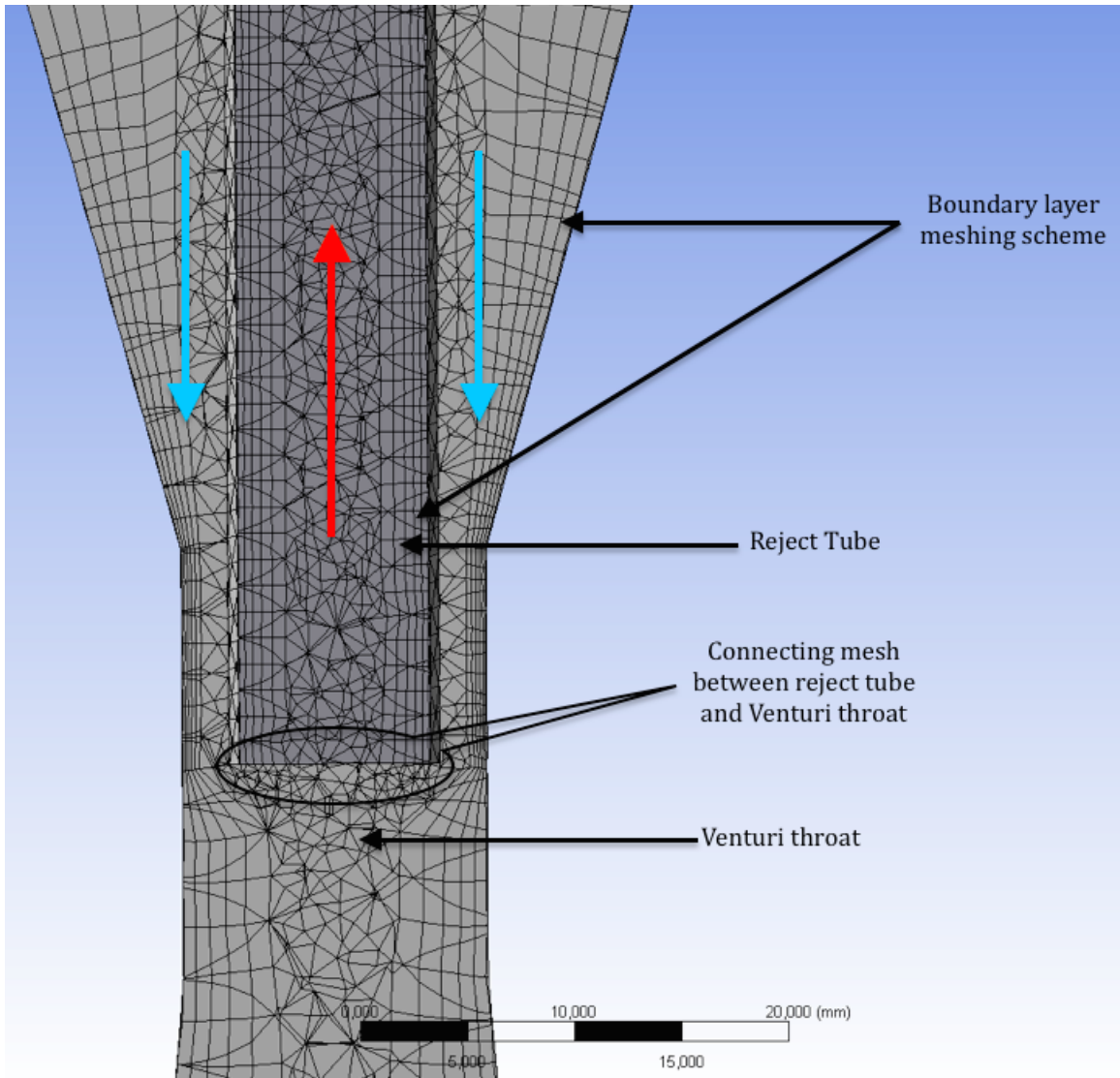
Figure 6.6: Meshed Venturi geometry

Boundary layer meshing scheme was used in the vicinity of the wall due to the uniformity of the flow in that region. Since the core of the geometry is turbulent, the grid size in this region is relatively coarse. The red and blue arrows indicate the flow direction. The meshed Venturi is shown in figure 6.6.

6.2.2 Subsystem 2 - Pressure balance rejects 1st and 2nd stage

1. Objective

The aim is to determine any back-flow of the slurry outlet **5** of the de-sander **1** into the overflow of the 2"
bulk de-oiling hydrocyclone **3**, figure 5.5. The outlet of the de-sander enters conduit **6** at a pressure of 138
[bar] and the outlet **3** of the bulk cyclone at 132 [bar]. Therefore a reducer will be placed at the slurry outlet
of the de-sander for flow assurance.

2. Simulation setup

With no pump installed at the riser, see figures 6.10 & 6.11, the reject fluid from the de-sander will flow
directly into the reject of the bulk de-oiling cyclone. This is due to the pressure difference of 138 [bar] vs.
132 [bar]. In order to find out how much this is, the pressure difference between the inlet and the overflow
of the bulk de-oiling cyclone will be set to zero, $\Delta P_{Over} = 0$. From the pressure-drop curve in figure 6.7
the reject rate curve in figure 6.8 can be constructed, by simply taking the pressure drop for different reject
rates at a fixed flow rate.
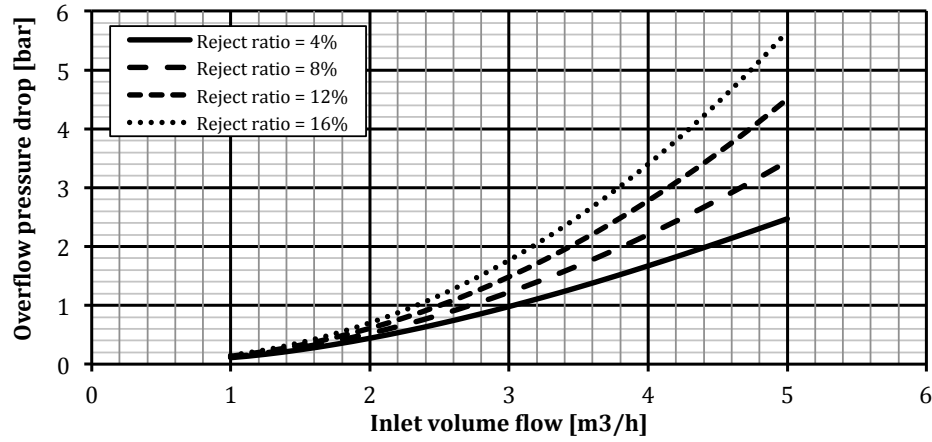
Figure 6.7: Overflow pressure-drop curve bulk de-oiling hydrocyclone
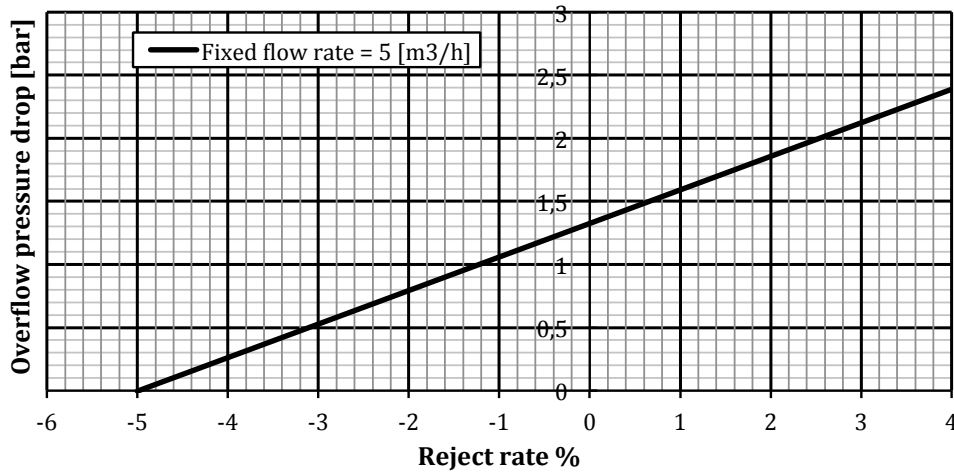
Figure 6.8: Reject rate curve bulk de-oiling hydrocyclone

This yields that there is a negative overflow rate of (-)5%, meaning that the fluid flow is backward into the bulk cyclone. In order to get fluid through the overflow of the bulk cyclone, $P_{BC;R} < P_{BC;In}$ and therefore $P_{DS;R} < P_{BC;In}$. To achieve this, a reducer will be placed at the reject of the de-sander (due to its higher erosion tolerance in comparison with an orifice or nozzle).

1. Since the DPR of the de-sander is practically 1, this gives:

$$P_{DS;R} = P_{DS;Out} \tag{6.7}$$

2. Outlet of the de-sander is the feed for the bulk cyclone:

$$P_{DS;Out} = P_{BC;In} \tag{6.8}$$

3. Since $dP_{BC;Over} = 0$:

$$P_{BC;In} = P_{BC;R} \tag{6.9}$$

4. And since (6.7) is equal to (6.8):

$$P_{BC;In} = P_{DS;R} \tag{6.10}$$

Although a pump is installed at the riser to create the suction from the rejects of the de-sander and the bulk cyclone, it is important that the DPR of the bulk de-oiling cyclone is maintained to achieve fluid through the overflow. When the reducer is eliminated in the system, the bulk cyclone cannot produce any reject. Figure 6.9 illustrates the situation without constriction where the fluid is flowing back into the bulk de-oiling cyclone. The sizing and erosion analysis of the reducer is performed in 6.2.3.
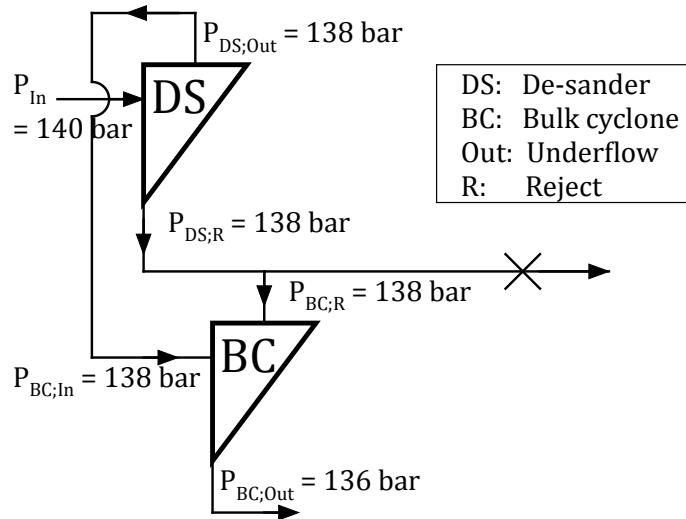
Figure 6.9: Pressure Balance de-sander & bulk de-oiling hydrocyclone

3. Boundary conditions

Some minor changes should be applied to the above Venturi model. When imposing a flow fraction (outflow) on both outlets as a boundary condition, Fluent gives as output the outlet pressures. When using the Venturi in a system, it is not possible to set the outlets to outflow. Moreover, in practice the pressure is regulated in order to control the flow. Therefore the same constraints will be imposed on the CFD model. Since the pressures are known at the different outlets, Fluent will give as output the volume flow rate. No boundary constraints will be imposed at the reject, only the porous jump value. By setting the other boundary conditions as below, it will be determined whether the bulk de-oiling cyclone Venturi can produce any reject. The second step is to determine how the pump inlet pressure influences the PDR of the bulk de-oiling hydrocyclone Venturi. In practice, when controlling the hydrocyclones downhole it is difficult to regulate the fluid flows at both outlets. A pressure inlet is imposed at the de-sander slurry outlet, and a pressure outlet is imposed at the underflow outlet of the CFD Venturi bulk de-oiling cyclone. We will then calculate the pressure at the overflow of the Venturi. The pressure at the outlet of the riser will be varied to investigate the relation between the PDR and pump inlet pressure. Figure 6.10 shows how the physical model is translated to a CFD model. An important aspect is that the de-sander outlet-tube is eliminated and its flow is directly imposed on the Venturi model. Figures 6.11 and 6.12 show the 3D mesh design before importing to Ansys Fluent.
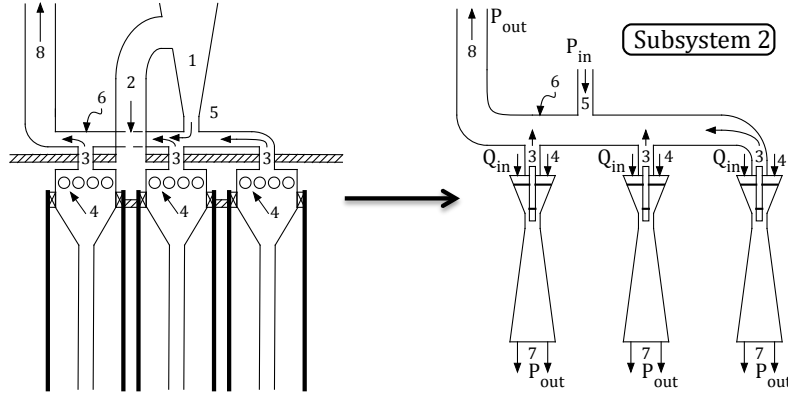
Figure 6.10: Translation schematic model to CFD model.

Table 6.2: Boundary conditions subsystem 2.

B.C.	Element	Type	Value	Unit
BC 3	Venturi Overflow	Interior	[-]	[-]
BC 4	Venturi Inlet (3x)	Mass flow inlet	1,2	[kg/s]
BC 5	De-sander outlet	Pressure inlet	Varying	[Pa]
BC 6	Conduit	Wall	[-]	[-]
BC 7	Venturi Underflow	Pressure outlet	136e+5	[Pa]
BC 8	Riser outlet	Pressure outlet	Varying	[Pa]
P.J.1	Porous Jump	$C_{2;1}$	64000	[1/m]
P.J.4	Porous Jump	$C_{2;4}$	10	[1/m]
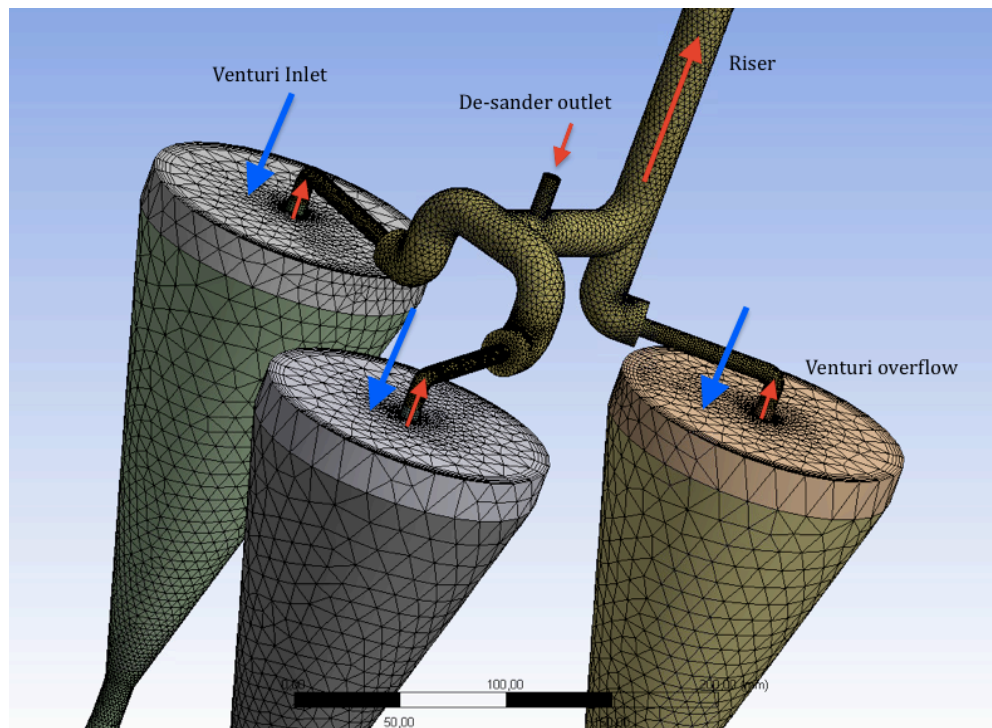
Figure 6.11: 3d CFD model.
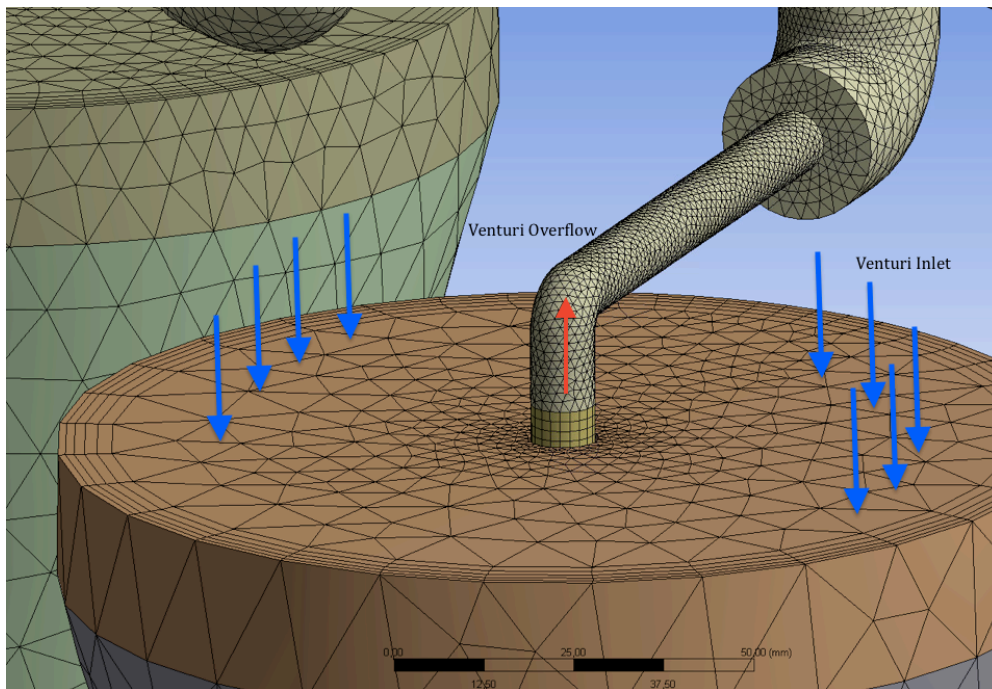
Figure 6.12: Detail 3D CFD model inlet and overflow Venturi

6.2.3 Subsystem 3 - Erosion analysis

1. Objective

This section examines the erosional wear of the reducer installed at the reject outlet of the de-sander. Two approaches are there, whereby the first assumes a fixed impact angle of a particle at 60°. The second approach uses CFD to determine the impact angle of multiple particles on the wall with particle tracking. The first approach will be used to verify the CFD model.

The model for the erosion rate in a flow reducer proposed in the "Recommended Practice RP O501 Erosive Wear in Piping Systems" [30] by DNV will be used to calculate the erosional wear.
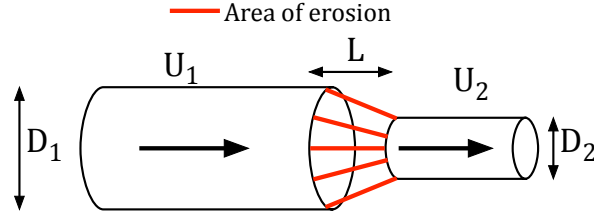
Figure 6.13: Schematic model flow reducer

2.Theory

The erosion on ductile and brittle material by solid particles was investigated by Finnie [29]. This study accounts for multiple particle impacts that involves two primary mechanisms of erosion, deformation wear and cutting wear.

The main difference between the two erosion mechanisms is that deformation wear occurs when the particles strike the material at high angles which deforms its surface layer while cutting wear takes place when the angle between particle and material collisions are low which leads to cuts and scratches on the surface. Since the material of the hydrocyclone is duplex, the erosion equations for ductile materials were used. The condensed Finnie model[29] is as shown:

$$\dot{E} = \dot{m}_p K U_p^n F(\alpha) \tag{6.11}$$

where $\dot{m}_p$ is the mass flow of sand, K the material constant, U_p the particle impact velocity (equal to the fluid velocity), n is the velocity exponent and $F(\alpha)$ the function characterizing ductility of the material.

$F(\alpha)$ is defined as:

$$F(\alpha) = A_1 \times \left(\gamma \frac{\pi}{180}\right) - A_2 \times \left(\gamma \frac{\pi}{180}\right)^2 + A_3 \times \left(\gamma \frac{\pi}{180}\right)^3 - A_4 \times \left(\gamma \frac{\pi}{180}\right)^4$$
$$+ A_5 \times \left(\gamma \frac{\pi}{180}\right)^5 - A_6 \times \left(\gamma \frac{\pi}{180}\right)^6 + A_7 \times \left(\gamma \frac{\pi}{180}\right)^7 - A_8 \times \left(\gamma \frac{\pi}{180}\right)^8 \tag{6.12}$$

with the constants

Table 6.3: Function distribution constants

A_1	A_2	A_3	A_4	A_5	A_6	A_7	A_8
9,370	42,295	110,864	175,804	170,137	98,398	31,211	4,170

From the obtained mass erosion rate, the lengthwise erosion rate can be further calculated using the equation below:

$$E_L = \frac{E_m}{\rho_t A_t} \times 3,15e + 10 \tag{6.13}$$

where E_L is the erosion rate [mm/year], ρ_t the target material density [kg/m^3] and A_t the target material surface area [m^2].
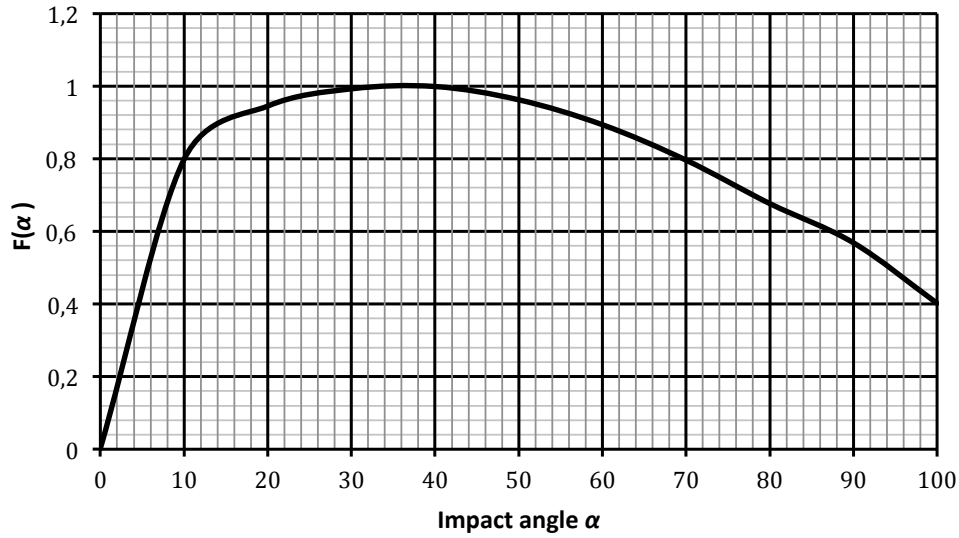
Figure 6.14: Function F_α for typical ductile materials

The F_α profile shows that the angle that induces the highest erosion rate is between 30 - 40°. Although this profile was based on experimental testing on various steel materials, the impact angles of this experiment only range from 1 - 9°where most of the ductile materials share similar F_α profiles [30].

Ductile materials, such as steel grades, attain maximum erosion attacks for impact angles in the range of 15 - 30°. Brittle materials, such as tungsten carbides with a metallic binder phase, attain maximum erosion attacks at normal impact angle [30].

3. Simulation setup

The dimensions of the reducer are obtained from the online JAVA Applet [11], as shown in figure 6.15, and the 3D geometry was built in CFD. In Fluent, single-phase flow is used and after steady state has been reached, particle tracking was applied to extract the particle's position and velocity in the x, y and z direction to compute the impact angle. From there, the k and n constants obtained from the DNV's "Recommended Practice RPO501 Erosive Wear in Piping Systems" were used in the erosion model to calculate the simulated erosion.
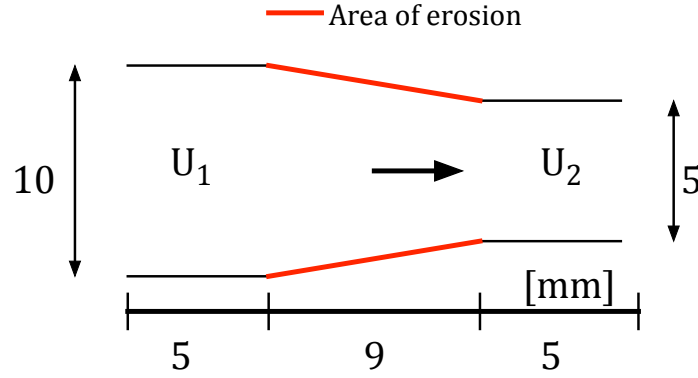
Figure 6.15: Dimensions flow reducer
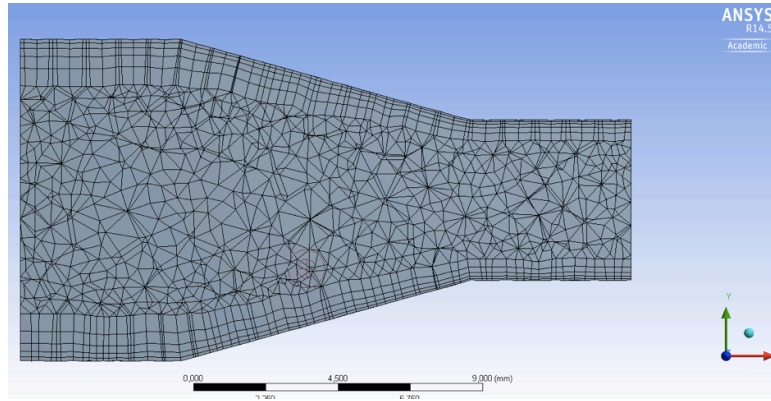
Figure 6.16: Meshed geometry of flow reducer

A flow reducer with an inlet diameter of 10 [mm], throat of 5[mm] and nozzle length of 9 [mm] was used, as shown in figure 6.15. Boundary layer meshing scheme was used in the vicinity of the wall due to the uniformity of the flow in that region. Since the core of the geometry is turbulent, the grid size in this region is relatively coarse. The meshed flow reducer is shown in figure 6.16.

The impact angle as described below:

1. Fluent gives as output the position in three dimensions (x, y & z), with its corresponding velocity vectors (u, v & w). With this the radial velocity can be calculated:

$$v_{rad} = \frac{yv}{r} + \frac{zw}{r} \tag{6.14}$$

with:

$$r = \sqrt{y^2 + z^2} \tag{6.15}$$

2. Determine the impact angle γ:

$$\alpha = \tan^{-1}\left(\frac{v}{u}\right) \tag{6.16}$$

$$\gamma = -\alpha + \beta \tag{6.17}$$
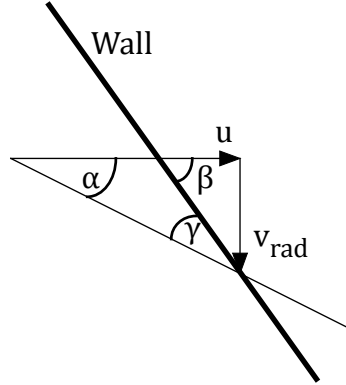
Figure 6.17: Impact angle γ to wall

The process conditions for the simulation are:

Table 6.4: Simulation of flow reducer boundary conditions

	Unit	Value
Mass flow rate	0,56	[kg/s]
Sand loading	5,5e-5	[kg/s]
Particle diameter DV_{50}	100e-6	[m]

6.3 Results & Discussion

In this section the simulation results from the three subsystems are presented. The Venturi model will be shown first, where the Excel fits are shown followed by the CFD pressure-drop curve as a proof of the performance. Hereafter this simulated Venturi is placed in the downhole separator to function as a subelement to compute the reject rate under various conditions. Finally the sensitivity of the element causing the pressure-drop at the outlet of the de-sander for erosion is computed. The section is concluded with a discussion about the obtained results.

6.3.1 Subsystem 1 - Venturi model

Figure 6.18 and figure 6.19 show the ASCOM and the Venturi model pressure-drop curve for two different reject rates for the 2,5" bulk de-oiling hydrocyclone. Only the pressure-drop curves of the 2,5" hydrocyclone and Venturi model are shown, the rest of the curves can be found in the Appendix B. For the sake of clarity the hydrocyclone pressure drop curves and Venturi model pressure drop curves are depicted in separate figures. Figure 6.19 resembles the fit calculated in Excel.
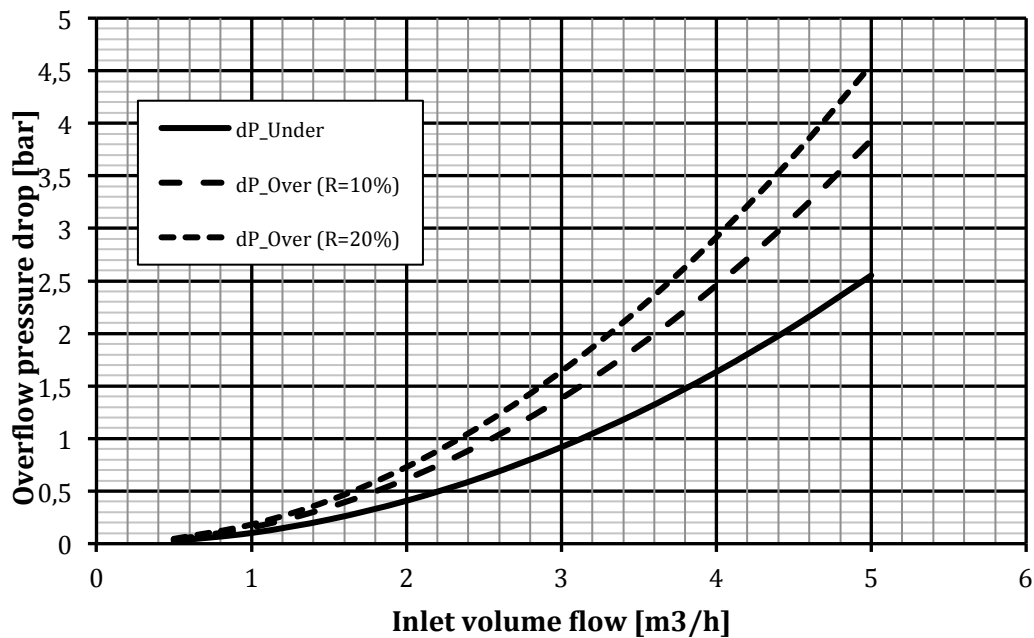
Figure 6.18: ASCOM pressure-drop curve for 2,5" bulk de-oiling hydrocyclone
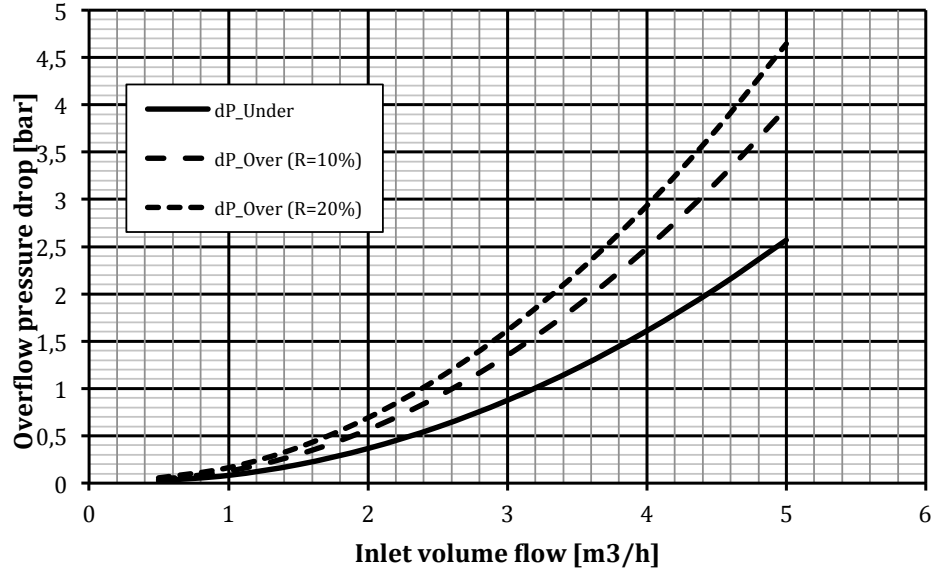
Figure 6.19: Venturi model pressure-drop curve for the 2,5" simulated bulk de-oiling hydrocyclone

The following table with coefficients are computed with the fit made in Excel (with a density of ρ=1000 [kg/m^3]). The Fluent C_2 curves are calculated according to equations (6.5) and (6.6).

Table 6.5: C_2 coefficients.

	1" Venturi Model		2" Venturi Model		2,5" Venturi Model	
	Excel C	Fluent C_2	Excel C	Fluent C_2	Excel C	Fluent C_2
Inlet C_1	18e+6	36e+3	1,55e+7	31e+3	3,19e+7	63,8e+3
Overflow C_4	95e+3	0,19e+3	70e+3	0,14e+3	5+e3	0,01e+3

The pressure-drop curve, figure 6.19, fits the curve in figure 6.18 with high accuracy. This is the case for all three the Venturi models. For a first simulation only the C_2 coefficients for the 2,5" Venturi model worked. The C_2 coefficients for the two other models were not functioning as expected, resulting in too high pressure-drops. The correct C_2 coefficients were found rather quickly with trial and error, as these can be seen in table 6.6.

Table 6.6: Verified C_2 coefficients.

	1" Venturi Model		2" Venturi Model		2,5" Venturi Model	
	Excel C	Fluent C_2	Excel C	Fluent C_2	Excel C	Fluent C_2
Inlet C_1	36000	9000	30000	15000	64000	64000
Overflow C_4	190	95	140	70	10	10

Six simulations were run with different reject rates (10% and 20%) and different flow rates (2, 3 and 4 [m^3/h]) to check if the CFD Venturi model is behaving as expected in Fluent. With CFD-Post[3] the pressure at the inlet, underflow and overflow have been determined and with these the pressure-drops have been calculated. Figure 6.20 gives the pressure-drop curve for the underflow and overflow with their corresponding C_2 values of 63800 and 10 respectively. The related graphs for the other cyclones can be found in Appendix C.
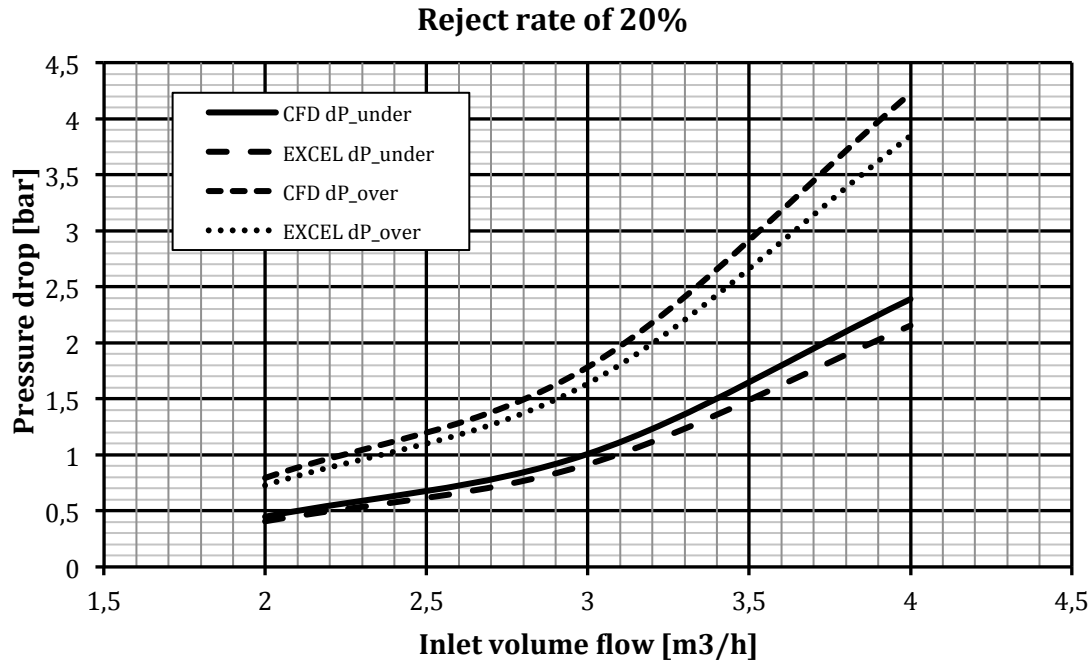
Figure 6.20: Venturi model pressure-drop curve for the 2,5" simulated bulk de-oiling hydrocyclone

Figure 6.21 illustrates the pressure contour of the simulated Venturi model, and the places where the porous jump is imposed can be clearly seen. To calculate the pressure at the different boundaries, Fluent takes an arbitrary level as zero reference level.

---

[3]CFD-Post is the name for post processing within Ansys Fluent.
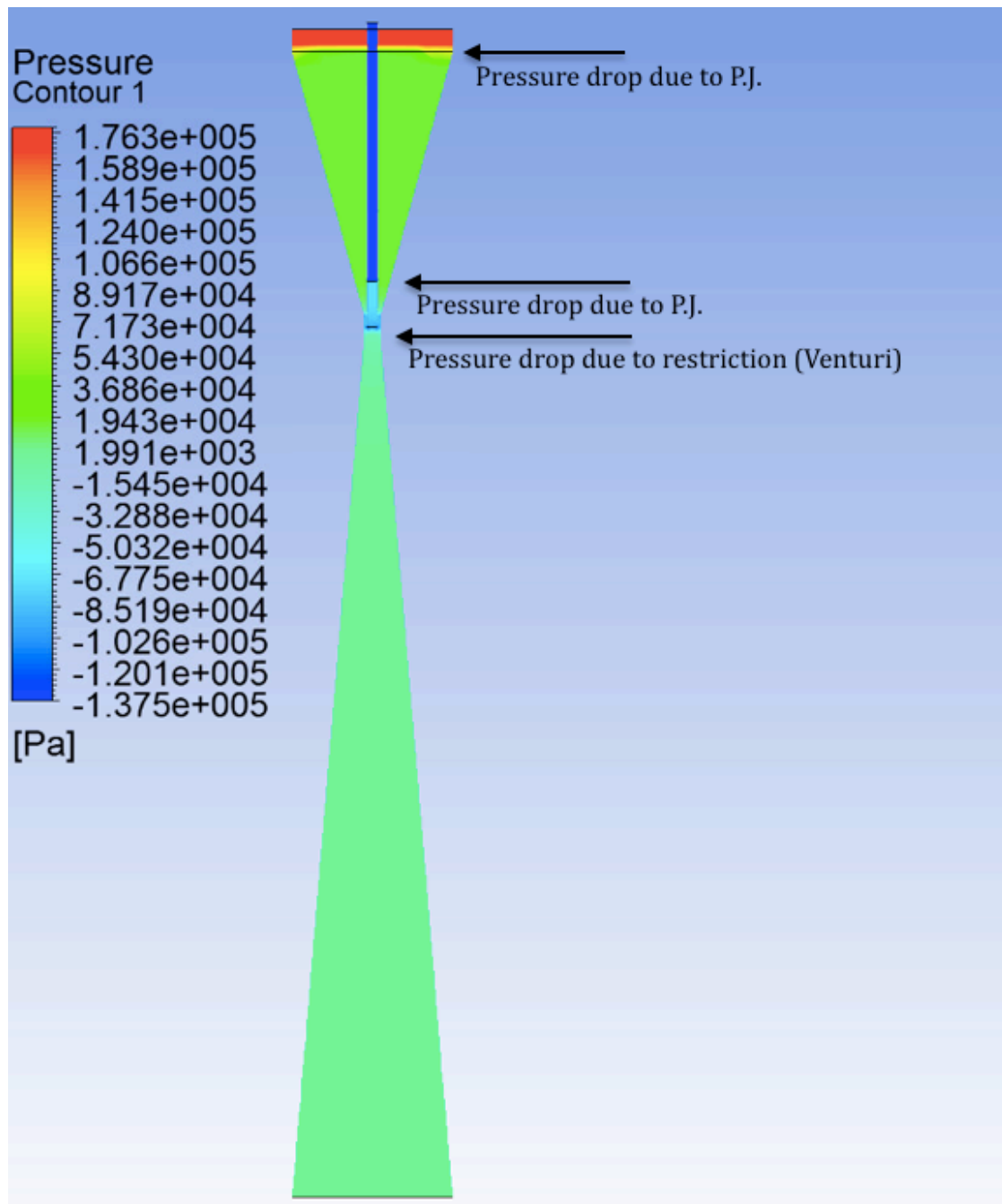
Figure 6.21: Pressure Contour Venturi model

6.3.2 Subsystem 2 - Pressure balance rejects 1st and 2nd stage

Five simulations have been run to investigate how the DPR behaves with respect to the de-sander outlet pressure and the pump inlet pressure. The de-sander outlet and the underflow pressures where fixed, whereby the pressure at the pump inlet was varied. The porous jump values remained the same for all simulations. The overflow rate is set at 20% by imposing a pressure-outlet condition at the underflow. The pressure of 134 [bar] is the pressure after the reducer.

Table 6.7: Input values CFD simulation

Boundary	Simulation 1	Simulation 2	Simulation 3	Simulation 4	Simulation 5	Simulation 6	Unit
Inlet Venturi	1,2	1,2	1,2	1,2	1,2	1,2	[kg/s]
DS Outlet	134	134	134	134	138	138	[bar]
Underflow	136	136	136	136	136	136	[bar]
Riser	134	133	132	130	134	138	[bar]

Table 6.8: Output values CFD simulation - Flow rate

Boundary	Simulation 1	Simulation 2	Simulation 3	Simulation 4	Simulation 5	Simulation 6	Unit
Inlet Venturi	4,3	4,3	4,3	4,3	4,3	4,3	[m3/h]
DS Outlet	0,3	2,9	4,1	5,9	6,8	1,2	[m3/h]
Underflow	3,3	3,1	2,9	2,5	1,9	5,6	[m3/h]
Overflow	1,0	1,2	1,5	1,9	0,6	- 1,3	[m3/h]

Table 6.9: Output values CFD simulation - Pressure

Boundary	Simulation 1	Simulation 2	Simulation 3	Simulation 4	Simulation 5	Simulation 6	Unit
Inlet Venturi	138	137	137	137	143	138	[bar]
DS Outlet	134	133	132	130	133	138	[bar]
Underflow	136	136	136	136	136	136	[bar]
Riser	134	133	132	130	134	138	[bar]
Overflow	134	133	133	131	137	137	[bar]

Table 6.10: Reject rates and DPR

Boundary	Simulation 1	Simulation 2	Simulation 3	Simulation 4	Simulation 5	Simulation 6	Unit
Reject	23%	29%	34%	43%	14%	-30%	
dP$_{Over}$	3,8	4,1	4,9	6,4	6,0	0,7	[bar]
dP$_{Under}$	1,9	1,4	1,4	1,2	7,0	2,0	[bar]
DPR	2,0	2,9	3,5	5,3	0,9	0,4	[bar]
DPR$_{fit}$	2,9	3,6	4,3	5,6	1,9		[bar]
P$_{Riser}$	134	133	132	130	134	138	[bar]

For simulation 1, the pressure at the de-sander (DS Outlet) and the riser are the same. By gradually lowering the pressure at the riser outlet (pump inlet) and maintaining the pressure at the de-sander outlet constant (simulations 2, 3 & 4) the change in PDR for the bulk de-oiling hydrocyclone can be computed, since Fluent calculates the pressure at the overflow. Table 6.8 shows that the pressure at the de-sander adjusts to the riser pressure, and since the pressure at the overflow of the bulk de-oiling hydrocyclone adjusts to the de-sander outlet the PDR of the bulk de-oiling hydrocyclone adapts to the pressure at the riser outlet. The lower the suction head of the pump, the more fluid is extracted trough the overflow of the bulk de-oiling hydrocyclone. The DPR$_{fit}$ gives the value of the DPR it should be based on the calculated pressure drop and corresponding reject rate.

Simulation 5 gives the scenario where there is no reducer installed at the outlet of the de-sander, as explained in section 6.2.2. Here the pressure at the de-sander outlet is higher than that of the bulk de-oiling hydrocyclone but the riser outlet is set at a lower value. Simulation 6 is a case where both the de-sander outlet and the riser outlet are higher than that of the bulk-de-oiling hydrocyclone hence resulting in back flow.
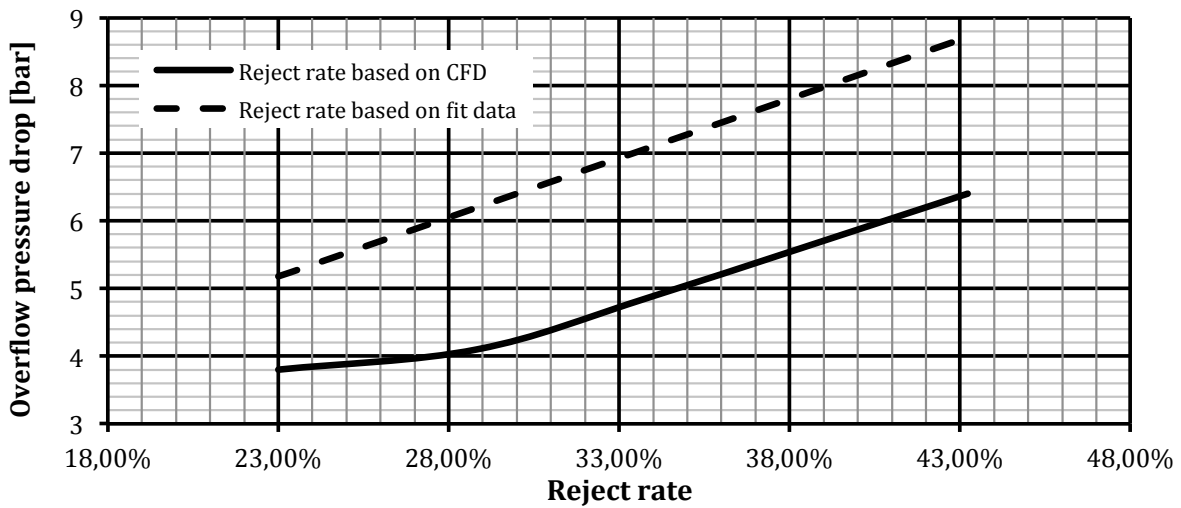
Figure 6.22: Overflow pressure-drop as function of reject rate

6.3.3   Subsystem 3 - Erosion analysis

The flow field in the geometry is found with Fluent and is used to calculate the particle trajectories (figure 6.24 and 6.25). The impact velocities and impact angles are then used to determine the resulting erosion attacks. The erosion rate is calculated by means of equation (6.13) for individual particles and added to give an estimate of the overall erosion profile in the geometry. The simulation has been conducted with one DV_{50}. Two models have been used, $k - \epsilon$ for the turbulent single phase flow and and the Discrete Phase Model (DPM) to track the solid particles.

Table 6.11: Axial & $v+w$ velocities

x [m]	Axial velocity [m/s]	Velocity v [ms]	Velocity w [m/s]
0	7,218	-0,000977	0,000121
0,002	7,217	0,0004225	0,0004364
0,004	7,207	0,00191	-0,0004
0,006	8,081	-0,00167	0,0001421
0,008	10,37	0,002114	-0,001141
0,010	13,82	0,0003105	0,003756
0,012	19,33	0,003809	0,004678
0,014	28,97	-0,007492	-0,0003
0,016	28,94	-0,00465	-0,0025
0,018	29,00	0,0008769	-0,01
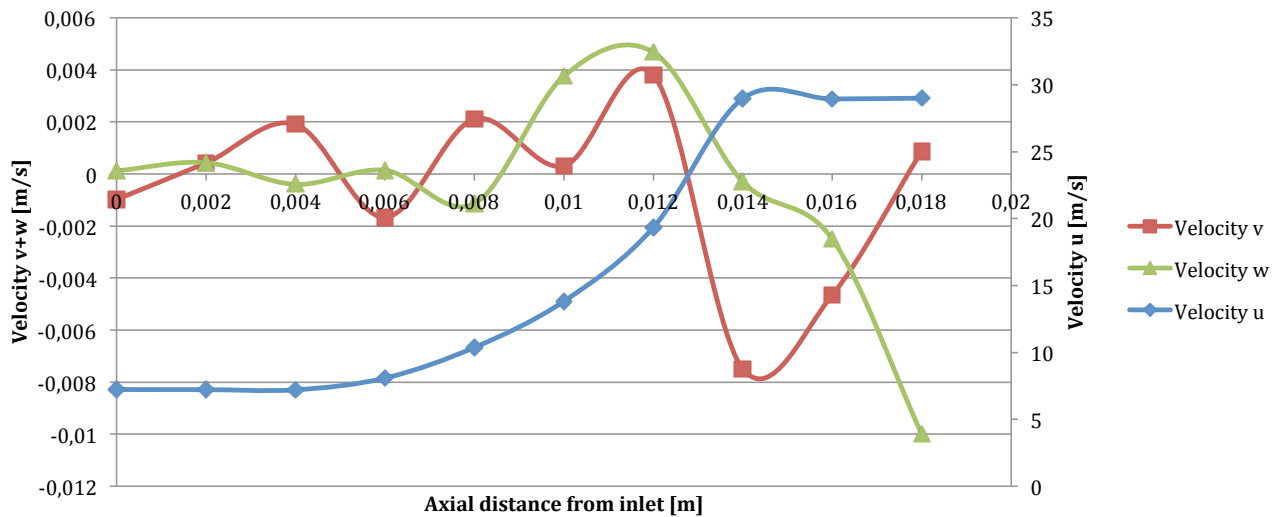
Figure 6.23: Axial & $v+w$ velocities

The velocity profiles, shown in figure 6.23, behave as expected where the axial velocity is lowest in the inlet where the cross-sectional area is largest and reaches a maximum at the section with the smallest diameter.

As for the radial velocity, it exhibits a profile that mimics the v and w velocity components combined. This can be explained by the rebound of a particle on the wall. The regime with a higher velocity profile will provide the particle with more velocity and therefore it has more energy to collide with the surface wall which sends it farther from the surface. The added distance in turn gives the particle more settling time for the transfer of energy from the fluid to the particle before striking the surface wall again.
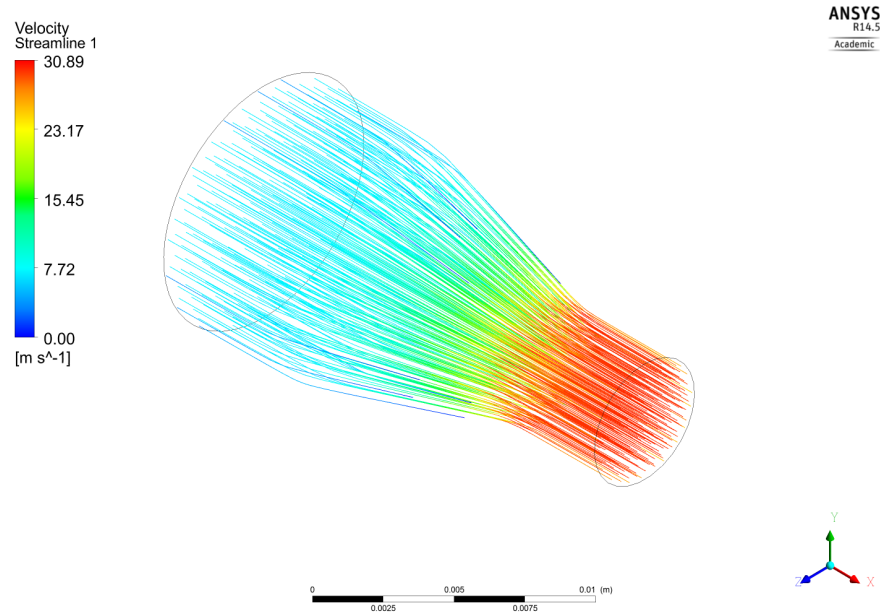
Figure 6.24: Streamlines
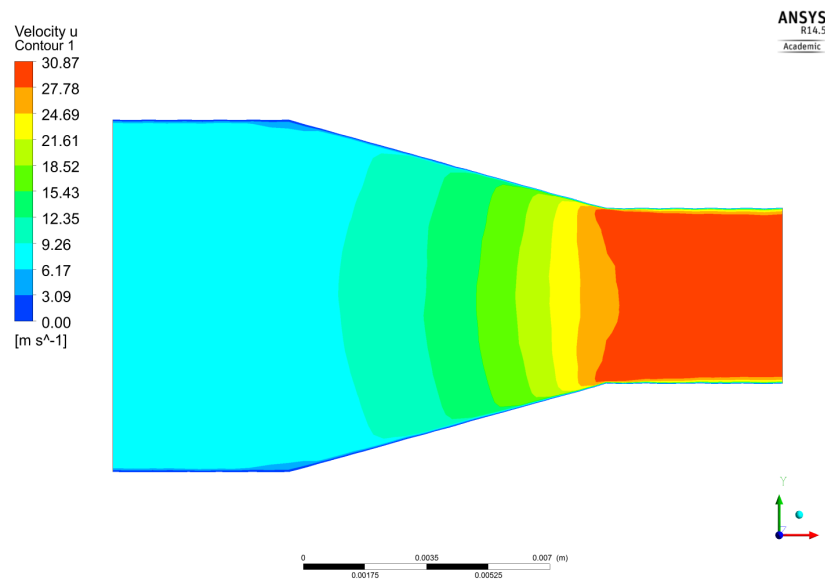
Figure 6.25: Axial velocity profile

To look at the overall erosion effects, the particle impacts in a section is summed up and divided by the respective surface area to obtain the overall erosion in length per year. Figure 6.26 shows the distribution of the DPM erosion rate at different locations of the flow reducer geometry for 100 microns sand particles with water velocity of 28,77 [m/s]. The location of maximum erosion at this condition is just before the throat inlet, at 13 [mm] from the inlet of the flow reducer. This is to be expected as the flowlines are most impeded just before the throat inlet.

Due to lack of available experimental results, validation of the CFD simulation was not performed. Although experimental validation was not presented, CFD simulation results presented in this section will shed some light on the relative magnitude and location of erosion in the flow reducer.
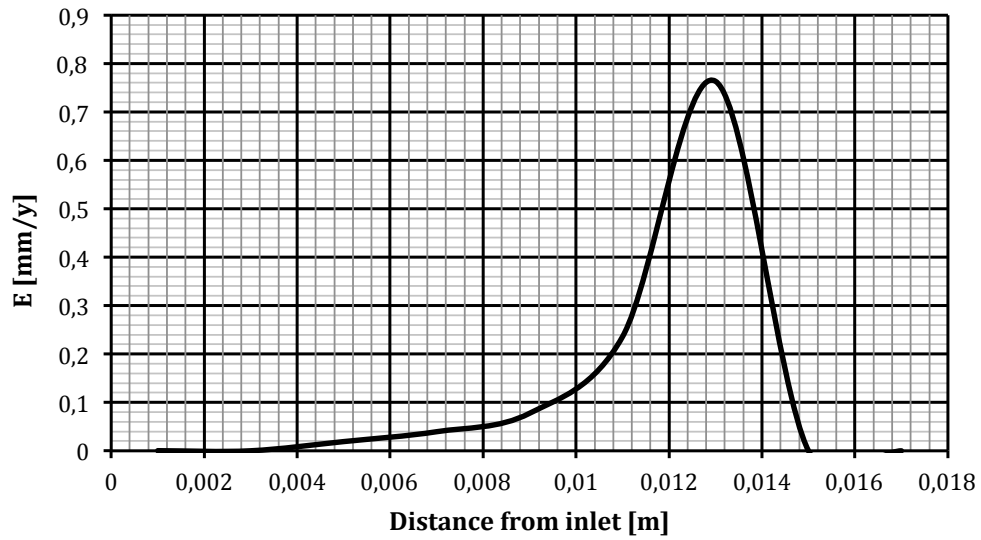
Figure 6.26: Theoretical erosion profile

6.3.4 Discussion

The main goal of the simulations is to provide a reliable estimation of some critical elements in the downhole separator. Some aspects of the simulation results will be discussed here together with the interpretation of the results.

Translation to CFD model
One of the major issues with the analysis of the downhole separator is the translation of a schematic model, as proposed in chapter 5, to a CFD model. Since CFD has a relatively weak predicting power we have chosen to look at the overall performance i.e. with respect to the flow assurance. We reviewed several options to compute the pressure balance in subsystem 2, of which one could simply be to impose a pressure inlet, with varying values, at the reject of the bulk de-oiling hydrocyclone and not implementing the Venturi. However in this fashion the performance of the hydrocyclone could not be taken into consideration since the amount of flow leaving the overflow of the bulk de-oiling hydrocyclone is dependent on its corresponding pressure-drop which is on its turn dependent on the pressure at the outlet of the de-sander and riser. Moreover, in order to make a model which corresponds to the behavior of an hydrocyclone the porous jump membranes were introduced. These arguments have led for the choice of a Venturi geometry for the flow and pressure mimic of an hydrocyclone.

Results accuracy
The calculated C_2 coefficients gave the correct pressure-drop relation in Excel. The fit in Excel, however, was not reliable for higher reject rates. The Venturi model overestimates the overflow pressure-drop. The 1" and 2" hydrocyclones were only fitting for reject rates up to 5% and the 2,5" up to 25%. The reason for this is because the overflow pressure-drop is more sensitive for the reject rate because of the quadratic term in equation 6.4. Since the fluid velocity v_4 in the reject tube is 5 - 10× higher than the inlet velocity v_1, the overflow pressure-drop becomes more sensitive for increasing velocitiy.
The C_2 coefficients did not work as expected in CFD initially. Several options were investigated to make the model working, e.g. a better mesh connection between the reject tube and the Venturi and altering the C_2 coefficients in FLUENT. The latter led to the correct pressure-drop relation.

Table 6.9 shows that the pressure at the overflow of the bulk de-oiling hydrocyclone adjusts to the pressure at the riser outlet and not at the de-sander. However, it was rather anticipated that the pressure would be corrected to that of the de-sander outlet and then to the riser outlet. Simulation 5, table 6.10, shows that with eliminating the flow reducer, the bulk de-oiling hydrocyclone can hardly produce any reject because the pressure at the outlet of the de-sander is too high. Simulation 6 confirms the theory as described in figure 6.8, whereby the riser outlet operates at the same pressure as the de-sander outlet and no fluid is flowing through the overflow. Therefore the bulk de-oiling hydrocyclone receives negative flow rate rather than producing any.

Consideration downhole conditions
Downhole conditions like temperature, viscosity, droplet size distribution and reservoir injectivity which alter the separation performance have not been taken into consideration for the simulation due to CFD's relative weak predicting power. However, they have been considered for the experimental tests (chapter 7).
On the other hand, the influence of downhole conditions did alter the design of the separator assembly by positioning a de-sander unit upstream the liquid-liquid hydrocyclones and placing the 2" and 2,5" hydrocyclones in series to prevent for example the settling of sand. For the simulation of the flow reducer reservoir parameters such as particle size and sand load have been used to predict the erosional.

Chapter 7

Multistage hydrocyclone performance testing

In order to verify the performance of the downhole separator experimentally, tests were conducted at Pro-LabNL. These tests were such that the real field conditions were mimicked as best as possible. Important aspects that verify the performance of the downhole separator are the droplet break up and the separation performance of the three consecutive separation stages.

7.1 Translation downhole separator to physical test model

Since the low pressure (LP) loop at ProLabNL is limited to 15 bars, the downhole separator as presented earlier is scaled down. This will however not influence the calculated separation efficiency in section 4.2.1. since it is independent on the number of liners. The number of liquid-liquid separation stages will not be altered.

Table 7.1: Downhole separator configuration

Stage	Type of liner	Number of liners	Flow capacity [m^3/h]
1st	2" De-sander	1	50
2nd	2,5" Bulk de-oiling hydrocyclone	3	5
3rd	2" Hydrocyclone	3	4
4th	1" Hydrocyclone	9	1

Existing system: At the ProLabNL facility a dedicated test loop was already available for performance testing. This existing system consists of two stages with 2 and 3 hydrocyclone liners respectively to test with higher flow rates.

Upgraded system: The upgraded system is based on the existing system in which its second stage is bypassed and added with two other hydrocyclone stages. The bypassed hydrocyclone will not be used due to its lower efficiency. This results in three consecutive stages that are placed in series such that the output of the 1st stage is the input for the 2nd stage and output of 2nd stage the input for the 3rd stage. Due to the flow rate

Table 7.2: Test model at ProLabNL configuration

Stage	Type of liner	Number of liners	Flow capacity [m^3/h]
1st	2,5" Bulk de-oiling hydrocyclone	2	5
2nd	2" Hydrocyclone	1	4
3rd	1" Hydrocyclone	1	1

(4 [m^3/h]), a closed loop system will be used where the outlet and rejects of the liners will be disposed in a 10 [m^3] vessel.

To gain a higher separation performance, it is advisable to operate the hydrocyclones and bulk de-oiling cyclone in their optimum flow range. However, this will create a higher-pressure drop for the three consecutive stages. Therefore a progressive cavity pump will be installed after the second stage to bring the pressure back to the desired level. Due to the existing material, only one hydrocyclone will be used but due to its lower capacity a part of the flow will be bypassed.

Since the 1" hydrocyclone is a scaled 2" hydrocyclone, the diameter is half of the 2" therefore allowing only $\frac{1}{4}$ of the flow.

$$Q_2 = Q_1 \left(\frac{d_2}{d_1}\right)^2 = \frac{1}{4}Q_1 \tag{7.1}$$

This means that a part of the flow should be bypassed in order for the 1" hydrocyclone to operate in its optimum flow range.

7.2   Experimental set-up

All tests have been done according to the test matrix (ref. Appendix D). The existing flow loop is a closed system where the outlets of the hydrocyclones are led back into a reservoir tank. Because of its capacity of 10 [m^3] and a flow rate of 4 [m^3/h] this would result in a maximum of 2,5 hour test. Nitrogen, oil and water are stored in the tank, in which Nitrogen is meant to prevent hazardous situations (due to its high flash point).

7.2.1   Test loop

The main loop of the upgraded test loop contains a water reservoir, a filter unit, separate screw pumps for oil and water, shear valve and the three-stage hydrocyclone system. The Process Flow Diagram is presented in figure 7.1.

1. As the water and oil are extracted from the plate pack separator, they are led through their respective pump (1 & 3) from where they are led to the shear valve.

2. The shear valve (2) is used for mixing the oil and water stream and generating oil droplets of different sizes. A more closed valve will create a higher pressure-drop over the valve, higher shearing forces in the water and therefore resulting in a smaller droplet size distribution.

3. Water and oil is routed trough a metering system where the pressures, temperatures and flow rates of the liquids are determined. The flow through the bulk de-oiling cyclone (3) is controlled digitally with software package LabVIEW. The two additional stages (6) & (7) are controlled manually by reading of the pressure at the pressure gages (PI) at the inlet and outlet and therewith setting the flow rate.

4. Hydrocyclone (4) is not used.

5. In order to obtain a reject flow, valves are installed (A, B & C) at the outlet (underflow). Fluid will flow through the lowest resistance and by choking this outlet, a part of the fluid is forced to move upwards through the reject.

6. Valves are also installed at the reject (overflow) in order to control the reject rate (e.g. 2%, 4%)

7. In order to compensate the pressure drop due to the 2nd and 3rd stages, a progressive cavity pump (PCP) will be installed after the first stage.

8. In order to gain good separation, the hydrocyclones and bulk de-oiling cyclones should be operated in their optimum flow range. Therefore the outlet of the 1st and 2nd stage is partly bypassed so that the next stage receives just the right amount of flow rate.

9. The filter unit removes very small oil droplets as far as those present at the exit of the water reservoir.

10. Tap points for taking samples are located in the main loop, upstream of the bulk de-oiler, between bulk de-oiler and 2nd stage hydrocyclone, between the 2nd stage hydrocyclone and 3rd stage hydrocyclone, and downstream of 3rd stage hydrocyclone.

11. Sampling means extracting fluid from the system, therefore the water level should be monitored at the end of each testing day and if needed be complemented.

12. An important parameter is to maintain the water level sufficiently high; otherwise the oil outlet will suck in gas (Nitrogen) leading to a decrease in performance of the screw pump.
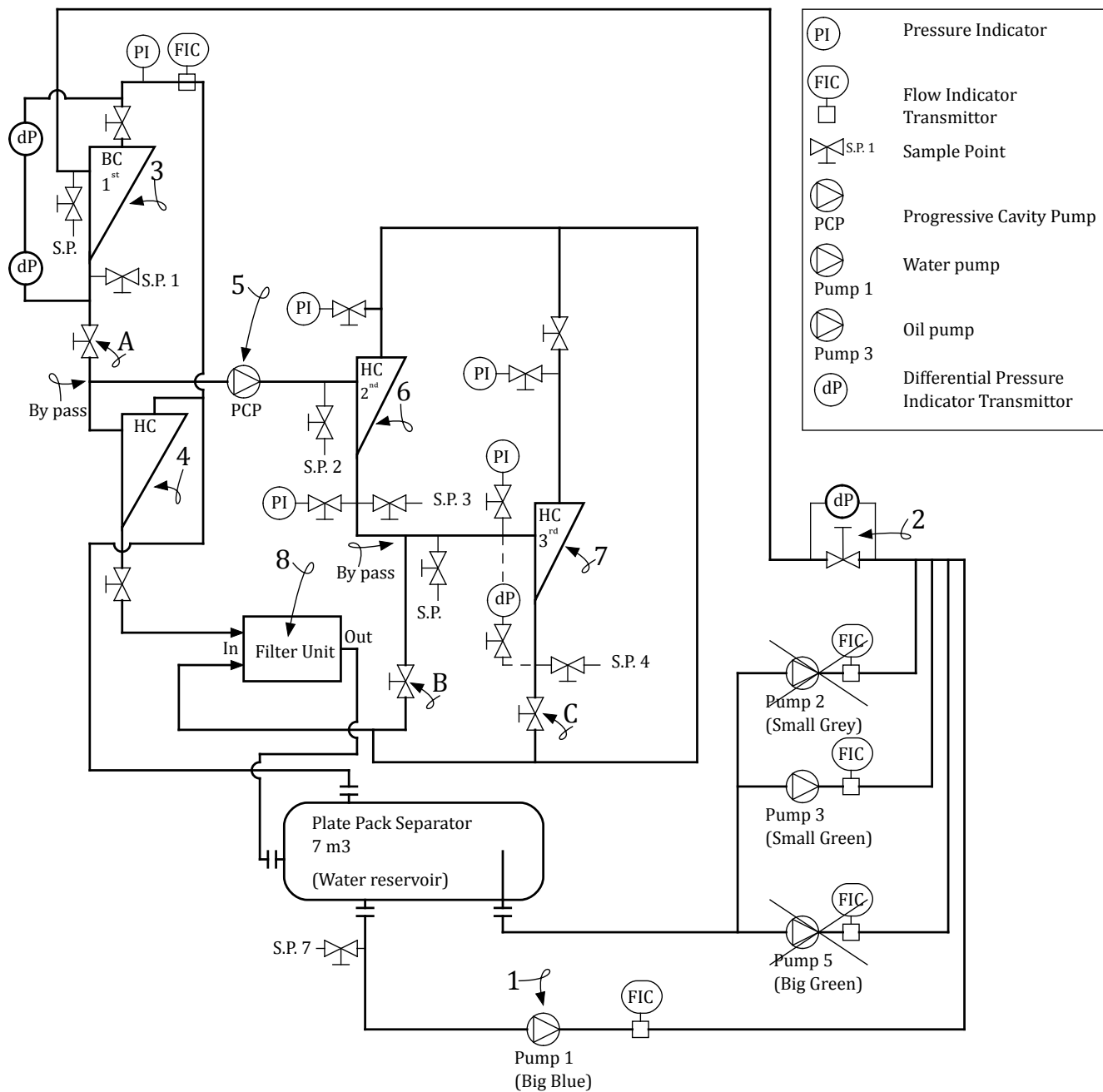
Figure 7.1: Process Flow Diagram three stage separation system

7.2.2 Flowloop elements

In figures 7.2 to 7.5 some components of the flowloop are shown.
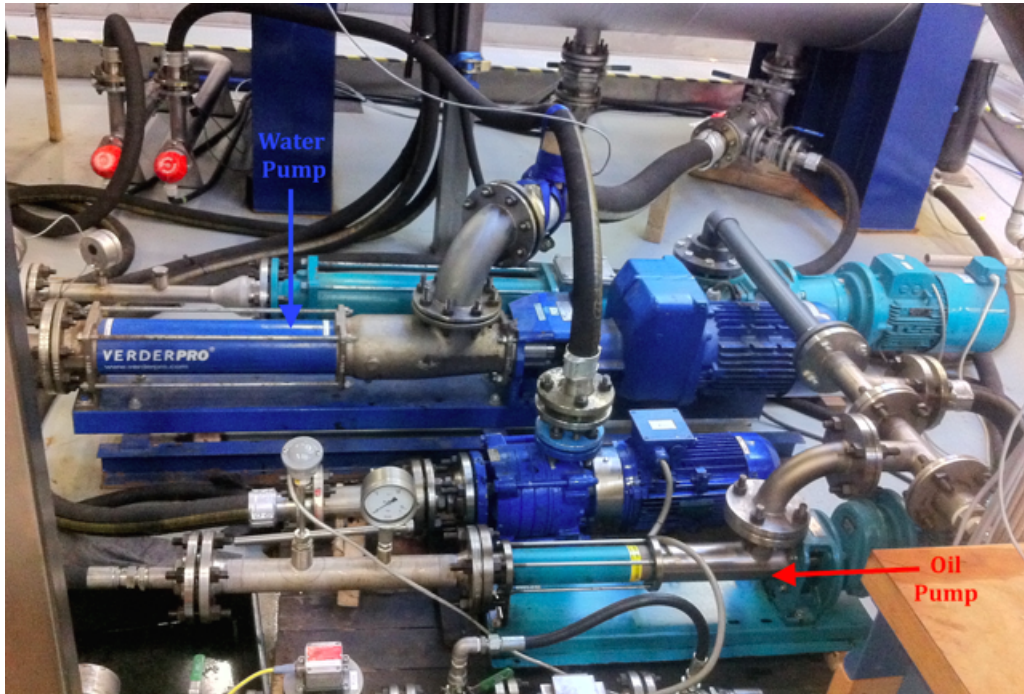
Figure 7.2: Oil and water pump
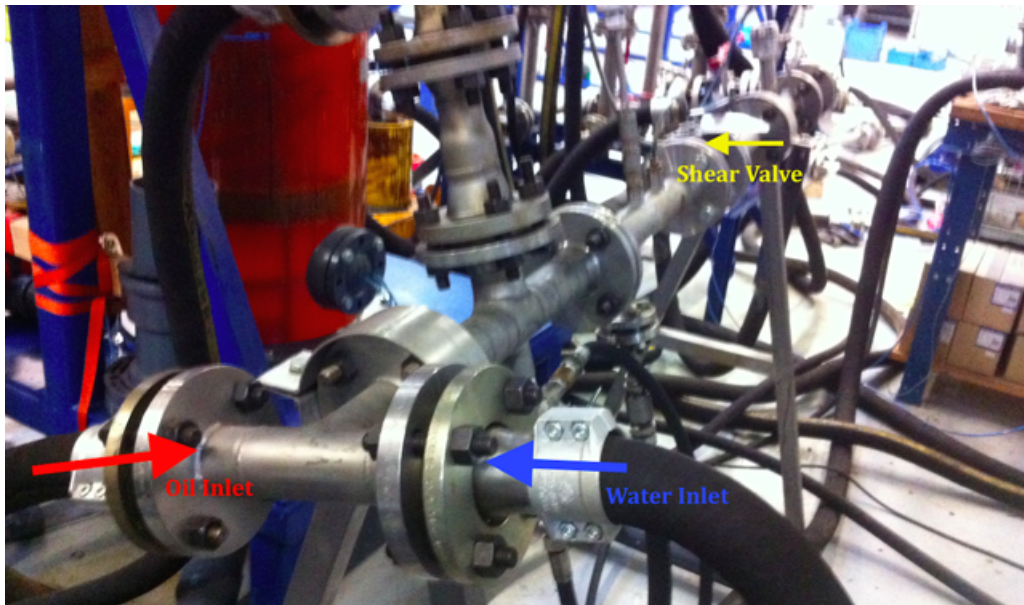
Figure 7.3: The oil and water inlet are the oil and water outlet of the pumps in figure 7.2. The shear valve is installed for creating droplet distribution
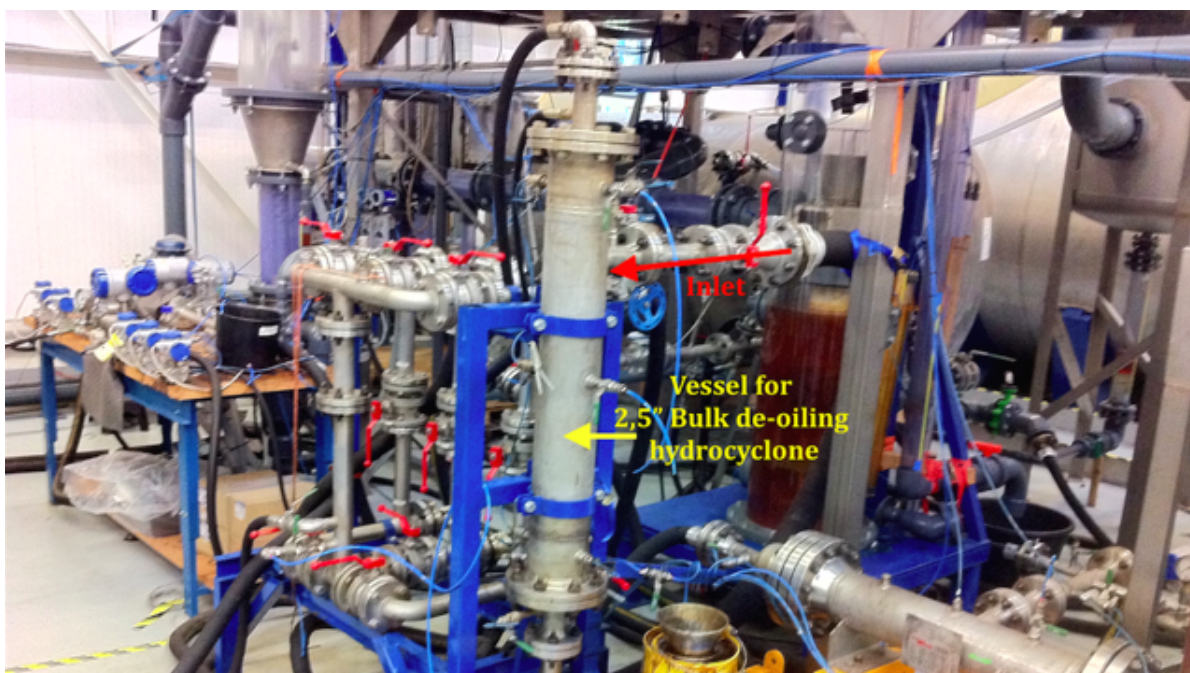
Figure 7.4: From the shear valve the fluids are directed to the 2,5" bulk de-oiling hydrocyclone vessel
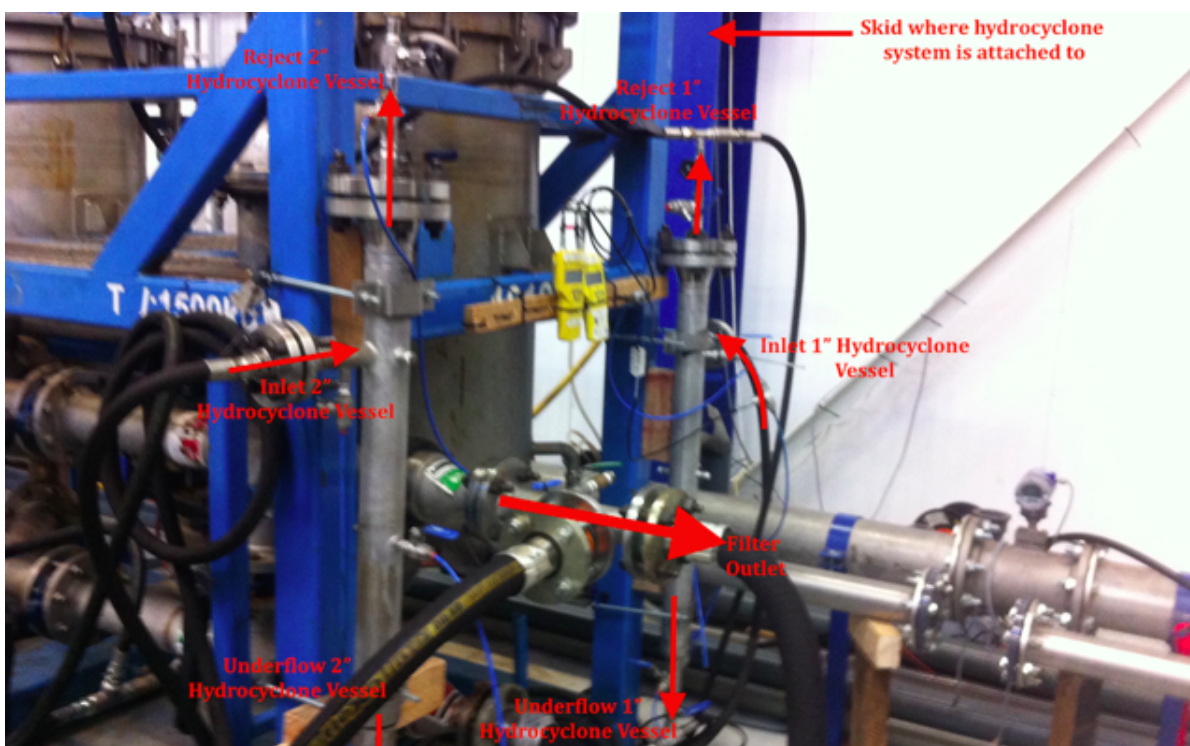
Figure 7.5: Vessels for the 2" and 1" hydrocyclones

7.2.3 Sampling procedure

For determining the separation efficiency of the hydrocyclone system, oil in water samples are taken. All samples are taken in transparent jars of 250 [ml]. The volume of the sample should be 200 [ml]. Depending on the amount of oil present in the samples, skimming or hexane extraction is to determine the amount of oil in water.

Skimming
If a substantial amount of oil is present in the sample (i.e. more than 1%, a distinct layer of oil is visible on top of the water) the skimming method is used. The oil layer is extracted from the sample using a pipette and collected in a graduated cylinder. The volume of oil and total sample volume are then noted.

Hexane extraction
If only a small amount of oil is present in the sample (i.e. no distinct oil layer is visible) hexane extraction is used to determine the amount of oil in the sample (in parts per million). ProLabNL uses a Turner Designs TD-500 hand-held Oil-in-Water meter (see figure 7.6a), which uses ultraviolet fluorescence to determine the amount of aromatic hydrocarbons in a sample. Assuming the fraction of aromatic compounds is constant for any given oil, the fluorescence intensity can be converted into the oil concentration of a sample when the device is calibrated for this oil.

(a) Turner Designs TD-500 hand-held Oil-in-Water meter and 4mm Minicell cuvettes

(b) Magnetic stirrer with water samples

Figure 7.6: Hydrocyclone polishing systems

1. Place a bottle containing a water sample on the analytical balance and note the weight.

2. Add 20 [ml] n-Hexane and weigh the bottle again. Subtract the weights to get the amount of hexane added (20 [ml] n-Hexane weighs approximately 13.2 grams).

3. Add a magnetic stirring bar to the bottle, close the cap tightly and shake the bottle to dissolve any oil stuck to the bottle.

4. Place the bottle on the magnetic stirrer (figure 7.6b) and stir them for at least 15 minutes. Longer stirring may be required in some cases.

5. Using a Pasteur's pipette, fill a cuvette with the solvent extract, wipe the outside and place it in the device. Press READ, wait until the device is ready and note the result.

6. If the result is higher than the calibration range, the reliability of the result cannot be guaranteed. In this case dilute the sample with clean solvent (n-Hexane) until the concentration is below the calibration concentration. Note the results as dilution factor x concentration [31].

7.2.4 Crude oil analysis

The crude oil used in the test loop has been analyzed for earlier test by Saybolt, a specialized company. The results are shown in the table below.

Table 7.3: Crude analysis

Test	Dimension	Grande crude
Kinematic Viscosity at 15 °C	[mm^2/s]	472,5
Kinematic Viscosity at 45 °C	[mm^2/s]	73,88
Kinematic Viscosity at 75 °C	[mm^2/s]	*)
Density at 15 °C	[kg/m^3]	939,4
Density at 45 °C	[kg/m^3]	919,9
Density at 75 °C	[kg/m^3]	**)
Flash Point (PM)	°C	<40

*) Viscosity at 75 °C cannot be done

**) Density at 75 °C cannot be done

7.2.5 Software package

LabVIEW (Laboratory Virtual Instrument Workbench), a product of National Instruments is a software system that accommodates data acquisition, instrument control, and data processing is used to control the temperature and flow rate (and therefore the pressure) in the test loop. The 2nd and 3rd stage are manually controlled by the frequency drive of the PCP and their flow rate can be determined with the pressure gauges.

7.3 Results

Tests have been performed with variations in the test matrix to gain a better insight into the separation process. The aim is to determine whether the three-stage polishing system is able to produce a water injectate below 100 ppm. The following test conditions have been used:

1. Inlet OiW: 5 - 10%

2. Temperature: 45 °C

3. Crude: Grane, 939 [kg/m^3]

4. Shear valve ΔP: 0,5 [bar]

Samples have also been taken at the overflow of the bulk de-oiling hydrocyclone to see if enough reject was produced ($\pm$ 45%). Since the outlet of the bulk de-oiling hydrocyclone is the feed for the 2" hydrocyclone, no sample analysis have been conducted.

Figure 7.7: Overview oil in water concentration for three consecutive stages.

Table 7.4: Sample analysis

Run	Sample Point	Oil-in-water [ppm]
L1	Water sample	212
L1	BCI	47000
L1	BCO	1340
L1	HCO 2"	368
L1	HCO 1"	224

Assuming the outlet of the bulk de-oiling hydrocyclone having the same oil-in-water concentration as the inlet of the 2" hydrocyclone, the following efficiency can be calculated:

Table 7.5: Efficiency

Sample point	Efficiency
BC	97%
HC 2"	73%
HC 1"	39%

The outlet of the last stage, HCO (1"), should have the same visible quality as drinking water. After several test trials it was concluded that the efficiency is as above, a follow-up experiment was set-up to determine the reason for this poor efficiency.

7.4 Determining droplet breakup in the flow loop

7.4.1 Introduction

After having run multiple tests with the three-stage hydrocyclone flow loop, it can be seen from the samples that the efficiency is significantly below the expected theoretical efficiency. The problem lies in the forming of smaller droplets, referred to as background noise. Initially the droplets are in the order of magnitude of 500 [μm] -1000 [μm], before entering the system (so on start-up). Once these droplets are introduced, they are broken up into smaller droplets. Since it is a closed loop system, meaning the oil and water are led back into the vessel and re-circulated, these smaller droplets are continuously re-introduced into the system and broken up into even smaller droplets. The objective of this paragraph is to find out the cause of the breaking up of the droplets. To examine the droplet size distribution of the oil droplets *ImageJ* is used, a free cross-platform image analysis tool [32].

7.4.2 Theory

The colored dashed line in figure 7.8 illustrates the path where the oil droplets are getting broken up, where the continous phase is water. Before start-up of the loop almost all the oil droplets have risen to the oil phase, resulting in a rather "clean" water phase.
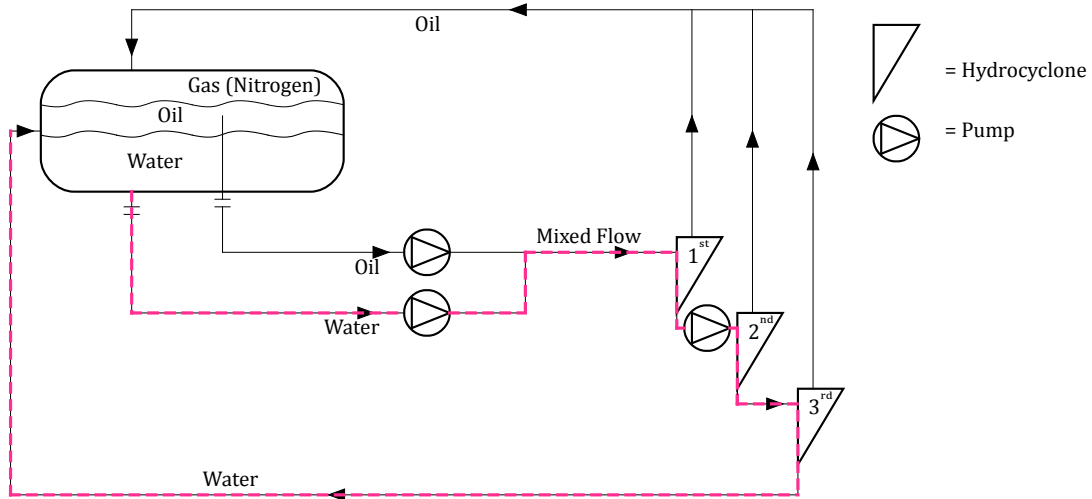
Figure 7.8: Simplified flow scheme three stage separation system ProLabNL.

However, once the system is turned on the particle size distribution of the oil in water phase starts shifting. This phenomenon is better depicted in figure 7.9a. It can be seen that the median shifts towards the left. As the droplets keep getting broken up, the amount of bigger droplets is reduced while the frequency of the smaller droplets increases.

(a) Change in droplet size distribution as function of shearing

(b) Oil droplet traveling time as function of droplet size
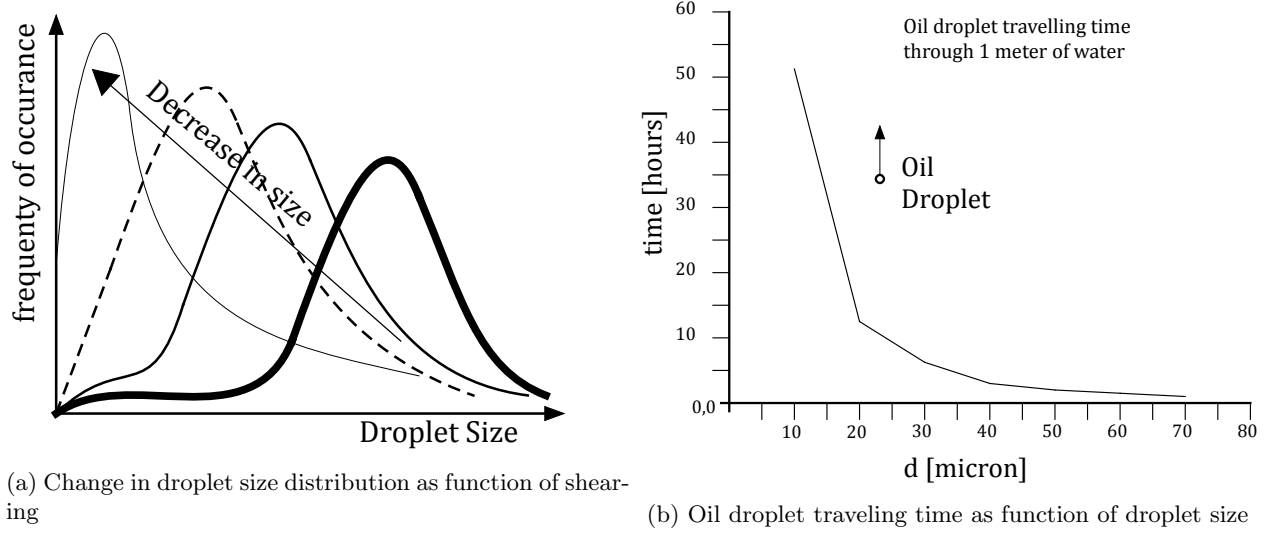
Figure 7.9: Droplet breakup and particle settling velocity

Based on Stokes-law a simple calculation can be conducted to see how long it will take for a small oil droplet to rise up to the oil layer.

$$v_{settle} = \frac{d^2(\rho_w - \rho_o)}{18\mu}g = \frac{d^2(1000 - 900)}{18 * 0,001}9,81 \tag{7.2}$$

where v_{settle} is the particle settling velocity [m/s] (vertically downwards if $\rho_o > \rho_w$, upwards if $\rho_o < \rho_w$), g is the gravitational acceleration [m/s^2], ρ_o and ρ_w are the mass density of the oil and water respectively [kg/m^3] and μ is the dynamic viscosity. Taking the viscosity of water, and a specific density of 0,9 for oil, the graph in figure 7.9b can be yielded. It can be seen that droplets below 40 [μm] have a traveling time between 5 - 50 hours. In this time span these oil droplets will leave through the water outlet (figure 7.10) and re-enter the system. Every time this oil droplet enters the water tank it can be broken up to even smaller fractions creating more background noise.
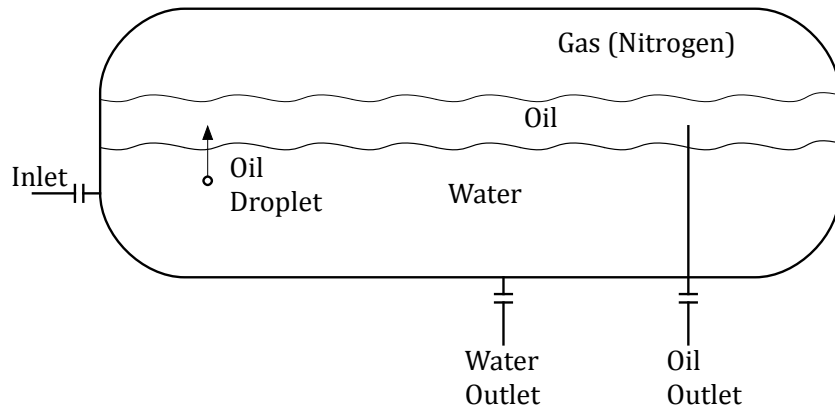
Figure 7.10: Reservoir tank

This phenomenon occurs due to a pressure difference along any resistance in the system. The following are some factors that can cause small droplet sizes:

- Centrifugal Pump

- Hydrocyclone

- Valves

- Other restrictions in flow like elbows, tees or small line sizes

There are several solutions to minimise the risk of droplet breakup, which are:

- Gravity flow (not pumped) to the inlet piping

- Inlet piping straight for at least 10x pipe diameter upstream the separator

- Inlet piping containing a minimum of elbows, tees, valves and other fittings.

Since the flow loop is equipped with multiple pressure gauges, it can be rather easily investigated where such a pressure-drop occurs. To determine the quantity, samples are obtained at different points in the flow loop and the droplet size distribution is investigated. In the Process Flow Diagram (PFD) in figure 7.11 these "sweet spots" are numbered from 1 to 7. The colored dashed lines are there to indicate the relative oil intensity in that particular fluid line.

In order to find out which of these elements has the highest potential to create droplet breakup, a risk table is made (table 7.6). Each element is ranked from 1 - 3, where 1 is least and 3 is most likely to create droplet breakup. The table is based on the experience of the author.

Figure 7.11: PFD ProLabNL with "liquid-lines"
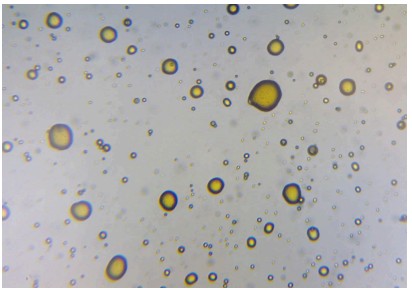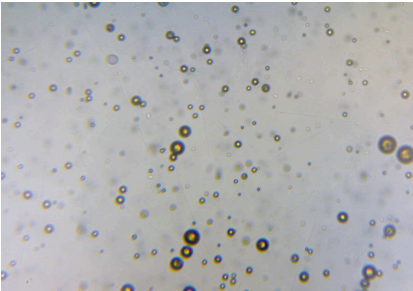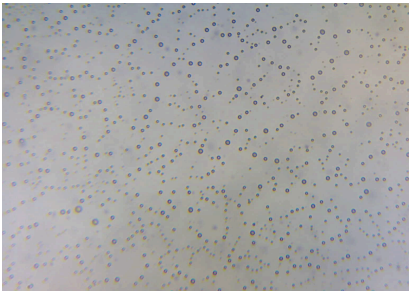
Table 7.6: Risk analysis

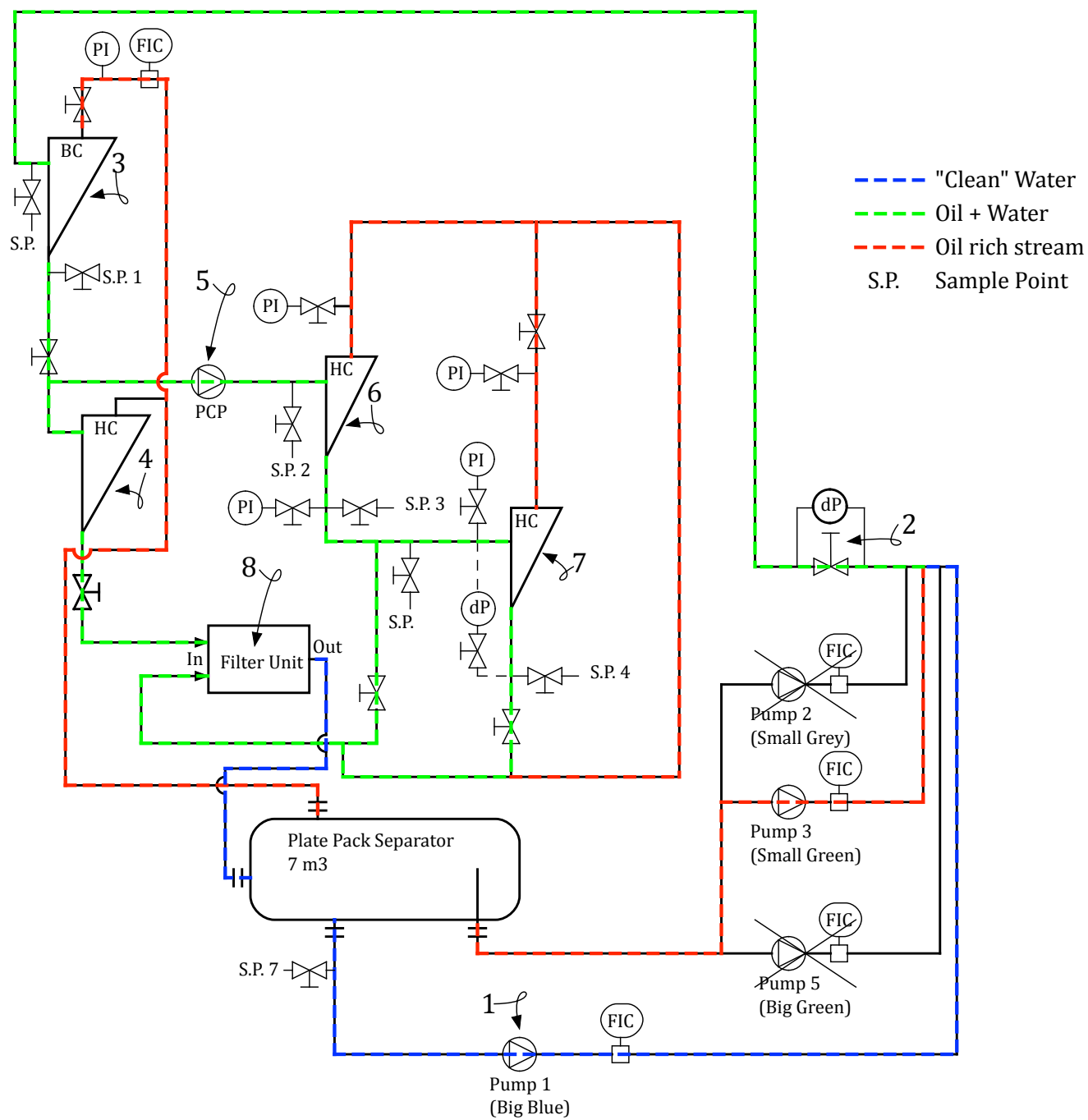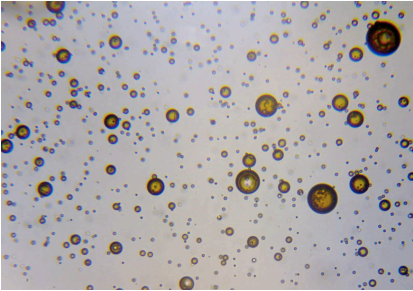| #	Component causing pressure-drop	Cause	Argument	Possibility
1	Water pump	Centrifugal Pump; creates shear because of the rotating impeller. The blades on the impeller wheel spin the water outwards with a high velocity.	Almost pure water, so OiW concentration is low, and therefore almost no droplets to be broken up.	1
2	Shear valve	Ball valve; mixes the oil and water into a homogenous oil-water mixture.	Pressure drop over valve is set at max. 0,5 [bar]. Based on previous experiments significant shearing starts at $\pm$ 3 - 4 bar dP.	1
3	2,5" Bulk de-oiling hydro-cyclone	Liquid-liquid cyclone; swirl is needed from high tangential velocities to achieve high accelerations leading to good separation. Turbulent shear stress and energy dissipation in the entry affect the size of the droplets.	Only swirling velocity with a pressure drop of $\pm$ 2 [bar] at the underflow, which is of importance since this flow will be directed as a feed for the next stage. This cyclone creates relative low shear due to its low swirl momentum at the blades of the cyclone.	1
4	2" Hydrocyclone	This hydrocyclone is not used for separation since its geometry/-model is out-dated.	Flow only exits through the lower outlet. This cyclone can be seen as a conduit with just a very low-pressure drop.	1
5	PCP	Progressive Cavity Pump; based on a stator and rotor principle, where fluids are pushed forwards. Are called low shear pump because of the low velocity.	This pump pushes an oil-water mixture forward, with a relative high OiW. Moreover a relative high pressure-drop is encountered over the pump. Both these cause a significant change in droplet size.	3
6	2" Hydrocyclone	Liquid-liquid cyclone; swirl is needed from high tangential velocities to achieve high accelerations leading to good separation. Turbulent shear stress and energy dissipation in the entry affect the size of the droplets.	Underflow pressure drop is $\pm$ 2,5x higher than the bulk cyclone. This hydrocyclone has been tested under ideal conditions (with separate oil and water tanks, so no background noise), which lead to almost no breakup of droplets.	1
7	1" Hydrocyclone	Liquid-liquid cyclone; swirl is needed from high tangential velocities to achieve high accelerations leading to good separation. Turbulent shear stress and energy dissipation in the entry affect the size of the droplets.	Underflow pressure drop is in the same range as the 2" hydrocyclone in point 6. This hydrocyclone has been tested under ideal conditions (with separate oil and water tanks, so no background noise), which lead to almost no breakup of droplets. However, based on the diameter (1"), the tangential velocity will be much higher than the 2" hydrocyclone.	2

7.4.3 Image analysis

For the image analysis *ImageJ* is used, which is a free cross-platform image analysis tool written by academics, and not commercial software developers. Below follows a stepwise description of determining the droplet size distribution based on the images in table 7.7. It must be noted that this procedure fits when the image has non-aggregating, spherical and high contrast objects when compared to the background. When the image is not suitable for automatic particle sizing, semi-manual or completely manual counting is performed.

Table 7.7: OiW samples before and after the pump

	Without hose	With hose
Pump in		
Pump out		

Automatic particle sizing

1. *Set scale.* In order for ImageJ to convert each pixel in the image to a length, the scale is set.

2. *Convert image to monochrome.* Here ImageJ converts the image to grey scale so that is does not need to worry about color, just about brightness.

3. *Set a threshold.* This is the most important part of the analysis. By setting the threshold, ImageJ exactly knows what comprises a droplet in this image. The aim is to define a "window of brightness" that represents particles in the image by changing the minimum and maximum brightness.

4. *Sizing.* ImageJ allows further tweaking of the image by setting controls on size and circularity. The latter is a measure of how circular each droplet is, whereby particles are modeled with ellipses. An ellipse with a circularity of 0 is a straight line, while an ellipse of 1 is a perfect circle.

Manual particle sizing

In case the image has a low contrast when comparing with the background, there is nothing for it but to manually select and measure the droplets. The problem is that there are numerous "vague droplets" at a lower depth in the image that are partially counted too. To solve this, the circumference will be drawn manually for which ImageJ then calculates the area.

7.4.4   Experimental setup

Table 7.6 now provides information on the elements to focus on. Components with a possibility of 1 or 2 will not considered for any further detailed analysis because based on the scenario description it can be concluded that they have a low possibility to create droplet breakup. This means that the progressive cavity pump will be analyzed for its influence on droplet breakup.

7.4.4.1   Test conditions

The test has been performed under one set of condition. Table 7.8 shows the outline of the test matrix. The values in the table are the settings.

Table 7.8: Conditions for droplet break-up test

	Setting	Dimension
Water flow rate	6,66	[m^3/h]
OiW	6%	
Oil flow rate	0,43	[m^3/h]
Flow to BC	7,09	[m^3/h]
Flow to HC 2"	3,00	[m^3/h]
Flow to HC 1"	0,7	[m^3/h]
Pressure outlet BC	4,75	[bar]
Pressure inlet HC	7,5	[bar]
Pressure drop over PCP	2,75	[bar]

7.4.4.2   Test procedure

Samples have been taken before and after the pump, being at S.P.1 and S.P.2 respectively, see figure 7.1. Since the digital OiW analyzer was not available, determination of the droplet size distribution has been performed in this fashion. In order to drain a representative sample, it is very important that the oil droplets are not broken up due to the pressure difference in the system and the sample bottle (atmospheric). Therefore a hose has been made where fluid is let into from which it is conveyed to the sample bottle by opening the hose very slowly. This procedure is illustrated in table 7.9.

Table 7.9: Sampling procedure

Diagram	Description
System S.P. — Hose Open Open Open	1 - Flushing the hose and remove all air
System S.P. — Hose Open Open Close	2 - Filling the hose by closing at one end
System S.P. — Hose Close Close Close	3 - System sample point and both hose valve are closed. Fluid is inside the hose.
System S.P. — Hose Close Close Open	4 - Slowly opening hose valve, reducing the pressure and fluid is conveyed to sample bottle. Fluids received upon opening hose valve are not used, since they may be broken up.

Only one hose has been used, so when draining at a different sample point the hose was flushed for 30 seconds with the fluid coming from that specific point. Moreover, in order to justify the advantage of draining with a hose also samples have been taken without a hose.

Immediately after sampling the samples have been analyzed with a microscope (type: Biolux NV 20x - 100x). The reason for this was because the oil droplets will separate out due to gravity and the sample will not be representative anymore. With a pipette fluid is extracted and a droplet is analyzed.

7.4.5 Results

ImageJ gives as output the area of a droplet. In order to obtain a distribution graph, the area is converted to the diameter. The settings for *ImageJ* are:

- Size: 0 - infinity
- Roundness: 0,00 - 1,00
- Scale: 1,071 pixels/Micron

The processing of the data is done with Excel, to which the output data from ImageJ is transferred. When plotting the distribution curve, a following curve is yielded:
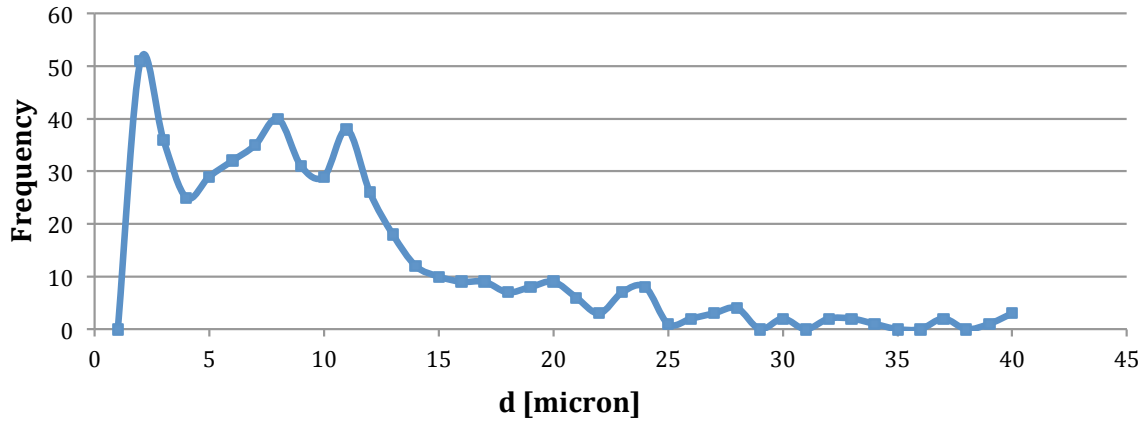
Figure 7.12: Distribution curve

When looking at the distribution graph in figure 7.12 it can be seen that it is not smooth[1]. There are spikes in the smaller diameters, which could be due to the following:

1. Droplets stacked on top of each other are being detected as one single one, giving a higher value to the range of droplets with bigger diameter.

2. Bigger droplets are easier to deform (due to fluid passing through a small orifice) which makes it more difficult to measure them.

3. Certain ranges not being detected will give a value equal to zero. This results in peaks.

4. Some ranges have not been detected well enough, which gives it a low value also resulting in some peaks.

In order to increase the accuracy of the results a possible approach could be to make a fit. The graph is assumed to be a lognormal distribution with skewness y $\neq$ 0.

Curve fitting
Since Excel does not have a built-in lognormal fit, this data will be fit with a Weibull distribution.

1. First the two unknown Weibull parameters λ & k need to be determined by linearization of the Weibull distribution:

$$y = 1 - e^{-(\frac{d}{\lambda})^k} \tag{7.3}$$

---

[1]Please note that this graph is only meant for illustrating the distribution based on the measured data.

$$\ln(1 - y) = \ln\left(e^{-\left(\frac{d}{\lambda}\right)^k}\right) \tag{7.4}$$

$$\ln(1 - y) = -\left(\frac{d}{\lambda}\right)^k \tag{7.5}$$

$$\ln(-\ln(1 - y)) = k \ln\left(\left(\frac{d}{\lambda}\right)\right) \tag{7.6}$$

$$\ln(-\ln(1 - y)) = k \ln(d) - k \ln(\lambda) \tag{7.7}$$

$$p = ax + b \tag{7.8}$$

with $a=k$ and $b=-k\ \ln(\lambda)$

2. Now that the equation has become linear, the parameters a & b can be determined by fitting the linear graph with Excel and displaying the equation on display.

3. Now that the parameters are determined the Weibull fit can be made.

4. A smooth curve based on the existing data is generated. This will result in the following red curve:
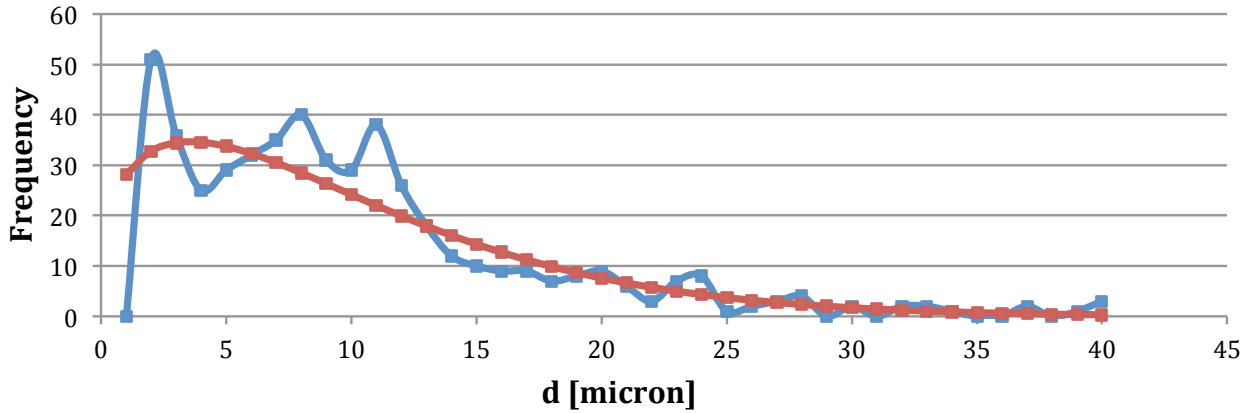
Figure 7.13: Non smooth distribution graph with fit

Still the results are not conclusive, because in the range of 0 - 10 [μm] the Weibull fit is not good enough. Moreover, what is missing in this graph is that even though there are bigger droplets their amount is negligible. Therefore the measured (blue) distribution curve will be weighted with the volume and then fitted with the Weibull distribution.

$$freq.(diameter) \rightarrow freq.(volume) = freq.(diameter) * \left(\frac{1}{6} * \pi * d^3\right) \tag{7.9}$$
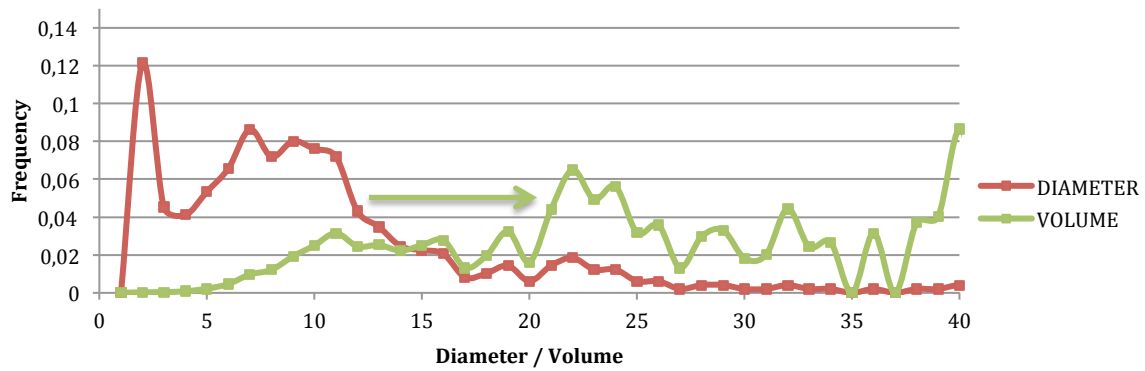
Figure 7.14: Weighted distribution graph with volume of droplets

Now when fitting the normalized volume distribution, the following Weibull graph can be yielded:
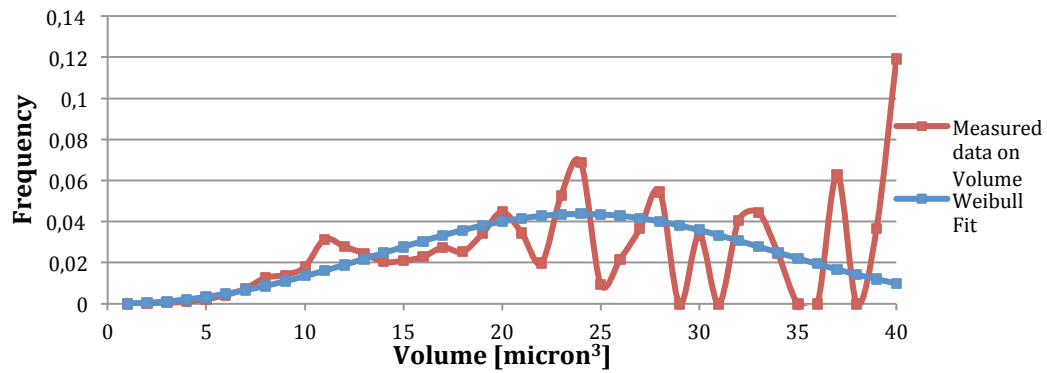
Figure 7.15: Weibull fit on volume distribution

From this graph it can be seen that the Weibull distribution is fitting the volume distribution better than the diameter distribution. In figure 7.16 the distribution curves are shown at the inlet and outlet of the pump. It is clearly visible that the curve shifts towards the left, concluding that the bigger droplets are broken up and fill up the range of the smaller droplets. The droplets of 40 micron are broken up and result in droplets of 10 micron.
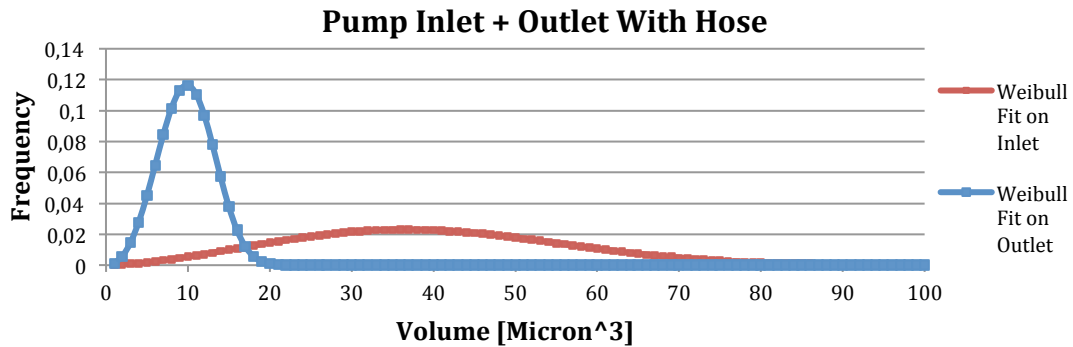
Figure 7.16: Weibull fit on volume distribution

Figure 7.17 shows that there are less small droplets on the background when using a hose as compared to sampling without a hose. The graph below shows that droplets are less sensitive to breakup when use has been made of a hose.

Table 7.10: OiW samples before and after the pump

	Without hose	With hose
Pump in		
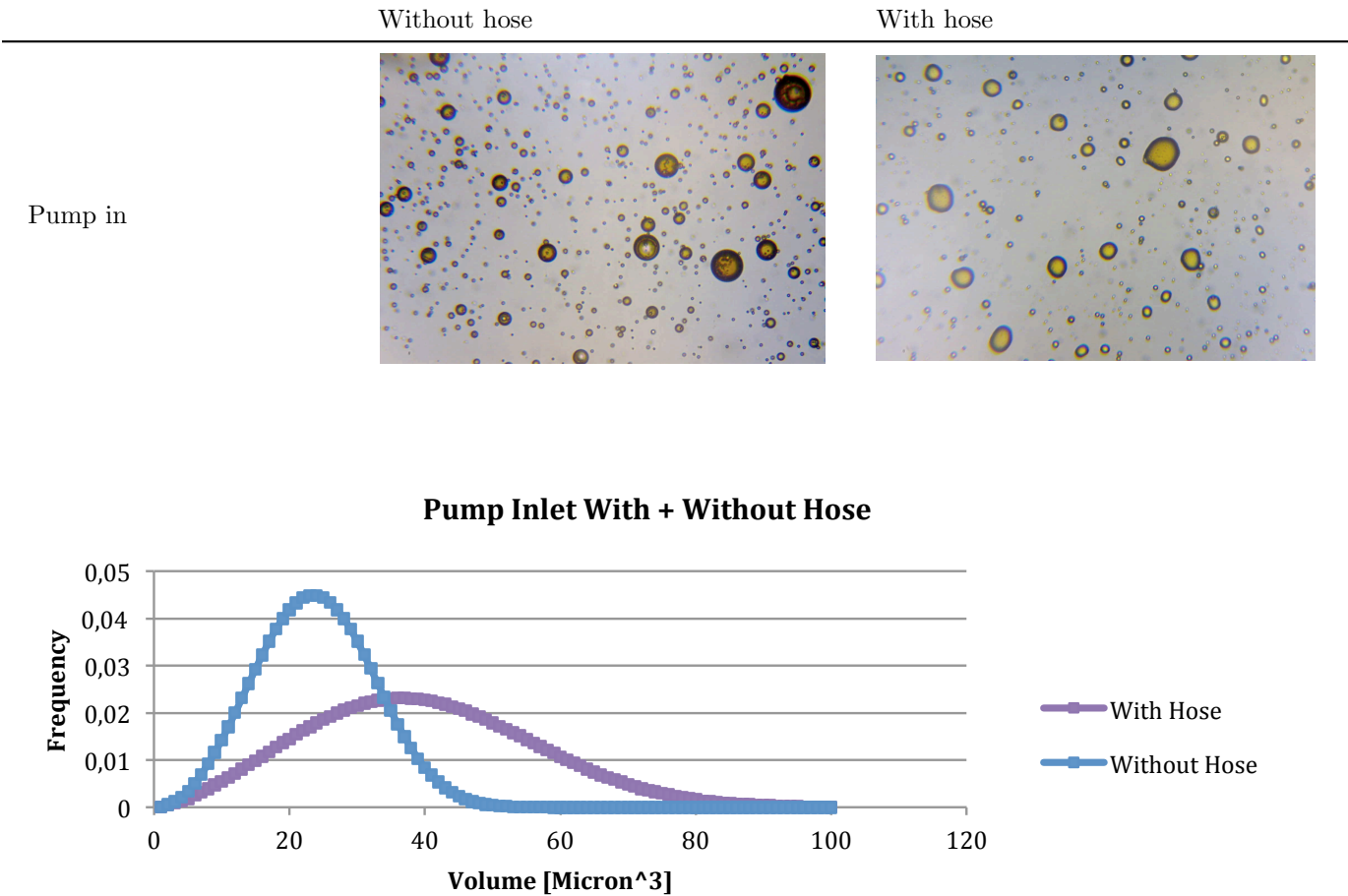
Figure 7.17: Influence of hose on droplet breakup

7.5 Discussion

The main goal of the experiments was to mimic downhole separation on topside facilities with downhole conditions. The de-sanding cyclone was not coupled with the three de-oiling stages in series due to the limitations of the test facility. Some aspects of the experimental results, and mainly why the expected efficiency could not be reached, will be discussed here.

Why the expected efficiency could not be obtained
Based on the results in section 7.3 it can be seen that the first stage separation, bulk de-oiling hydrocyclones, have a good performance. The bulk of the oil is separated out whereby the underflow outlet is the feed for the 2" hydrocyclone.
Having all other fluid properties the same, the droplet size distribution is severely altered as the fluid is lead to the next stage. It was found out that the pump in between the first and second stage causes most of the shearing. Before investigating the influence of the PCP due to shearing, several steps were carried out to alter the process and mechanical conditions to reach the desired results.

- The OiW% was changed from initially 10% to 5% and even as low as 2% to see if the bulk de-oiling hydrocyclone was capable of separating out such high oil concentration. Since the oil droplets in the reservoir tank need time to rise to the surface, the flowloop was paused for 1 day every time. As a rule of thumb (Chapter 4) the bulk de-oiling hydrocyclone should produce $\pm$ 50% reject, which was the case (sample jar "BCR" in figure 7.7 illustrates this). However, the change in oil concentration did not lead to a change in the overall separation efficiency.

- The temperature was increased from an initial 45 to 75 °C to alter the water viscosity. The heating took one day, after the desired temperature was reached the flowloop was operated. The performance was enhanced but after $\pm$ 30 min the quality of the water started showing a steep decrease. Only one frequency-drive was available (to either drive the heater or the PCP) it was used to operate the PCP and therefore the temperature of the water went down.

- The 2" and 1" hydrocyclones were bypassed and the 2,5" bulk de-oiling hydrocyclone was tested separately. This showed an oil concentration in the reject jar of $\pm$50% which is a good reference of the performance.

The reason this turndown in separation efficiency was not anticipated is due to preceding experimental tests with two separation stages with promising results. One of the mistakes was the assumption that the PCP would be less susceptible to shearing, even for higher pressure-drops. Two solutions are proposed to increase the separation efficiency:

- One of the great benefits of installing a cyclonic separator downhole is the benefit of oil droplets being in the mm-range [1], enhancing the separation efficiency. In order to mimic this situation for topside testing a suitable solution would be to use three reservoir tanks (instead of one), one with water, one with oil and one for disposal. In this manner the background noise is eliminated out of the system. However by doing so the original flowloop should be modified too much leading to higher costs which is beyond the scope of this project.

- Another option could be to "chop" the three separation stages into two separate systems and correlate the data with each other. A possible setup could be to couple the 2,5" & 2" cyclones and separately test the 1" hydrocyclone. However, even though this strategy has been performed in the past, the results cannot be taken as conclusive in comparison with three consecutive separation stages because the outlet conditions of the 2" hydrocyclone, being the flowrate, OiW% and the droplet size, are set manually to the inlet of the 1" hydrocyclone. It is practically impossible to set the outlet conditions the same as the inlet conditions.

Results accuracy

The analysis of the samples as depicted in figure 7.7 is performed in-house by skilled ProLabNL personnel in the fluid property characterization laboratory. The results are therefore accurate. The droplet breakup during sampling (from system pressure to atmospheric bottle pressure) is not relevant since only the concentration is important.

As mentioned earlier the digital OiW analyzer was not available and a fast and a relative reliable way was proposed by using a hose to minimize the droplet breakup and *ImageJ* to determine the droplet sizes. The benefit of such a system is the simplicity and time efficiency, since samples were able to taken within ± 1 hour. The disadvantage is the lack of data to verify the results with. Even though the aim is to see a shift in droplet size distribution before and after the pump, the quantity is important to verify arguments made in table 7.6 based on the experience of the author. Secondly, it can be incorporated in the hydrocyclone model in order to judge whether the amount of breakup influences the efficiency. The use of a hose can be argued, even though the results are as expected, droplets in the hose can coalesce or the sample droplet on the microscope is a lucky shot. Multiple drains need to be conducted at several places with precision to confirm that a hose is less sensitive to droplet breakup.

As described in section 7.5.3. the most important step for automatic particle sizing is setting the threshold, which is an effective method for measuring complex attributes in an image. This step replaces a time consuming task by hand by only shifting two sliders. However, when a humans eye looks at an image it is extremely good at filtering out what we are interested in, regardless of how complex the image may be. *ImageJ* has no intuitive moves and will take all the information in the image and treat it equally. If a lost pixel falls within a threshold range it will be counted, even though the humans eye sees it as a false.

Chapter 8

Conclusions & Recommendations

8.1 Conclusions

A prototype downhole separator with a de-sanding unit was designed and tested both numerically and experimentally. After considering several equipment configurations, it was concluded from processing and mechanical versatility, that it would be best to have a system that separates out most of the sand out of the total flow before de-oiling. The separation performance of the three liquid-liquid stages in series were established but the desired results could not be met due to droplet breakup caused in the system.

The conclusions are divided into four sections, whereby the first is regarded to the design of the downhole separator. Secondly, conclusions are drawn regarding the CFD simulations after which conclusions on the experimental procedures are shown.

Design of the downhole separator

- The performance of the hydrocyclones are highly sensitive to droplet breakup. Therefore no ESP will be installed prior to the separator.

- The separation efficiency is dependent on the DPR and therefore influenced by the suction of the upstream ESP.

- To prevent erosion of the 3 consecutive hydrocyclone stages a de-sander is installed. The author reviewed several options for the position of the de-sander and the most viable position was to place it above all the other elements to knock out the most of the sand before de-oiling.

- A recital has been made between storing the sand downhole or flushing it to the surface with the rejects of the hydrocyclones. The latter has been chosen, with both the consideration of erosion and not optimal DPR of the bulk de-oiling hydrocyclones, however, ensuring continuous sand transportation to the surface.

- A packer was placed between the production and injection intervals to isolate the zones.

- Two DOWS designs are proposed. The second design where the 2,5" and 2" hydrocyclones are placed in a tubular is most favorite for work-over reasons, rigidness and relative easy assembling.

- The configuration of the liners and tubulars in a narrow wellbore is successfully solved.

Use of CFD for downhole separation

- The simulated Venturi model has been successfully implemented to investigate the PDR of the bulk de-oiling hydrocyclone for different pump inlet pressures.

- Even though a flow reducer is installed at the outlet of the de-sander, the pressure and therefore the reject rate is strongly dependent on the pressure at the riser outlet. Since the ESP is mounted at the riser outlet, the inlet pressure should be maintained at the same value as the de-sander outlet.

- The aim is to create a pressure drop of 6 [bar], from 138 to 132 [bar]. By doing so, the restriction becomes very narrow and the angle of the wall, β (figure 6.17), becomes steep resulting in a higher erosion rate. A recital should be made between generating the desired pressure-drop and accepting the corresponding high erosion rate or a somewhat lower pressure drop due to the sensitivity of the reducer to higher erosion and not having the correct DPR of the bulk de-oiling hydrocyclones.

Experimental procedures

- The bulk de-oiling hydrocyclone shows high separation performance as it separates out most of the oil in the first stage, reaching an efficiency of 97%.

- The 2" and the 1" hydrocyclone show poor separation efficiency due to the PCP which imparts the oil droplets.

- A follow-up experiment is needed with sand in order to say something about the behavior of the three liquid hydrocyclones in series.

8.2   Recommendations

The recommendations are grouped in the same fashion as the conclusions. The first is regarded to the design of the downhole separator, the second is regarding the CFD simulations after which follows the experimental procedures.

Design of the downhole separator

- As stated in paragraph 5.3 the fluid column in the wellbore can pass the inlet of the DOWS, which could potentially lead to only influx of water. A further analysis should be performed to examine the performance of the DOWS with respect to the change in reservoir production.

- The second design is preferred over the first design as such a system has an advantage in the assembly and de-assembly of the parts since only a single tubular piece needs to be replaced.

- Examine the DOWS design from a mechanical design point of view.

- Outline the factors that make up the economic decision whether to install such a system.

Use of CFD for downhole separation

- In order to minimize the erosion impact, the steepness of the nozzle part of the reducer should be lowered, i.e. a longer nozzle length.

- Couple the third and fourth separation stage to the first and second separation stage.

Experimental procedures

- Operating the flowloop with two people.

- The influence of the filter unit has to be investigated on the shearing effect in the flowloop.

- Use separate liquid reservoir tanks to test the flowloop.

- Conduct a physical test on the reducer to examine the erosion rate to verify the CFD model.

Nomenclature

α	Impact angle of particles hitting the wall	[°]
Δm	Thickness of porous medium	[m]
δ	Permissible pressure ratio	[-]
ε	Density ratio between motive and suction fluid	[-]
μ	Fluid viscosity	[cP]
μ	Mass flow ratio between motive and suction fluid	[-]
μm	Micro meter	[m]
η	Separation efficiency	%
ω	Angular velocity	[m/s]
ρ	Fluid density	[kg/m^3]
ρ_t	Density of target material	[kg/m^3]
A_t	Area exposed to erosion	[m^2]
C_i	Porous jump coefficient at position i	[1/m]
D	droplet diameter	[m]
D_o	Diameter overflow outlet Colman-Thew hydrocyclone	[m]
ΔP_{over}	Pressure-drop at overflow	[Pa]
ΔP_{under}	Pressure-drop at underflow	[Pa]
ΔP_{DOWS}	Pressure-drop over the downhole separator	[Pa]
$\Delta P_{P.J.}$	Pressure-drop over porous jump	[Pa]
DS	De-sander cyclone	
D_u	Diameter underflow outlet Colman-Thew hydrocyclone	[m]
DV_{50}	Median particle size by volume	[m]
$\dot{E}$	Erosion rate	[mm/year]
E_L	Erosion rate referred to depth	[mm/year]
E_m	Erosion rate referred to the mass of eroded material	[mm/year]
ESP	Electrical Submersible Pump	

$F(\alpha)$	Function characterizing ductility of the material	[-]
g	Gravitational constant equal to 9.81	[m/s^2]
HC	Hydrocyclone	
K	Material constant	[(m/s)$^{-n}$]
LLC	Liquid-liquid cyclone	
ln	Logarithm with base e	
$\dot{M}$	Mixed mass flow	[kg/h]
$\dot{M}_p$	Mass flow of sand	[kg/s]
n	Velocity exponent	[-]
OiW	Oil in Water	%
P	Pressure	[Pa]
P_{abs}	Absolute pressure	[Pa]
P_{atm}	Atmospheric pressure	[Pa]
$P_{BC;In}$	Pressure at inlet of bulk de-oiling hydrocyclone	[Pa]
$P_{BC;R}$	Pressure at reject of bulk de-oiling hydrocyclone	[Pa]
PDR	Pressure difference ratio	[-]
$P_{DS;R}$	Pressure at de-sander reject	[Pa]
$P_{DS;Out}$	Pressure at de-sander outlet	[Pa]
P_{gauge}	Gauge pressure	[Pa]
P_{in}	Inlet pressure	[Pa]
P_{over}	Pressure at overflow outlet	[Pa]
ppm	Parts per million	[-]
P_{res}	Reservoir pressure	[Pa]
P_{under}	Pressure at underflow	[Pa]
Q	Volumetric flowrate	[m^3/h]
r	Radius of the circular path inside the hydrocyclone	[m]
R	Reject rate	%
U_p^n	Particle impact velocity	[m/s]
v	Velocity	[m/s]
v_{rad}	Radial velocity	[m/s]
V_t	Terminal settling velocity	[m/s]
y	Skewness factor	[-]

Appendix A

Discretization of the Navier Stokes equation

For an incompressible and homogenous fluid, considering the pressure, external forces and viscous stresses, the Navier-Stokes equation can be written as follows:

$$\frac{\delta v}{\delta t} + (v \cdot \nabla) + \nabla p = \mu \Delta v \tag{A.1}$$

In this equation v and p are the unknowns, the velocity and pressure of (for example) running water and μ is the viscosity. When putting $\mu=0$, then (A.1) becomes the Compressible Euler equation. The symbol ∇ is also present in the right hand side of equation (A.1):

$$\nabla \cdot v = 0 \tag{A.2}$$

Equation (A.2) represents the incompressibility of the fluid. The left hand side of (A.1) describes how under the influence of pressure differences and other in water acting forces the flow and corresponding pressure changes. Two equations for two unknowns, from which p can be eliminated. The problem is that nobody knows whether equation (A.1) is sufficient to describe the flow. The acceleration term is not only

$$\begin{pmatrix} \frac{\partial v_1}{\partial t} \\ \frac{\partial v_2}{\partial t} \\ \frac{\partial v_3}{\partial t} \end{pmatrix} \tag{A.3}$$

the vector with the partial derivatives

$$\frac{\partial v_1}{\partial t}, \frac{\partial v_2}{\partial t}, \frac{\partial v_3}{\partial t}, \tag{A.4}$$

of v_1, v_2 and v_3 with respect to t, but also contains a part in which $v \cdot \nabla$ works on v. Here ∇ denotes for gradient operator:

$$\nabla = \begin{pmatrix} \frac{\partial}{\partial x_1} \\ \frac{\partial}{\partial x_2} \\ \frac{\partial}{\partial x_3} \end{pmatrix} \tag{A.5}$$

and the point denotes the dot product, so:

$$v \cdot \nabla = \begin{pmatrix} v_1 \\ v_2 \\ v_3 \end{pmatrix} \cdot \begin{pmatrix} \frac{\partial}{\partial x_1} \\ \frac{\partial}{\partial x_2} \\ \frac{\partial}{\partial x_3} \end{pmatrix} = v_1 \frac{\partial}{\partial x_1} + v_2 \frac{\partial}{\partial x_2} + v_3 \frac{\partial}{\partial x_3} \tag{A.6}$$

such that

$$(v \cdot \nabla)v = v_1 \frac{\partial v}{\partial x_1} + v_2 \frac{\partial v}{\partial x_2} + v_3 \frac{\partial v}{\partial x_3} \tag{A.7}$$

In the second equation of the Navier-Stokes, (A.8) resembles the *divergence* of v.

$$\nabla \cdot v = \begin{pmatrix} \frac{\partial}{\partial x_1} \\ \frac{\partial}{\partial x_2} \\ \frac{\partial}{\partial x_3} \end{pmatrix} \begin{pmatrix} v_1 \\ v_2 \\ v_3 \end{pmatrix} = \frac{\partial v_1}{\partial x_1} + \frac{\partial v_2}{\partial x_2} + \frac{\partial v_3}{\partial x_3} \tag{A.8}$$

If the first component v_1 in the x_1-direction increases or decreases, then, downstream, the fluid will be pulled apart or pushed together. The same holds for the x_2 and x_3-direction. The extent to which this happens is quantified by:

$$\frac{\partial v_1}{\partial x_1}, \frac{\partial v_2}{\partial x_2}, \frac{\partial v_3}{\partial x_3} \tag{A.9}$$

But due to the fact that water is incompressible and non extendable, these three have to compensate each other. In other words, the sum of the three partial derivatives should be zero.

$$\nabla \cdot v = \begin{pmatrix} \frac{\partial}{\partial x_1} \\ \frac{\partial}{\partial x_2} \\ \frac{\partial}{\partial x_3} \end{pmatrix} \begin{pmatrix} v_1 \\ v_2 \\ v_3 \end{pmatrix} = \frac{\partial v_1}{\partial x_1} + \frac{\partial v_2}{\partial x_2} + \frac{\partial v_3}{\partial x_3} = 0 \tag{A.10}$$

Appendix B
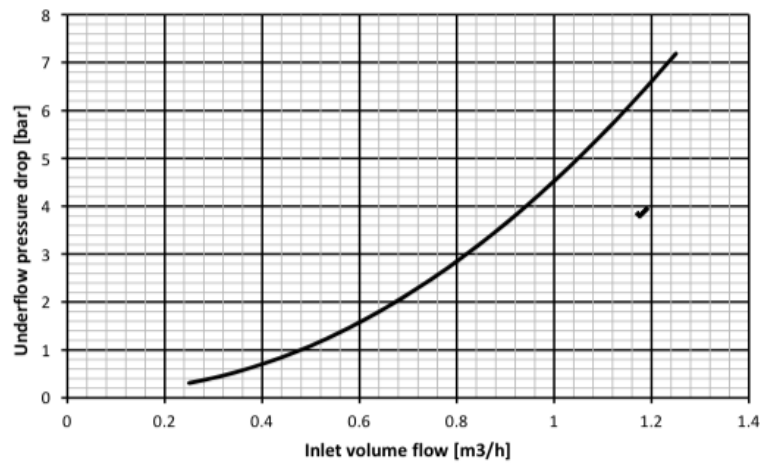
Hydrocyclone pressure-drop curves

Figure B.1: 1" hydrocyclone underflow pressure-drop
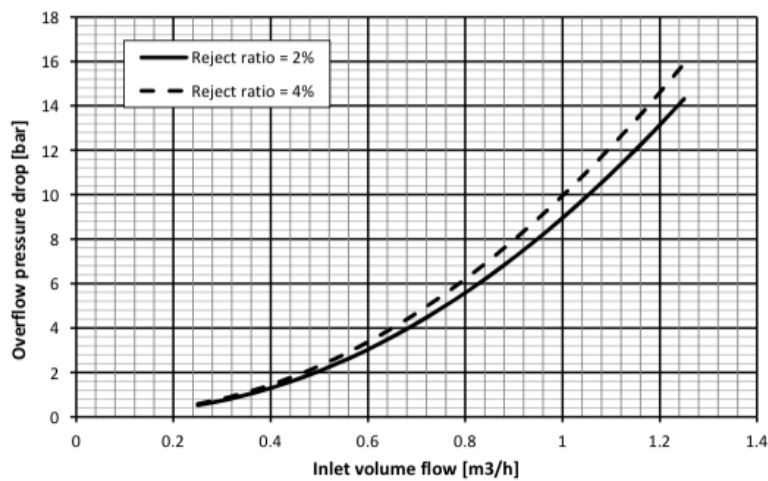
Figure B.2: 1" hydrocyclone overflow pressure-drop
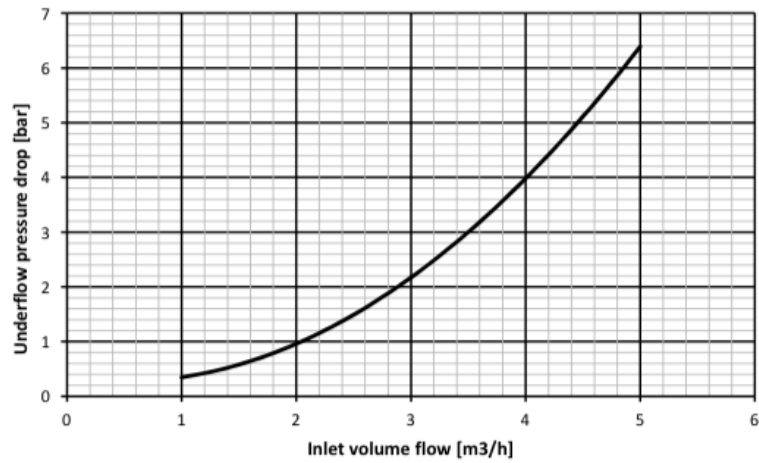
Figure B.3: 2" hydrocyclone underflow pressure-drop
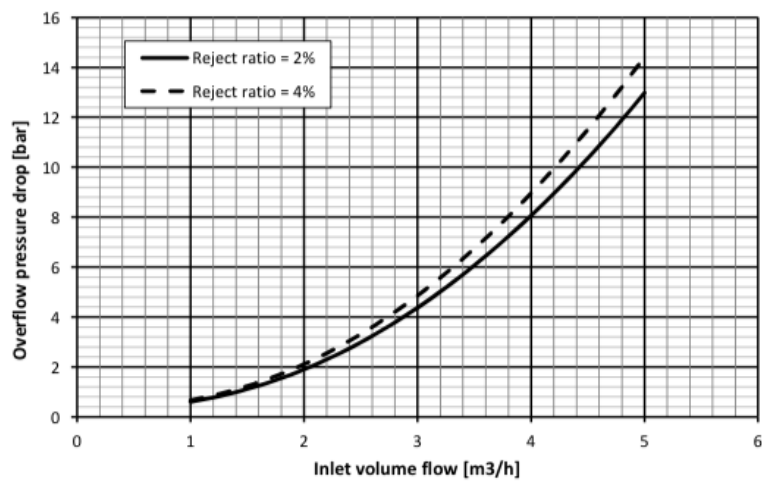
Figure B.4: 2" hydrocyclone overflow pressure-drop

Appendix C

CFD Venturi model pressure-drop curves
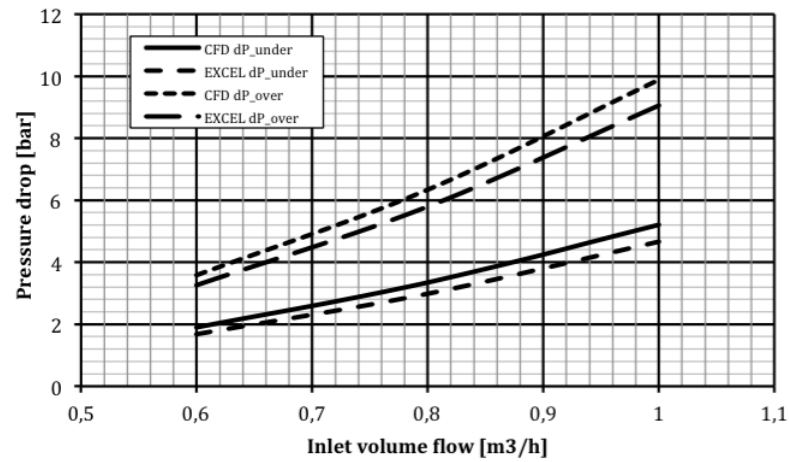
Figure C.1: 1" hydrocyclone CFD Venturi model pressure-drop curve at 2% reject rate

Figure C.2: 1" hydrocyclone CFD Venturi model pressure-drop curve at 4% reject rate

Figure C.3: 2" hydrocyclone CFD Venturi model pressure-drop curve at 2% reject rate

Figure C.4: 2" hydrocyclone CFD Venturi model pressure-drop curve at 4% reject rate

Appendix D

Test matrix

Water	1000	kg/m3	
Oseberg	835	kg/m3	
Grane	939,4	kg/m3	(density based on 15°C)

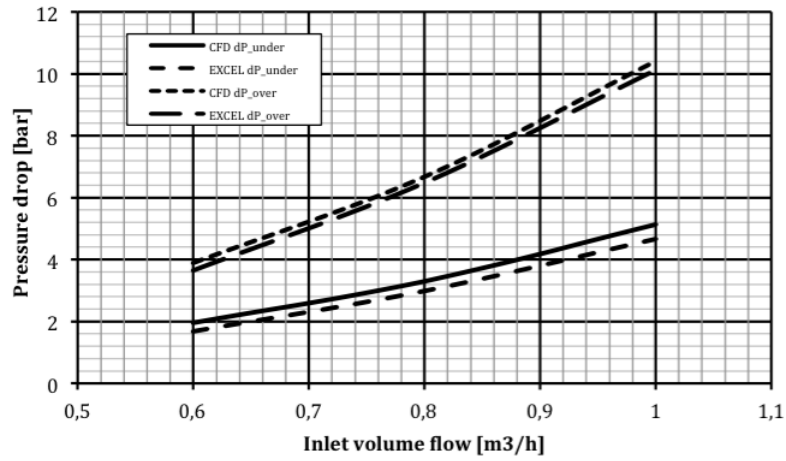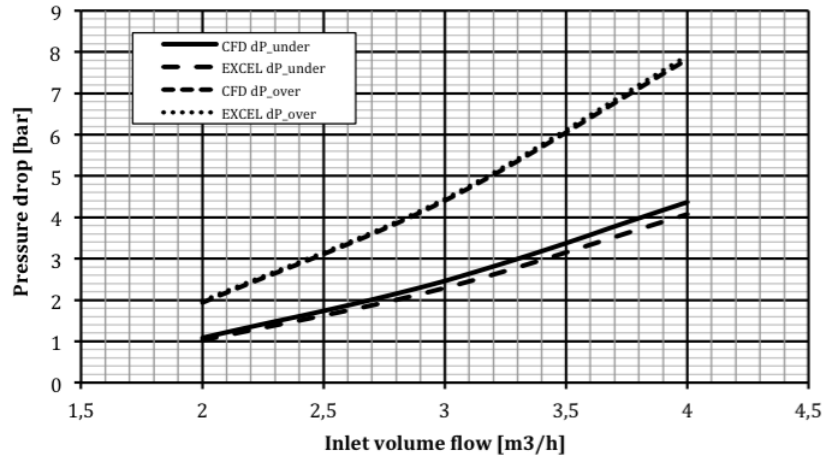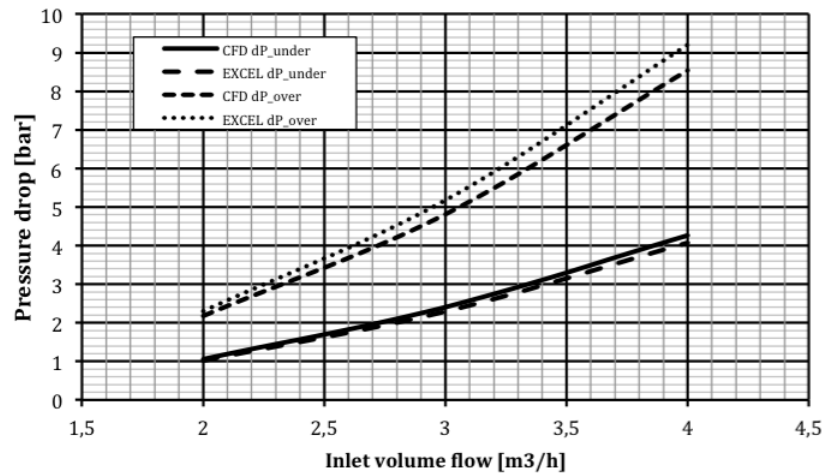| INUT DATA														
Measurement nr	PFD	# Active bulk liners	# Active hydrocyclone liners	# Active hydrocyclone liners	Type oil	Oil density	Layout	Temperature	Shear Valve dP	Water Flow to BC	Oil Flow to BC	Total Flow to BC	Flow to HC	Flow to HC
		D0904-011-FAB-0450	D0904-009-FAB-080	D0904-009-FAB-103						FAB 050	FAB 050	FAB 050	FAB 081	FAB 103
		Bulk De-Oiling Cyclone	Hydrocyclone	Hydrocyclone		[kg/m3]	-	[°C]	[Bar]	[m3/h]	[m3/h]	[m3/h]	[m3/h]	[m3/h]
L1	Rev1	2	1	1	Grane	939,4	BC + HC+HC	45	0,00	6,66	0,21	6,87	3,00	0,7
L2	Rev1	2	1	1	Grane	939,4	BC + HC+HC	45	0,00	6,66	0,21	6,87	3,00	0,9
L3	Rev1	2	1	1	Grane	939,4	BC + HC+HC	45	0,00	6,66	0,43	7,09	3,00	0,7
L4	Rev1	2	1	1	Grane	939,4	BC + HC+HC	45	0,00	6,66	0,43	7,09	3,00	0,9
L5	Rev1	2	1	1	Grane	939,4	BC + HC+HC	45	0,00	6,66	0,74	7,40	3,00	0,7
L6	Rev1	2	1	1	Grane	939,4	BC + HC+HC	45	0,00	6,66	0,74	7,40	3,00	0,9
L7	Rev1	2	1	1	Grane	939,4	BC + HC+HC	45	0,00	9,34	0,29	9,63	3,00	0,7
L8	Rev1	2	1	1	Grane	939,4	BC + HC+HC	45	0,00	9,34	0,29	9,63	3,00	0,9
L9	Rev1	2	1	1	Grane	939,4	BC + HC+HC	45	0,00	9,34	0,60	9,94	3,00	0,7
L10	Rev1	2	1	1	Grane	939,4	BC + HC+HC	45	0,00	9,34	0,60	9,94	3,00	0,9
L11	Rev1	2	1	1	Grane	939,4	BC + HC+HC	45	0,00	9,34	1,04	10,38	3,00	0,7
L12	Rev1	2	1	1	Grane	939,4	BC + HC+HC	45	0,00	9,34	1,04	10,38	3,00	0,9

Inlet OiW	Reject Rate BC	Reject Rate BC	Reject Rate HC	Second Bypass		dP_Out	dP_rej	dP_Out	dP_rej	dP_Out	dP_rej
To FAB 050	FAB 050	FAB 050	FAB 081	To Filter Unit		FAB 050	FAB 050	FAB 081	FAB 081	FAB 103	FAB 103
[%]	[%]	[m3/h]	[%]	[m3/h]		[Bar]	[Bar]	[Bar]	[Bar]	[Bar]	[Bar]
3%	6%	0,41	4%	2,18		1,09	1,56	2,17	4,34	2,16	4,32
3%	6%	0,41	4%	1,98		1,09	1,56	2,17	4,34	3,64	7,28
6,00%	12%	0,85	4%	2,18		1,09	1,56	2,17	4,34	2,16	4,32
6,00%	12%	0,85	4%	1,98		1,09	1,56	2,17	4,34	3,64	7,28
10%	20%	1,48	4%	2,18		1,09	1,56	2,17	4,34	2,16	4,32
10%	20%	1,48	4%	1,98		1,09	1,56	2,17	4,34	3,64	7,28
3%	6%	0,58	4%	2,18		2,23	3,19	2,17	4,34	2,16	4,32
3%	6%	0,58	4%	1,98		2,23	3,19	2,17	4,34	3,64	7,28
6,00%	12%	1,19	4%	2,18		2,23	3,19	2,17	4,34	2,16	4,32
6,00%	12%	1,19	4%	1,98		2,23	3,19	2,17	4,34	3,64	7,28
10%	20%	2,08	4%	2,18		2,23	3,19	2,17	4,34	2,16	4,32
10%	20%	2,08	4%	1,98		2,23	3,19	2,17	4,34	3,64	7,28

Figure D.1: Test matrix

Appendix E

Derivation set of equations for CFD Venturi model

The equations below are based on the geometry in figure 6.4.

1. The pressure-drop in the throat can be described by the Bernoulli equation:

$$\Delta P_{Bernoulli} = \frac{1}{2}\rho v_3^2 - \frac{1}{2}\rho v_1^2 \tag{E.1}$$

2. An inlet resistance will imposed, being a porous jump coefficient C_1. This creates the pressure drop from the inlet to the outlet (underflow):

$$\Delta P_{P.J.1} = C_1 v_1^2 \tag{E.2}$$

3. A porous jump coefficient C_4 will be imposed at the overflow to ensure the PDR for different reject rates:

$$\Delta P_{P.J.4} = C_4 v_4^2 \tag{E.3}$$

4. The pressure drop at the overflow will be the sum of:

$$\Delta P_{overflow} = \Delta P_{P.J.1} + \Delta P_{Bernoulli} + \Delta P_{P.J.4} \tag{E.4}$$

$$C_1 v_1^2 + \left(\frac{1}{2}\rho v_3^2 - \frac{1}{2}\rho v_1^2 \right) + C_4 v_4^2 \tag{E.5}$$

5. The "Pressure Difference Ratio" is defined as the ratio between pressure drop from inlet $\rightarrow$ overflow and inlet $\rightarrow$ underflow:

$$DPR = \frac{\Delta P_{overflow}}{\Delta P_{P.J.1}} \tag{E.6}$$

6. The pressure at porous jump C_1 is equal to the pressure at the underflow:

$$P_{P.J.1} = P_{underflow} \tag{E.7}$$

7. R being the reject rate:

$$Q_{overflow} = R * Q_{in} \tag{E.8}$$

8.

$$v_1 = \frac{Q_{in}}{A_{in}} \tag{E.9}$$

9.

$$v_3 = \frac{v_1 A_1}{A_3} \tag{E.10}$$

10.

$$v_4 = R\frac{v_1 A_1}{A_4} \tag{E.11}$$

Bibliography

[1] Danyluk, T.L, Chachula, R.C. and Solanki, S.C. 1998. "Field Trial of the First Desanding System for Downhole Oil/Water Separation in a Heavy-Oil Application". 1998 SPE Technical Conference and Exhibition, New Orleans, Louisiana, September 27-20. SPE 49053.

[2] Scaramuzza, J. L., Fischetti, H., Strappa, L., and Figliuolo, S. "Downhole Oil/Water Separation System-Field Pilot-Secondary Recovery Applicaation Project". SPE paper 69408 presented at the SPE Latin Ameerica and Caribbean Petroleum Engineering Conference, Buenos Aires, Argentina, March 25-28. 2001.

[3] Alhoni, M.A., Jerbi, K.Khalid, Drawil, T.A., and Zekri, A.Y. "Application of Downhole Oil-Water Separation: A Feasibility Study". SPE paper 80485 presented at the 2003 SPE Asia Pacific Oil and Gas Conference, Jakarta, Indonesia, 9-11 Sept.

[4] J.A. Veil and J.J. Quinn. "Performance of Downhole Separation Technology and its Relationship to Geologic Conditions". *SPE*, March 2005, SPE 93920

[5] Verbeek P.H.J and Smeenk R.G. "Downhole separator produces less water and more oil". SPE 50617. 1998 SPE European Petroleum Conference, The Hague, The Netherlands, 20-22 October 1998.

[6] Kjos, T., Sangesland, S., Michelet, J.F., Kleppe, J., 1995. "Downhole water?oil separation and water reinjection through well branches". SPE 30518. Presented at SPE Annual Technical Conference and Exhibition, Dallas, TX, October 22?25.

[7] S. Suarez and A. Abou-Sayed. "Feasibility of Downhole Oil/Water Separation and Reinjection in the GOM", SPE paper 57285, presented at the 1999 SPE Asia Pacific Improve Oil Recovery Conference, Kuala Lumpur, October 25-26.

[8] Ogunsina, O.O., Wiggins, M.L. "A Review of Downhole Separation Technology", SPE paper 94276 presented at the 2005 SPE Production and Operations Symposium, Oklahoma, April. 16-19.

[9] Loginov, A., and Shaw, C. "Completion Design for Downhole Water and Oil Separation and Invert Coning", SPE paper 38829, Proc. 72nd Annual Technical Conference and Exhibition of SPE, San Antonio, Texas, October 5-8, 1997; J. Petroleum Technology, March 1998.

[10] Bowers B.E , Brownlee R.F and Schrenkel P.J. "Development of a downhole oil/water separation and reinjection system for offshore application". OTC 8865. OTC Houston, Texas , 4-7 May 1998.

[11] Ed. Sheridan, Ian Ayling, Jordan Hixson. Downhole Oil and Water Separation: A New Start. March 2013. IPTC 16914.

[12] B.R. Peachy, S.C. Solanki, T.A. Zahacy, K. Piers. Downhole Oil/Water Separation Moves into High Gear. July 1998, Volume 37, No. 7, The Journal of Canadian Petroleum Technology.

[13] John A. Veil and John J. Quinn. "Downhole Separation Technology Performance: Relationship to Geologic Conditions". Prepared for U.S. Department of Energy, National Energy Technology Laboratory. November 2004.

[14] Veil, J.A., Langhus, B.G., Belieu, S. "Feasibility evaluation of downhole oil/water separator (DOWS) technology". In: Report prepared for US Department of Energy under Contract W-31-109- Eng-38, January 1999.

[15] J.E. Mendonca. Deepwater Installation of an Electrical Submersible Pump in Campos Basin, Brazil. *OTC*, May 1997.

[16] Jan-Dirk Jansen. Nodal Analysis of Oil and Gas Production Systems. Lecture notes for course AES1360 'Production Optimisation'. Version 12a, May 2013.

[17] Janssen, P.H.: "Characterisation of oil-water mixtures produced in high-watercut oil wells", Ph.D.-thesis, Delft University of Technology, June 2000.

[18] Young, G., Walkley, W., Taggart, D., Andrews, S. and Worrel, J., 1990, "Oil-Water Separation Using Hydrocyclones: An Experimental Search for Optimum Dimensions". American Filtration Society, Advances in Filtration and Separation Technology, Vol.3, Conference held in Baton Rouge, Louisiana.

[19] Jeff Knight et al., Petroleum Technology Transfer Council. Downhole water separation technologies

[20] Muecke, N. B., Kappelhoff, G. H. and Watson, A. 2002. ESP Design Changes for High GLR and High Sand Production; Apache Stag Pro- ject. Paper SPE 77801 presented at the SPE Asia Pacific Oil and Gas Conference and Exhibition, Melbourne, Australia, 8?10 October.

[21] Zhang, N.S., Somerville, J.M., and Todd, A.C. 1993. An Experimental Investigation of the Formation Damage Caused by Produced Oily Water Injection. Paper SPE 26702 presented at Offshore Europe, Aberdeen, 7?10 September.

[22] M. Narasimha, R.Sripriya, P.K. Banerjee, 2003, "CFD modelling of hydrocyclone-prediction of cut size", International Conference on Quantitative approaches in mineral processing (QAMP-2003), held on July 3-5, at Bhubaneswar, India.

[23] Staff, November 24 2010. "Taqa's Rijn oilfield opens after 12 years". http://www.emirates247.com/business/energy/taqa-s-rijn-oilfield-opens-after-12-years-2010-11-24-1.320713

[24] Liquid jet liquid pump, General information. GEA Wiegand GmbH. www.gea-wiegand.com

[25] Buret, S., Nabzar, L., and Jada, A. 2010. "Water Quality and Well Injectivity: Do Residual Oil-in-Water Emulsions Matter?" SPE J. 15 (2): 557-568. SPE-122060-PA.

[26] T.E.W. Nind, J. H. Nind (1989). "Hydrocarbon Reservoir and Well Performance". New York, USA. Chapman and Hall.

[27] Ansys Fluent 15.0 User Manual, ANSYS Inc., November 2013.

[28] Software-Factory Norbert Schmitz. "Pressure-drop calculator". http://www.pressure-drop.com/Online-Calculator/

[29] I. Finnie: "Erosion of Surfaces by Solid Particles". Wear 1960; 3:87-103

[30] DNV RP O501 (Revision 4.2 - 2007), "DNV Recommended Practice RP O501 - Erosive Wear in Piping Systems", (DNV)"

[31] ProLabNL Personnel. "Oil-in-Water analysis Procedure".

[32] Ferreira, T., and W. Rasband, 2011. "ImageJ User Guide". IJ 1.46r